Progress in Materials Science 159 (2026) 101656

Contents lists available at ScienceDirect

Progress in Materials Science

journal homepage: www.elsevier.com/locate/pmatsci

Tunable physicochemical properties of PDMS@nanoparticle composites: modifications, mechanisms, and emerging applications

B.D. Cardoso [a], G. Nobrega [a,b], I.S. Afonso [a,b,c], A. Souza [a,b,e], L.B. Neves [a,b,c], C.L. Faria [a,e], J.L. Diaz de Tuesta [f,g], J.E. Ribeiro [b,d], R.A. Lima [a,h,i,*]

[a] *Mechanical Engineering and Resource Sustainability Center (MEtRICs), Mechanical Eng. Dep., University of Minho, Campus de Azurém, 4800-058 Guimarães, Portugal*
[b] *Centro de Investigação de Montanha (CIMO), Instituto Politécnico de Bragança, Campus de Santa Apolónia, 5300-253 Bragança, Portugal*
[c] *International Iberian Nanotechnology Laboratory (INL), 4715-330 Braga, Portugal*
[d] *Instituto Politécnico de Bragança, Campus de Santa Apolónia, 5300-253 Bragança, Portugal*
[e] *CMEMS-UMinho, Univ. of Minho, Campus de Azurém, Guimarães, Portugal*
[f] *Chemical and Environmental Engineering Group, Universidad Rey Juan Carlos, C/Tulipan, s/n, 28933 Móstoles, Comunidad de Madrid, Spain*
[g] *Instituto de Investigación de Tecnologías para la Sostenibilidad, Universidad Rey Juan Carlos, C/Tulipan, s/n, 28933 Móstoles, Comunidad de Madrid, Spain*
[h] *Transport Phenomena Research Center (CEFT), Faculdade de Eng. da Univ. do Porto (FEUP), Rua Roberto Frias, 4200-465 Porto, Portugal*
[i] *Faculty of Engineering, Associate Laboratory in Chemical Engineering (ALiCE), University of Porto 4200-465 Porto, Portugal*

ARTICLE INFO

Keywords:
PDMS composites
Nanoparticles incorporation
Interfacial engineering
Multifunctional elastomers
Nanostructured materials
PDMS applications

ABSTRACT

Polydimethylsiloxane@nanoparticles (PDMS@NPs) composites represent a versatile class of advanced elastomers whose physicochemical behavior can be finely tuned through nanoscale interfacial design and nanofiller morphology. Owing to their inherent flexibility, transparency, and chemical stability, PDMS based systems have emerged as model platforms for developing multifunctional materials with optimized mechanical, thermal, electrical, optical, acoustic and wetting properties. This review systematically elucidates the structure property relationships in PDMS@NPs composites and the interaction mechanisms between NPs and polymer chains that enable tunable control over bulk and interfacial behavior, with particular emphasis on how NPs dimensionality and aspect ratio (0D, 1D, and 2D fillers) regulate stress transfer, transport pathways, and functional interconnectivity within the matrix. Three main NP incorporation strategies, (namely, physical mixing of presynthesized NPs, *in situ* synthesis on cured PDMS, and *in situ* formation within uncured matrices) are critically compared in terms of interfacial coupling, dispersion stability, and processing scalability. Particular attention is given to how interfacial engineering, nanofiller morphology, and hierarchical architecture govern stress transfer, phonon transport, charge percolation, and optical or surface responses. In addition, a property design prospective is presented that links interphase design and nanofiller morphology to mechanical, thermal, electrical, optical, acoustic and wetting-controlled surface properties. This review further critically examines the limiting factors that reduce the applicability of PDMS@NPs composites, including performance degradation, interface instability, and limited recyclability, as well as long-term stability under mechanical, thermal, optical, and environmental conditions.

* Corresponding author.
E-mail address: rl@dem.uminho.pt (R.A. Lima).

https://doi.org/10.1016/j.pmatsci.2026.101656
Received 23 April 2025; Received in revised form 6 January 2026; Accepted 11 January 2026
Available online 13 January 2026

Emerging directions such as green filler synthesis, recyclable PDMS matrices, dynamic and hierarchical interphases, and predictive modeling of morphology-dependent dynamic interfaces are outlined. Overall, this review provides a comprehensive and critical perspective on PDMS@NPs composites as a next generation of soft, functional, and sustainable elastomeric materials, opening new avenues for advances in flexible electronics, soft robotics, biomedical devices, and adaptive coatings.

1. Introduction

Silicone, also known as polysiloxane, consists of a silicon-oxygen backbone with organic side groups (carbon), which gives it a combination of organic and inorganic properties. Silicone is considered an 'organometallic' polymer due to the presence of carbon [1]. The main forms of silicones are oils, elastomers, gels, and resins, and are usually categorized as biocompatible, non-toxic, flexible, and chemical inertness [1–4]. The core properties of silicone materials can also be tuned through molecular-level modifications, which include control over polymer molecular weight, the addition of organic functionalities to the backbone or end groups, branching, crosslinking density, and copolymerization with organic polymers [5]. Such tunability support their widespread use in, for instance, implants, medical devices, tissue engineering, antimicrobial and water-repellent coatings, insulation, and soft robotics [6–10].

Polydimethylsiloxane (PDMS) is a soft synthetic polymer and one of most used silicone in the industry, due to its high flexibility, chemical stability, optical transparency, low surface energy, tunable mechanical properties and biocompatibility.

As shown in Fig. 1, the development of pure PDMS and PDMS-based composites has gone through several historic stages from the 1940 s to the present. In the 1940 s, PDMS was first synthesized by the General Electric Company and Dow Corning corporation [11,12]. The idea of the reinforcement of PDMS with particulate fillers appeared in the middle of the 20th century. In 1955, Warrick and Lauterbur showed that particle size of filler, for instance, silica (SiO_2), affects mechanical properties of silicone rubbers [13]. In 1957, Bueche performed measurements of modulus and swelling in PDMS reinforced by different fillers, such as SiO_2 and alumina (Al_2O_3). The results indicated that the main reasons for modulus increase, and swelling reduction are polymer-filler attachments [14]. In the 1970 s, Boonstra and his colleagues reported the effect of SiO_2 in elastomers by investigating mechanisms such as bound-rubber formation and the influence of SiO_2 surface chemistry [15]. These first works positioned SiO_2 as a successful reinforcing filler in PDMS elastomers and outlined the importance of nanoscale interfacial interactions for dictating macroscopic performance.

The 1990 s marked a turning point with the development of soft lithography (Fig. 1 **A**), where pure PDMS revolutionized microfabrication and enabled the low-cost production of microfluidic devices [16,17]. This microfabrication technique proved highly successful and has had a huge impact on a wide range of microfluidics applications, from the early 21st century to the present, as illustrated in Fig. 1 **A-E, I-K**. In the early 2000 s, with the development of nanoscience, PDMS entered an era of research directed toward multifunctional composites. The addition of various nanofillers was carried out to provide electrical, optical, thermal, and biochemical properties in addition to mechanical reinforcement (Fig. 1 **F-H**). For instance, Paul et al. (2006) [18] reported on the mechanics of prestressed PDMS@carbon nanotube (CNT) composites and gave early insights into the alignment and reinforcement of nanotubes. Shortly after that, Khosla and Gray (2009) [19] developed multi-walled carbon nanotube (MWCNTs) for PDMS used in microelectromechanical systems (MEMS), showing the potential for flexible conductive materials. In the meantime, Goyal et al. (2009) [20] pioneered the *in situ* synthesis of metal NPs embedded in PDMS films, opening a path towards multifunctional composites with tunable electrical, optical, and thermal properties (Fig. 1G). Since then, graphene, boron nitride nanosheets, quantum dots, liquid metals, and various other organic/inorganic NPs have been incorporated in PDMS matrices. These composites have enabled applications ranging from sensors, actuators and heat sinks to membranes, filters, sponges, and even protective face masks developed during the COVID-19 pandemic (Fig. 1 L-P).

Despite the advantages and successful applications of the PDMS, pure PDMS has several limitations. Mechanically, it has a low elastic modulus and poor fracture toughness, which makes it likely to develop cracks. It is unsuitable where high stiffness or strength is required [35,36]. Structural failure can also arise from weak adhesion to substrates like glass or metal. In biomedical contexts, hydrophobicity and absorption of small molecules make PDMS unsuitable for long term cell culture and drug studies. While surface treatments such as oxygen plasma can temporarily render PDMS hydrophilic, hydrophobic recovery inevitably occurs [11,37]. Also, PDMS is electrically insulating [38,39] and permeable to gases and water vapor, which can cause corrosion or device failure in electronics [40,41]. For cell culture specifically, the bulk PDMS surface is poorly conducive to long term adhesion and proliferation, so modifications are often required.

Modern PDMS-based composites address many of these limitations by the controlled incorporation of NPs into the polymer matrix (forming PDMS@NPs composites), enabling tunable enhancement of mechanical, optical, electrical, thermal, wettability, and acoustic properties depending on filler specifications and processing strategy. The overall effect of NPs is strongly dependent on synthesis methods, particle size and shape, surface chemistry, incorporation techniques, concentration, and dispersion quality.

2. Molecular structure and main properties of PDMS

PDMS are linear polymeric organosilicon compounds with unique physicochemical features [42]. Its molecular structure is obtained from repeating dimethylsiloxy ($-SiO(CH_3)_2$-) units with terminal trimethylsilyl ($-Si(CH_3)_3$) groups [43], overall expressed as $CH_3[Si\ (CH_3)_2O]n\ Si\ (CH_3)_3$ (Fig. 2 **A and B**). The "n" defines the number of repeating unit and, as a result, the molecular weight and

the resulting viscoelastic properties [44].

The siloxane (Si-O) backbone confers high flexibility, good thermal stability, and low surface energy. The Si-O bond has a high ionic character due to silicon-oxygen electronegativity difference (with an estimated 37–51% ionic contribution), which increases its strength and thermal stability [45]. The latter occurs since the dissociation energies of the Si-C bonds are higher than for Si-O bonds.

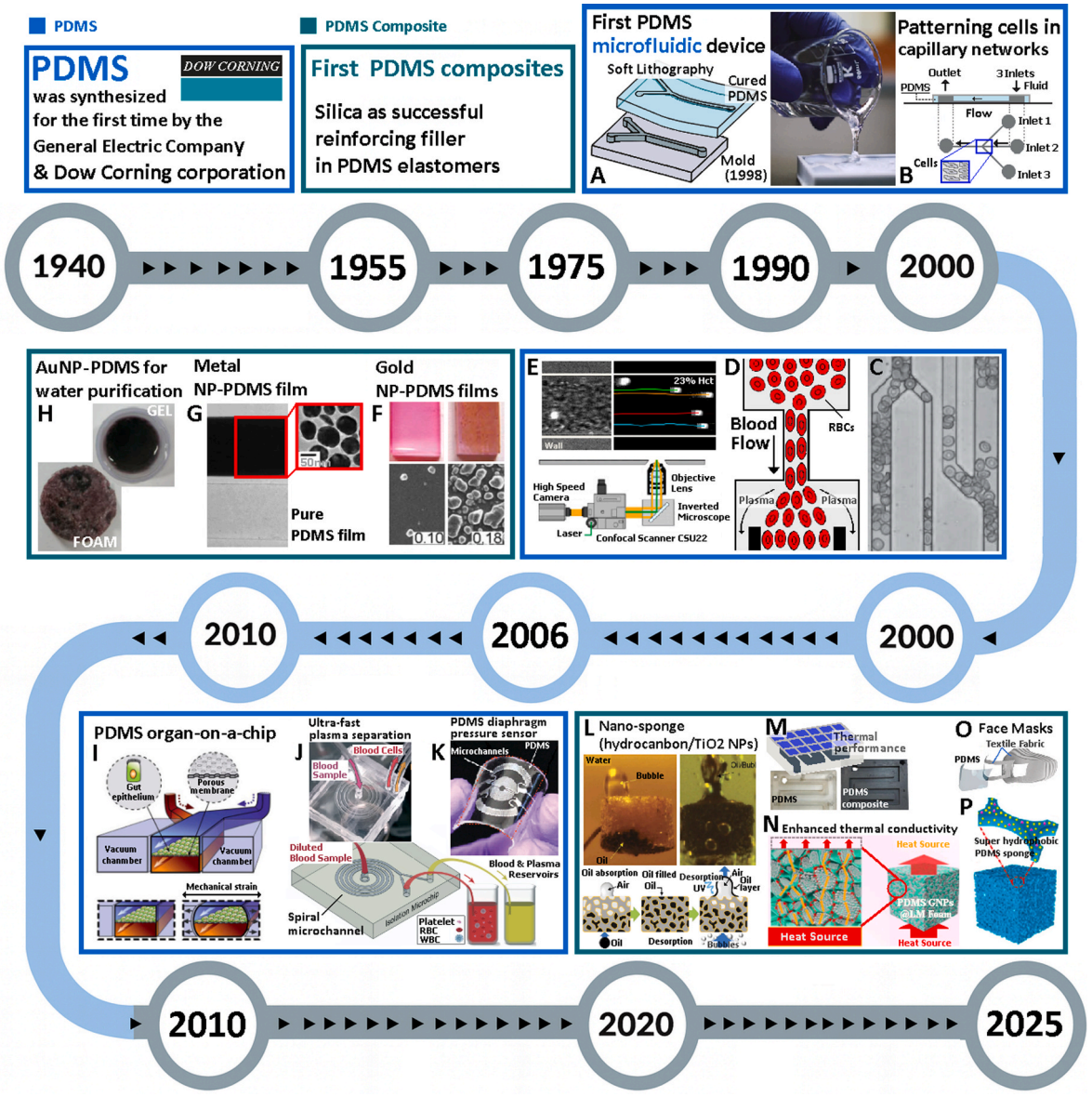

Fig. 1. Representative applications of pure PDMS and PDMS-based composites from the 1940 s to the present. (A) Development of soft lithography has revolutionized the application of microfluidic devices in wide variety of fields [16,17,21]. (B) Patterning cells in a PDMS microfluidic device adapted from [22], copyright (1999) National Academy of Sciences, U.S.A. (C) Direct assessment of the impact of impaired red blood cells (RBCs) deformability on the flow of blood in a PDMS microfluidic device [23]. (D) PDMS microdevice to separate blood plasma [24]. (E) Confocal micro-PIV/PTV blood flow assessment [25]. (F) Application of PDMS-gold NPs composite films in microfluidic systems to immobilize biomolecules, adapted from [26]. (G) Metal NPs (silver, gold, platinum) embedded in PDMS films for a variety of applications, adapted from [20]. (H) AuNP/PDMS nanocomposites for water purification and drug delivery, adapted from [27]. (I) PDMS organ-on-a-chip having a flexible porous membrane and two vacuum chambers, adapted from [28]. (J) PDMS spiral microfluidic device for cell focusing and ultra-fast plasma separation, adapted from [29]. (K) microfluidic diaphragm pressure sensor for pulse and tactile monitoring, adapted from [30]. (L) UV-responsive nano-sponge and its underwater oil absorption and desorption process, adapted from [31]. (M) Thermal performance of PDMS composite heat exchangers, adapted from [32]. (N) Heat transfer mechanism in a PDMS/graphene nanoplatelets@liquid metal (PDMS@GNPs-LM) composite foam with a dual network structure, adapted from [33]. (O) Face mask composed by PDMS and textile fabrics, developed during the COVID-19 pandemic [21], (P) Super-hydrophobic PDMS@SiO_2-WS_2 sponge for oil recovery, adapted from [34].

Thus, the initial degradation of PDMS is mainly governed by the cleavage of Si-C bonds, while the Si-O-Si backbone remains intact at high temperatures [46]. Also, the partial overlap of the empty *d* orbitals of Si with O *p* orbitals also imparts partial double-bond character, which also contributes to the thermal stability of the siloxane backbone [45]. This feature ensures that the PDMS maintain its mechanical properties and performance under thermal stress, making it highly suitable for application in automotive, aerospace, electronics industries, where the material is exposed to high temperatures [47–49].

Furthermore, PDMS Si–O–Si bond has a very broad bond angle, typically ranging between 120° and 180°, resulting in its inherent flexibility [50]. This flexibility is also due to the absence of energy variation in the given angular range, which allows the bond to undergo structural changes without breaking [51]. Elastomeric properties in a wide temperature range, which is most relevant for flexible electronics, wearable devices, and sensors, enable comfortable skin contact and efficient signal acquisition. These features ensure flexibility with no deterioration. Furthermore, by changing the mix ratio of the base polymer/curing agent, fine tuning of its mechanical properties is possible, allowing high tunability with respect to specific mechanical properties [52].

The backbone also contributes for the inherent transparency of PDMS (refractive index of PDMS is approximately 1.4) as a result of the low absorption of visible light by silicon-oxygen bonds [53,54]. Transparency is a feature highly pursued for microfluidic, biomedical devices and optical examination, since it enhances the performance of devices that require precise fluid manipulation and clear visibility [55–57]. It is also explored for tissue-mimicking phantoms due to its ability to mimic the optical and mechanical properties of biological tissues [58–60]. In coating, it is advantageous for applications as self-cleaning surfaces and anti-icing. The high transparency of PDMS-based coatings allow, for instance, a high visibility of windows (up to 93.6%) and enhanced performance in subzero environments [61].

The molecular structure of PDMS is responsible for its hydrophobicity due to the presence of methyl groups (CH_3) oriented outward [4]. Since CH_3 is non-polar, it creates a low energy surface that repel water, contributing to the high water contact angle observed on PDMS surfaces [4]. Some of the most significant structure property relationships are presented in Fig. 2 **C**. Even though this feature can be useful in several applications (anti-icing, self-cleaning surfaces, and fluid drag reduction), it can pose challenges in fields requiring hydrophilic surfaces (as some biomedical devices). In the latter cases, several treatments can be applied to modify the hydrophobicity of PDMS. For instance, oxygen plasma treatment introduces functional groups such as silanol (Si-OH) to turn it hydrophilic. Nonetheless, this effect is temporary since the low molecular weight siloxane chains migrates from the bulk to the surface [62]. Another surface modifications include UV-ozone treatment, polymer grafting and nanomaterials incorporation [62–64]. Table 1 summarizes the main physicochemical properties of cured PDMS.

3. Methods of incorporating NPs into PDMS

The physicochemical performance of PDMS@NPs composites depends on how the NPs are introduced into the elastomer matrix. The incorporation way determines dispersion uniformity, interfacial bonding, and long-term stability. Different studies have reviewed PDMS modification strategies, covering physical blending, sol–gel hybridisation, plasma-assisted deposition, and microfluidic synthesis [56,75]. Despite this progress, achieving strong and durable PDMS@NPs interfaces remains challenging due to the intrinsic

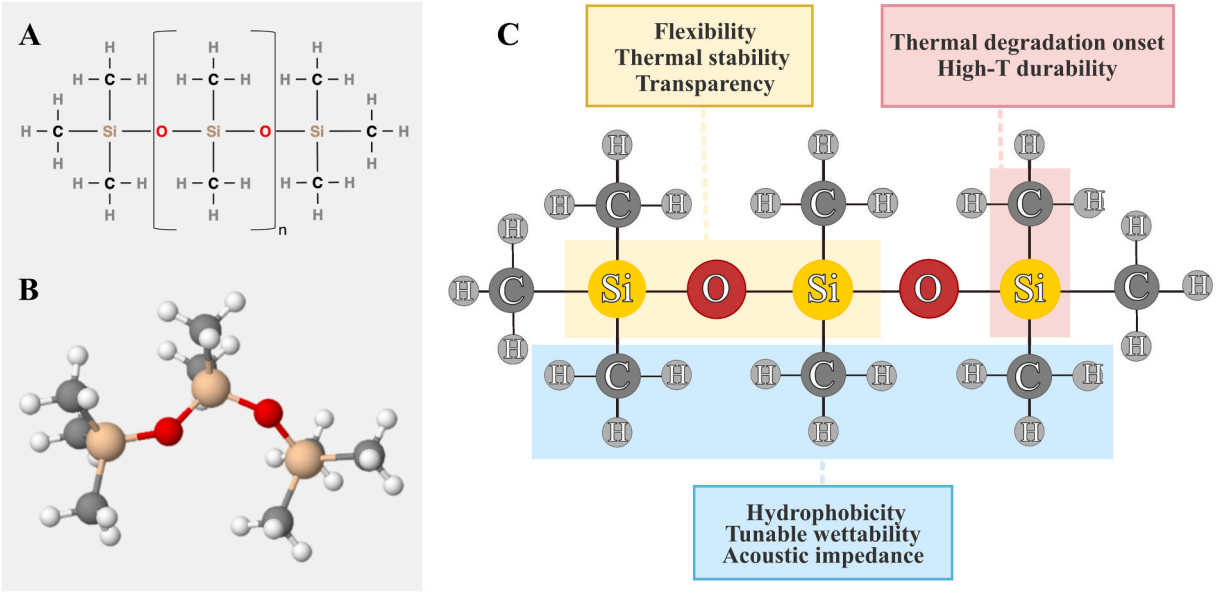

Fig. 2. (A) Chemical structure of PDMS showing repeating –[Si(CH$_3$)$_2$–O]– units; (B) 3D molecular model of PDMS illustrating the Si–O–Si backbone and flexible organic side groups; (C) Structure–property relationships: the Si–O backbone confers flexibility, thermal stability, and transparency (yellow box); methyl side groups contribute to hydrophobicity, tunable wettability, and acoustic impedance (blue box); and the Si–C provides high-temperature durability and delayed thermal degradation onset (red box).

mismatch between the apolar siloxane network and the typically polar or metallic nanophases [21,63].

In this section, NP incorporation methods are classified according to the degree of interaction between NPs and the PDMS network, rather than by processing technique. This aims to compare the effects of interfacial structure and curing dynamics on the resulting composite properties. The three main incorporation methods are: (i) Physical addition of pre-synthesised NPs into uncured PDMS; (ii) Synthesis of NPs on cured PDMS, which modifies the elastomer surface through controlled nucleation and reduction of precursors; and (iii) *In situ* generation of NPs within uncured PDMS during curing, where concurrent crosslinking and NP formation yield chemically integrated hybrids [76,77].

Although not being consensual, the term composite typically denotes a material in which two or more constituents coexist as physically distinguishable phases, even after processing. The components may interact mechanically or through secondary forces, but their identities remain separate within the final architecture [78]. Conversely, the term hybrid is typically used for systems in which organic and inorganic building blocks interact at the molecular or nanoscale level, often through covalent bonding, strong coordination interactions, or the formation of co-continuous networks. These interactions generate structural environments and properties that cannot be predicted by simple physical mixing [78]. Thus, throughout this chapter, the term PDMS@NPs composite refers to systems in which PDMS and NPs form distinguishable phases. In contrast, hybrid PDMS systems denote covalently integrated networks or co-continuous organic–inorganic phases.

3.1. *Pre-synthesized NPs introduced into uncured PDMS*

The direct dispersion of pre-synthesised NPs into uncured PDMS (prepolymer PDMS with curing agent) is the simplest and still the most widely adopted incorporation method (Fig. 3 A). Common fillers include carbon nanostructures such as CNTs, carbon dots, and graphene, as well as noble metals (Ag, Au) and oxides such as Fe_3O_4 and SiO_2. They are typically mixed into uncured PDMS by stirring or ultrasonication, methods that are reliable but offer limited control over uniformity [79,80]. Organic solvents such as toluene or hexane are often added to reduce viscosity and facilitate NPs distribution [81,82] temporarily. Ethanol is also commonly used to disperse SiO_2 before mixing with PDMS, and then evaporated [83,84]. Mixing and curing protocols are usually standardised according to the manufacturer's specifications. The curing of PDMS is often performed at room temperature for 24–48 h or at higher temperatures (60–150 °C) for a few hours. Degassing under vacuum (~0.1–10 kPa) is used to remove entrapped air [85]. The overall process and typical outcomes of direct dispersion are illustrated in Fig. 3, which highlights representative preparation steps, rheological behaviour, and microstructural features of PDMS@NPs composites.

Table 2 compiles representative PDMS@NPs systems from recent studies, illustrating how filler chemistry, loading, and dispersion modify the balance between mechanical, thermal, and functional performance.

Despite its simplicity, this approach is limited by poor dispersion control and weak interfacial adhesion. PDMS@Graphene composites often show non-uniform distribution and reduced chain mobility, consistent with the heterogeneous and shear-dependent morphologies observed in Fig. 3 B [86]. At the same time, aggregation and sedimentation are recurrent, especially at high filler loadings where viscosity rises sharply, as confirmed by the pronounced increase in the viscosity and yield-stress behaviour of PDMS@CNT composites shown in Fig. 3C [87]. In silica-based systems, Colijn et al. [96] demonstrated that dispersion quality governs both nanoscale and bulk dynamics, and that PDMS coated SiO_2 enhances miscibility, viscosity and interactions between particles.

Ultrasonication and solvent-assisted mixing can momentarily improve uniformity [97], as confirmed by the more homogeneous filler distribution visible in Fig. 3 D. Yet these gains tend to fade: Mugemana et al. [98] found that apparent homogeneity on day one often gives way to NP migration and performance decay over time. Characteristic agglomerates and voids observed in fractured PDMS@NPs surfaces (Fig. 3 E) further illustrate the intrinsic instability of this simple blending method.

Direct dispersion is ideal for prototypes and compositional screening, where throughput and filler freedom matter more than long-term stability. However, unpredictable dispersion, solvent residues, and weak matrix filler coupling limit its use in demanding or durable devices [77].

Table 1
Main physicochemical properties of PDMS.

Property	Value	Ref.
Density	~0.97 g/cm^3	[65]
Transmittance	> 90%	[66]
Index of refraction	1.4	[65]
Glass transition temperature	−120 °C	[67]
Thermal stability	Stable up to −300 °C	[68]
Surface tension	19–21 mJ m^{-2}/~20 mN/m	[69]
Thermal conductivity	0.12–0.35 W/mK	[70]
Specific heat	1.46 kJ/kg·K	[65]
Hydrophobicity	105° to 110°	[71,72]
Tensile strength	2.24–6.7 MPa	[65]
Young's modulus	360–870 KPa	[73]
Dielectric strength	2.3–2.8 kV/mm	[65]
Electrical conductivity	4×10^{13} Ωm	[65]
Poisson ratio	0.5	[74]
Magnetic permeability	0.6x10^6 cm^3/g	[65]

3.2. NPs on cured PDMS

NPs can also be deposited or patterned onto cured PDMS surfaces using either *in situ* synthesis or transfer-based methods. These methods enable spatial control and surface functionality without disrupting the bulk elastomer network. Fig. 4 summarizes the main strategies, from *in situ* surface synthesis (Fig. 4A) to microcontact and plasma assisted NP transfer (Fig. 4 B).

3.2.1. In situ synthesis of NPs

PDMS's hydrophobic, insulating, and chemically inert nature provides excellent stability but limits its application in conductive and catalytic devices. A strategy to overcome these intrinsic constraints is the *in-situ* synthesis of NPs directly on the cured PDMS surface, enabling strong adhesion and conformal coverage without compromising elasticity. This method eliminates transfer steps and ensures intimate metal–polymer interfaces, producing hybrid surfaces suitable for flexible electronics, sensing, and photonic applications.

Because PDMS possesses few polar functional groups, heterogeneous nucleation of NPs is nontrivial. Surface activation is required to create hydroxyl or silanol sites that serve as anchors for metal precursors. Oxygen plasma, UV/ozone, or acidic oxidation create Si–OH and Si–O–Si sites that raise surface energy and allow precursor ions to anchor (see Fig. 4 A (i)) [63,76]. Once reduced, either chemically or photochemically, these ions nucleate into metallic NPs directly bound to the PDMS network. The resulting morphology depends on the competition between nucleation rate, growth rate, and surface diffusion. Excessively rapid reduction promotes agglomeration, while controlled kinetics favor uniform nanocrystal distributions. This concept has been demonstrated by Park et al.

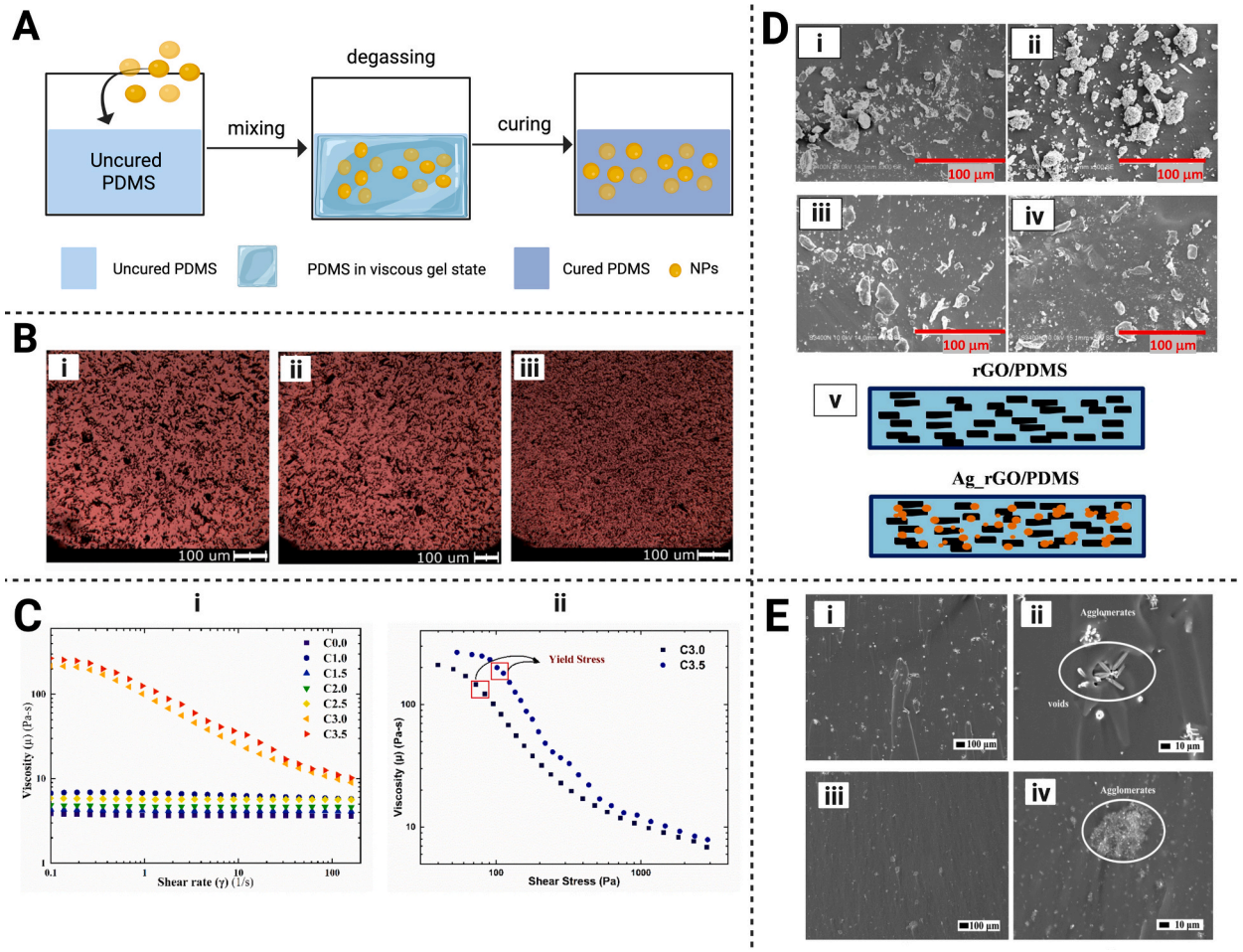

Fig. 3. (A) Schematic illustration of the direct dispersion of pre-synthesised NPs into uncured PDMS process, including mixing, degassing, and curing of PDMS. (B) Polarising-interference micrographs of PDMS@graphene composites prepared by different mixing methods: (i) magnetic stirring, (ii) stirring + calendering, and (iii) microfluidisation, illustrating the evolution from heterogeneous to uniform filler dispersion, adapted from [86]. (C) Rheological response of PDMS@CNT composites showing the rise in viscosity and the onset of yield-stress behaviour with increasing CNT loading ((i) viscosity vs shear rate; (ii) viscosity vs shear stress; adapted from [87] (D) Morphology and nanofiller distribution in PDMS composites: SEM images of (i) PDMS@ Graphene Oxide (GO), (ii) PDMS@Ag, (iii) PDMS@reduced graphene oxide (rGO), and (iv) PDMS@Ag-rGO samples, and (v) schematic representation of filler alignment within the PDMS matrix, adapted from [88]. (E) Fractured surface SEM images of 5 wt % PDMS nanocomposites showing agglomerates and interfacial voids for (i,ii) PDMS@nanofibre and (iii,iv) PDMS@NPs systems, adapted from [89].

[99] who, with the help of ridge-assisted nucleation, have grown Au NPs directly on PDMS and have shown that surface microcracks promote controlled *in situ* growth and uniform distribution (Fig. 4 A (ii)), while Paghi et al. [103] have expanded the approach to 3D PDMS foams, exploiting the enormous internal surface area and compressibility of porous networks. By immersing foams in aqueous silver fluoride (AgF) solutions, they have achieved spontaneous reduction of Ag^{+} to Ag^{0} at room temperature, generating tunable NP coverages (0–70%) simply by adjusting the reaction time and precursor concentration. Electrical percolation and piezoresistivity were maximised at intermediate coverage, where the network formed stable conductive pathways that responded reproducibly to micro-pressures as low as 25 Pa. The produced foams demonstrated long term durability and excellent recovery, underlining how percolation threshold and interparticle distance control macroscopic electromechanical performance.

A related strategy by Kim et al. [104] used $AgNO_3$ reduction on plasma-treated PDMS to produce antibacterial films for implantable devices. The *in situ* formed Ag NPs have shown strong bactericidal activity and negligible cytotoxicity, confirming that careful control of precursor concentration and reduction conditions can reconcile antimicrobial functionality with biocompatibility. Beyond these works, Ahmed et al. [100] reported a multicomponent PDMS@Au/CdTe QD surface composition, in which Au NPs were first grown *in situ* on PDMS and afterwards overlayered with CdTe quantum dots, forming photoluminescent composites that exhibit metal enhanced fluorescence (Fig. 4 A (iii)). These studies make one point clear: surface activation and reduction kinetics critically define final performance.

The coverage connectivity trade-off represents another universal design constraint: dense coatings improve conductivity and plasmonic intensity but reduce flexibility and increase the risk of cracking under strain. In contrast, sparse coatings preserve elasticity at the cost of incomplete percolation. Optimising intermediate coverage, as demonstrated by Paghi et al. [103], achieves mechanically resilient and electrically active architectures suitable for strain-sensing and stretchable optoelectronic platforms. Even with these advances, stability and uniformity still need further improvements. Silver oxidises, clusters coalesce, and coatings fatigue under strain. Thin Au or oxide shells slow the decay, but at the cost of extra processing. Scaling to wafer scale areas may require microreactor based coating or vapour assisted reduction, allowing for a more reliable and reproducible control over the reaction kinetics.

3.2.2. Surface patterning and NPs transfer onto cured PDMS

Stamp-based NP transfer, through microcontact printing (μCP) or related soft-lithographic techniques, patterns NPs onto cured PDMS by conformal contact. A PDMS stamp inked with NP dispersions or molecular precursors is brought into contact with the PDMS target surface; upon removal, a patterned NP layer remains, as exemplified in Fig. 4B (i).

The process of μCP is a mature and versatile method for nanoscale patterning, encompassing several transfer modes that differ in how material is deposited or retrieved from the substrate [105,106]. These approaches are schematically illustrated in Fig. 4B (ii), which compares additive, subtractive, and intaglio transfer configurations, where PDMS stamps are sequentially inked, contacted, and released to generate patterned NP or QD films [101]. Redolat et al. [107] reached submicron precision by defining wetting domains on PDMS stamps, while Xie et al. [108] and Lin et al. [109] used similar principles to build flexible Surface-Enhanced Raman Scattering (SERS) platforms based on Au and Ag nanostructures. Jalajamony et al. [102] went further, printing Ag NP circuits directly onto PDMS using plasma-assisted contact (Fig. 4B (iii)). Each variation pursues the same goal: precision without compromising flexibility. Beyond planar or monolayer transfers, Schnee et al. [110] expanded the concept of PDMS stamping to replicate 3D nanostructured coatings. In their work, a two-photon lithography master was used to create micropyramid arrays, which were subsequently replicated using PDMS stamps inked with a germanium (Ge) NP epoxy composite. The method enabled the repeated fabrication of 3D anti-reflective surfaces with low reflectivity in the short-wave infrared region, as well as the reuse of the PDMS stamp across multiple cycles. Recent strategies also improve reliability and interfacial resistance in nanowire and NP networks on PDMS. For instance, Park et al. [111] inhibit galvanic replacement to deposit conformal Au coatings on PDMS@Ag nanowire electrodes, thereby largely reducing contact resistance

Table 2
Properties of representative PDMS@NPs composites prepared via direct dispersion or solution mixing, and incorporating metallic (Ag, Au, CuO), oxide (SiO_2, TiO_2, ZnO, Fe_3O_4, $BaTiO_3$), and carbonaceous (graphene, CNTs) NPs.

NP Type	NP Size (nm)	Loading (wt. %)	Properties achieved	Ref.
Ag	~20–40	–	Enhanced adhesion, modified viscoelastic modulus; microwave-assisted cure demonstrated	[85]
Ag–rGO	Ag: ~20–50; rGO: 2–4	0.1–1	Improved dielectric properties, reduced agglomeration, and flexible sensors	[88]
Au	~10–50	0.5–2	Plasmonic response, stretchable conductivity, enhanced adhesion	[90]
$BaTiO_3$	~200	7–23 vol%	Piezoelectric response, dielectric tuning, energy harvesting	[91]
CuO	~23	<2	Improved antibacterial and anticorrosion properties; optimal performance at 0.5–1 wt% CuO; excess CuO leads to agglomeration and reduced biocompatibility; PDMS-SiO_2-CuO coatings are promising for temporary bone implants	[79]
Fe_3O_4	~44–65	1–10	Changes in stress–strain, fracture toughness, thermal properties for hyperthermia applications	[92]
Graphene; CNTs	–	>5	Increased hardness and reduced surface resistance with concentration	[93]
Reduced graphene	~50–100	0.05–1.5	Tuned transparency, roughness, contact angle (TENG optimisation)	[94]
TiO_2	~70	8	Frequency-independent dielectric permittivity; low dielectric losses; suitable for microwave and terahertz applications; TiO_2 acts as a crystallisation centre, improving structural stability.	[95]
ZnO	~50	10	Enhanced piezoelectric response under compression; flexible sensor performance; voltage generation up to 4.2 V depending on ZnO morphology	[89]

in organic transistors.

Adhesion and reproducibility are dependent on surface cleanliness and interfacial chemistry, whereas residue transfer can be reduced and pattern fidelity improved by plasma pretreatment [111]. However, repeated use may cause nanogap drift or contamination unless NP anchoring layers, such as thiols, silanes, or conformal coatings, are introduced [112].

Surface patterning remains central to flexible optics and sensing, where the geometry is more relevant than the bulk composition. A major challenge is to keep these delicate interfaces stable over extended periods and at scale. Hence, future progress will depend on tougher interfaces, less distortion during contact, and scalable pattern transfer [113,114].

3.3. *In situ synthesis of NPs on uncured PDMS (during or before curing)*

In situ synthesis generates NPs within the PDMS phase during or immediately prior to curing, improving dispersion and interfacial contact compared with *ex-situ* methods. Mechanistically, it relies on the chemical conversion of embedded precursors (e.g., hydrolysis condensation, redox reduction, or thermal decomposition) concurrent with siloxane crosslinking, which fosters strong NP matrix coupling and minimises aggregation [115].

Fig. 5 summarises the main mechanistic pathways encompassed by this concept, ranging from precursor reduction and polymerisation growth to sol–gel condensation, flash nanoprecipitation, and emerging microfluidic and surface-assisted strategies. These approaches differ not only in the chemistry driving NP nucleation but also in the resulting degree of network integration, scalability, and process control.

For PDMS@SiO_2 composites, sol–gel based *in situ* formation yields significant gains in mechanical and thermal stability, while Fourier Transform Infrared Spectroscopy (FTIR) and X-ray Photoelectron Spectroscopy (XPS) confirm silica incorporation without disrupting the PDMS backbone. Both the catalyst type (acid or base) and the tetraethyl orthosilicate (TEOS)-to-PDMS ratio significantly

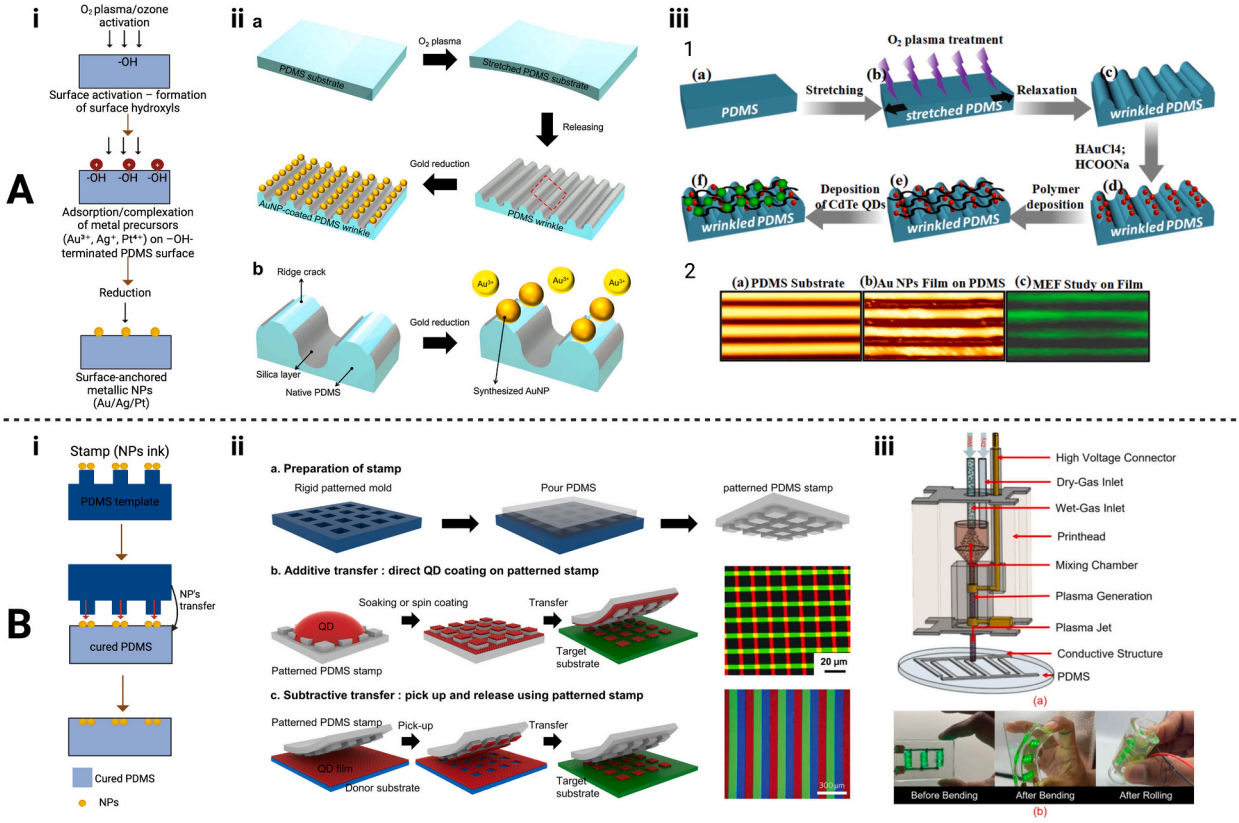

Fig. 4. NP deposition and patterning strategies on cured PDMS surfaces. (A) In situ surface synthesis: plasma or ozone activation generates hydroxylated PDMS sites that adsorb and reduce metal precursors into surface-anchored NP. (i) Schematic overview. (ii) wrinkle and ridge assisted growth of Au NPs on PDMS, adapted from [99] (iii) in situ-synthesis of Au NPs and CdTe QDs on plasma-treated PDMS; 1 a–f schematic of the stretching, plasma treatment, relaxation, reduction, polymer deposition and QD loading steps; (i) 2 a–c optical micrographs of the PDMS substrate, Au NP film, and MEF study on the resulting film; adapted from [100]. (B) Patterning and printing approaches: (i) NP or precursor inks can be transferred or directly printed onto cured PDMS using soft-lithographic or plasma assisted techniques. (ii) additive and subtractive microcontact printing strategies showing preparation of patterned PDMS stamps and direct transfer of QD/NP layers, adapted from [101]. (iii) plasma assisted inkjet printing of Ag NP inks on PDMS (ii) a schematic of the plasma jet printer, (b) photographs of the flexible circuit before, after bending and after rolling; adapted from [102].

influence the condensation rate, particle size, and mechanical response [116,117]. However, the tight chemical coupling that underpins these advantages also narrows the formulation window, as hydrolysis and condensation kinetics are highly sensitive to humidity, pH, and solvent polarity, and as a result, compromising the reproducibility and scale-up [115,118].

3.3.1. *In situ polymerisation*

In situ polymerization yields NPs directly inside the curing PDMS matrix, usually by reducing or decomposing the dissolved precursors as cross-linking proceeds. Metal salts, organometallic complexes, or silane monomers are incorporated into the PDMS prepolymer and subsequently transformed into NPs under thermal, photochemical, or chemical initiation (Fig. 5 A) [115].

The main strength of this method lies in control: nucleation within the viscous PDMS favors smaller, well-dispersed domains, which often translate into better mechanical, dielectric, or optical behaviour. This ability to form well integrated domains is exemplified in the work of Wang et al. [119], who achieved the *in situ* polymerization of an epoxy phase within PDMS (Fig. 5 (i)), uniformly distributed throughout the matrix. *In situ* growth of Ag and Au NPs has also been shown to improve electrical conductivity and long-term stability [120,121]. At the same time, silica generated within PDMS matrices enhances thermal resistance and modulus [117]. Moreover, chemical anchoring of NPs to the forming siloxane network can provide superior durability compared with post synthesis addition. However, these benefits come at a cost, since reaction kinetics and curing must remain perfectly balanced. If precursors or by-

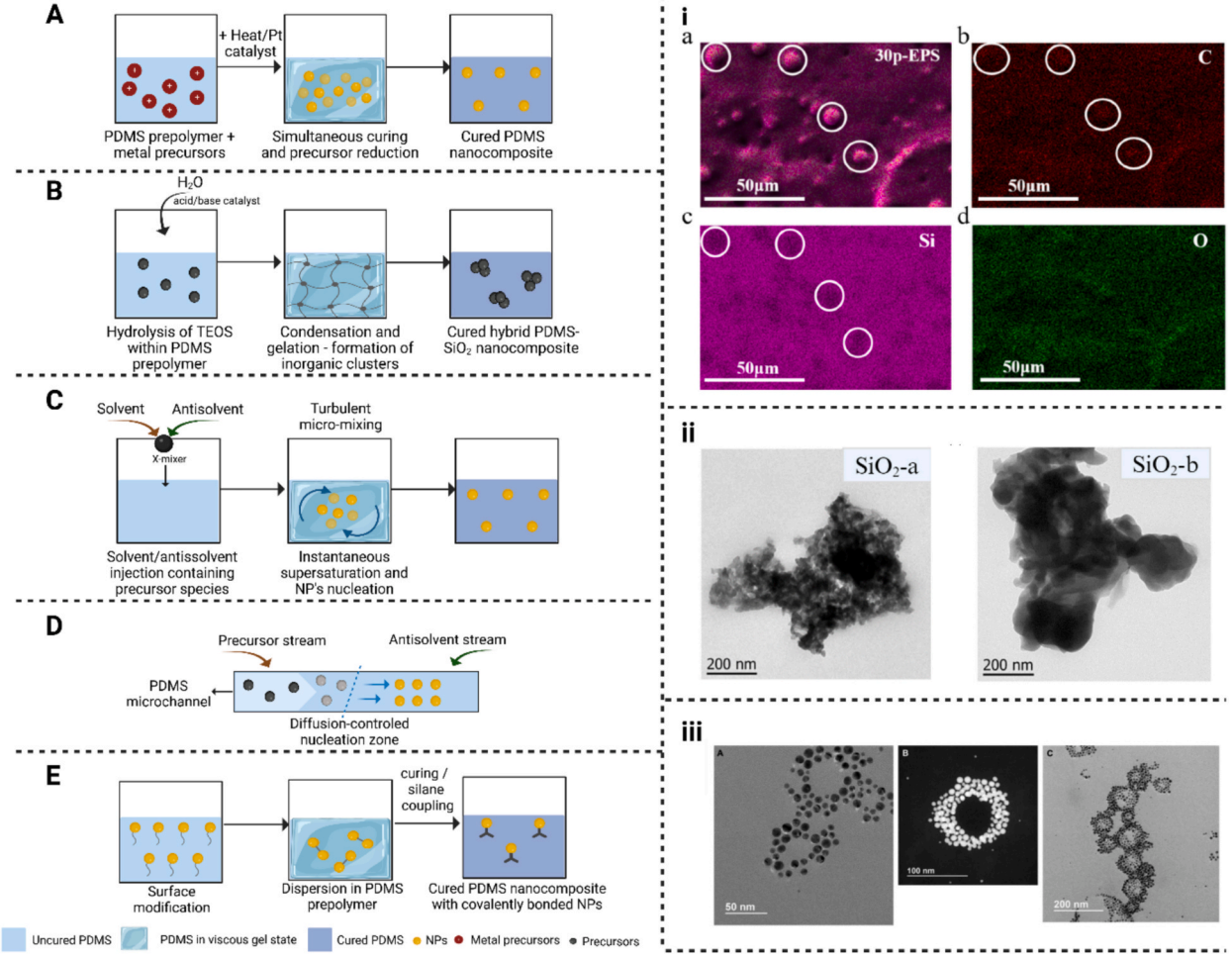

Fig. 5. In situ synthesis methods for PDMS@NPs nanocomposites: representative mechanisms and experimental evidence. (A) In situ polymerization or precursor reduction: curing and NP formation occur simultaneously within PDMS. Example shown for the in situ polymerisation of an epoxy phase (EPS) inside PDMS, where elemental mapping of carbon, silicon, and oxygen ((i) a–d) confirms homogeneous dispersion of the epoxy phase, adapted from [119]. (B) Sol-gel condensation of alkoxysilanes within PDMS: (ii) hydrolysis and condensation of TEOS in the PDMS prepolymer yield SiO_2 nanodomains distributed throughout the matrix. TEM images show silica particles synthesized under acidic (SiO_2-a) and basic (SiO_2-b) conditions, adapted from [116]. (C) Flash nanoprecipitation: rapid solvent antisolvent micromixing leads to instantaneous supersaturation and NP nucleation inside PDMS nanodroplets. Scanning Transmission Electron Microscopy/Transmission Electron Microscopy (STEM/TEM) ((iii) A-C)) images reveal Au NPs arranged in ring like morphologies within PDMS droplets, adapted from [116]. (D) Microfluidic coflow synthesis: controlled diffusion between precursors and antisolvent streams in PDMS microchannels allows diffusion limited, size tunable nucleation. (E) Surface modification assisted curing: NP surfaces functionalized during PDMS crosslinking form covalently bonded PDMS@NPs networks.

products interfere with hydrosilylation, crosslinking can stand altogether [122]. Hydrolysis condensation rates are highly sensitive to pH, humidity, solvent polarity, and catalyst choice, often resulting in nonuniform particle sizes or incomplete NP formation [118]. Reproducibility is therefore a persistent issue, particularly when scaling beyond laboratory batches.

3.3.2. Sol-gel processing

The most mature of the *in situ* methods is the sol–gel processing. This involves introducing inorganic nanodomains into uncured PDMS through hydrolysis and condensation of alkoxysilanes, such as TEOS or trimethoxymethylsilane (MTMS), in the presence of water and catalysts [118]. This method forms SiO_2 or TiO_2 networks under mild conditions compatible with PDMS curing, allowing covalent or semi-covalent integration into the elastomer matrix [116]. The partial hydrolysed silanes that condense with siloxane chains can yield strong interfacial bonding, thereby improving mechanical reinforcement, thermal resistance, and surface functionality compared to *ex situ* mixing approaches (Fig. 5B) [116,123,124].

Representative TEM images (Fig. 5 (ii)) from Córdoba et al. [117] show SiO_2 NPs synthesised under acidic and basic conditions, where acidic catalysis yields smaller, more homogeneous domains, whereas basic environments promote aggregation. This process is extremely versatile because it is tunable. Adjusting the precursor functionality, catalyst, or solvent polarity enables control over domain size and distribution [56]. Such properties are valuable in various applications, including microfluidic devices, stretchable electronics, and protective coatings that require transparency, hardness, or particular dielectric properties [56]. Organic-inorganic hybrid networks generated through sol–gel chemistry also generally exhibit increased swelling and chemical degradation resistance compared to unmodified PDMS, extending the utility of PDMS under conditions where standard PDMS would deteriorate rapidly [125].

The major scaling challenges for sol–gel synthesis in PDMS relate to reaction rates, which can be influenced by factors such as humidity, pH, and catalyst concentration. These effects make reproducibility between batches more difficult [116,126].

Yet the same rigid siloxane chains that reinforce the network can also stiffen it. Beyond a critical loading, the composite turns brittle. To contextualize the diversity of sol–gel chemistries applied to PDMS systems, Table 3 summarises representative formulations and outcomes reported in the recent literature.

3.3.3. Flash nanoprecipitation

Flash nanoprecipitation (FNP) relies on a high-speed mixing of a solvent and antisolvent streams in confined microchannels, driving supersaturation and NPs nucleation within milliseconds [130]. This fast mixing produces narrow size distributions and enables encapsulation of hydrophobic species within polymer or copolymer matrices (Fig. 5 C) [131,132].

A study by Lteif et al. [133] encapsulated metallic and oxide NPs (Au, Fe_3O_4, SiO_2) within amino-terminated PDMS nanodroplets, which were stabilised by polystyrenesulfonate shells. Unmodified PDMS aggregated instantly in polar media, but end functionalisation stabilised the droplets into narrow and reproducible dispersions. TEM analysis (Fig. 5 (iii)) revealed Au NPs arranged in concentric ring-like morphologies along the PDMS interface, a feature characteristic off diffusion limited growth during FNP. This study established FNP as a method for liquid PDMS nanocomposites, although integration into solid PDMS remains a research challenge [133].

Mechanistically, the method's strength lies in the precise control of the nucleation growth balance. However, translating FNP to viscous prepolymers or curing matrices introduces new complexities involving diffusion, interfacial tension, and cure kinetics. Sequential or microfluidic variants may mitigate these constraints but remain in early development for PDMS systems [130,134].

3.3.4. Co-flow focusing

Co-flow focusing is a microfluidic assisted synthesis technique that uses laminar flow within a microfluidic device to control mixing and reaction regions, allowing reproducible NP formation within PDMS microchannels [135]. It yields narrower particle distributions than batch methods, though the complexity of obtaining the drops and designing the devices is high [136]. Its ability to localise reactivity is particularly advantageous for patterned or compartmentalised devices, although weak NP matrix bonding still limits long term stability [137].

3.3.5. Surface functionalization (in situ context)

In situ surface functionalization involves adjusting the PDMS or NP precursors during particle formation to stabilise interfaces and maintain curing compatibility. Functional silanes, polyethylene glycol (PEG)ylated chains, or siloxane additives regulate nucleation kinetics and suppress phase separation [56,116]. When designed correctly, these additives greatly improve the dispersion and adhesion; when overused, they can inhibit crosslinking or plasticise the network [115].

3.4. Comparison between incorporation methods

The incorporation of NPs into PDMS encompasses a continuum of approaches that differ not only in when the inorganic phase is introduced, but in how deeply it interacts with the polymer network. As outlined in Section 3, these can be broadly grouped into three main regimes, where each method defines a distinct balance between control, interfacial coupling, and processing freedom.

As summarised in Table 4, direct dispersion of NPs remains the simplest method. They are quick, modular, and compatible with most filler chemistries, making them an appealing combination for prototyping or exploratory studies. Yet, their simplicity is also their weakness, as poor dispersion, residual solvents, and weak interfacial bonding often limit their long-term reliability. The result is a composite that performs well enough to demonstrate a concept, but rarely well enough to survive real operation. Deposition or growth of NPs on cured PDMS offers a step forward. Here, the emphasis shifts from mixing chemistry to interfacial design, i.e., from surface

energy, adhesion, and topology to the creation of functional skins. These surface integrated structures have transformed PDMS into flexible plasmonic, catalytic, and sensing platforms. Still, they demand strict control over activation and reduction kinetics. Note that excessive plasma treatment or accelerated reduction can compromise surface compliance, thereby diminishing the properties that make PDMS a valuable material. When NPs are generated *in situ* within uncured PDMS, the governing mechanisms change again. Now, inorganic and organic phases develop together, interlaced chemically and kinetically. The result of this joint formation yields exceptional mechanical and thermal resistance, sometimes even new optical or dielectric properties, but at the cost of reproducibility. Slight changes in humidity, catalyst ratio, or pH may affect particle size or the kinetics of crosslinking, thereby converting a smooth hybrid into a stiff solid.

As seen above, these approaches can be seen as points along a gradient of increasing interfacial coupling and decreasing process tolerance: physical addition prioritises compositional freedom; surface deposition integrates morphological and adhesive control; and *in situ* generation couples polymerisation and nucleation into a single, reactive step. Ultimately, as interfacial strength rises, scalability and flexibility fall. The challenge ahead lies not in finding new methods, but in mastering when and how to combine them, achieving chemical intimacy without losing the manufacturability that makes PDMS so indispensable.

3.5. Role of nanofiller morphology in PDMS composites

Beyond the choice of incorporation technique, the morphology of the nanofiller is decisive in determining how NPs interact with the PDMS matrix. A measure of this morphological variation is the aspect ratio (AR), defined as the ratio of the filler's characteristic lateral dimension to its length or thickness (d_p/L, where d_p is the lateral dimension and L is the length or thickness). Differences in ARs place NPs into distinctive structural categories, each characterised by a propensity to establish interfacial contacts, to align under flow or curing-induced stresses, and to assemble into percolated domains that can support mechanical, thermal, or electrical transport [140].

NPs with AR $\approx$ 1, or zero-dimensional fillers (0D), are mainly spheres that interact with the matrix as isolated inclusions, a behaviour that makes their performance almost entirely dependent on the quality of the local polymer–particle interface. This happens because their small contact area limits stress transmission across the interface, confining reinforcement to polymer segments in direct contact with the particle surface and promoting extensive phonon scattering, particularly when the particles are well dispersed but unable to establish meaningful connectivity, thereby preventing the formation of mechanically or thermally continuous pathways [140]. In PDMS systems, spherical NPs such as silica or alumina, typically achieve good dispersion but still fail to establish the sustained particle–particle contacts required for long-range connectivity [77]. As a result, improvements in stiffness are modest and heat-transfer pathways remain largely discontinuous unless loadings are sufficiently high, because spherical fillers, being isotropic, require markedly larger volume fractions before a percolated network can emerge [76].

One-dimensional (1D) fillers behave very differently. Nanotubes [141–143], nanorods and nanowires [144] introduce continuous, elongated elements capable of transmitting load and heat along their longitudinal axis, readily developing extended points of contact with the surrounding polymer. Because of their high AR (AR > 1), these fillers have a higher probability of forming partially connected or percolated networks at low filler loadings, which can promote interconnected thermal pathways within the PDMS matrix [140,145]. Even when incorporated through simple mixing routes, mild shear during processing or contraction during curing can induce partial alignment, further enhancing their ability to bridge neighboring regions of the elastomer. These axial pathways reduce interfacial resistance and facilitate both phonon bridging and charge percolation at comparatively low filler contents [146]. In PDMS-based composites, CNTs are a representative example: long CNTs form conductive and load-bearing networks at lower concentrations,

Table 3
Selected sol–gel formulations for PDMS@SiO_2 and hybrid siloxane nanocomposites.

Precursor system / catalyst	PDMS ratio / solvent environment	Curing /reaction conditions	NP size /morphology	PDMS improvement properties	Main limitations	Ref.
TEOS in acidic (HCl) or basic (NH_4OH) sol–gel methods	PDMS:TEOS = 15:1 → 5:1 (5–15 wt% SiO_2)	*In situ* hydrolysis/ condensation during PDMS cross-linking, 60–80 °C thermal curing	SiO_2 ≈ 50–60 nm (acidic method, well dispersed); larger aggregates under basic conditions	↑ Tensile strength (+30%), ↑ thermal stability; good electrical insulation	Agglomeration and local brittleness at > 10 wt% loading due to rapid condensation	[116]
Water based TEOS PDMS sol–gel coating (H_2O/ EtOH, acid catalysis)	TEOS:PDMS molar ratio ≈ 1: 0.25	Pad dry cure process, 80 °C, 20 min	Amorphous SiO_2 network forming nanoscale roughness (SEM)	Superhydrophobic surface (WCA ≈ 155°); enhanced abrasion resistance	Reduced adhesion after repeated washing; sensitive to humidity during gelation	[127]
Vinyltrimethoxysilane (VTMS)/TEOS hybrid sol–gel on Ti substrates	VTMS:TEOS ≈ 1: 1	100 °C condensation followed by anneal at 150 °C (2 h)	Densely cross-linked siloxane network with 30–40 nm domains	↑ Hardness (+40%), ↑ adhesion to substrate, hydrophobic (θ ≈ 118°)	High temperature step limits use with soft PDMS substrates	[128]
MTMS/TEOS/ Diethoxydimethylsilane (DEDMS) cocondensed ORMOSIL	Typical TEOS: MTMS ≈ 2 1	Sol-gel + postbake at 120 °C	Homogeneous SiO_2 network (20–40 nm)	↑ Mechanical strength (Young's modulus ~ 5–6 GPa), ↑ hydrophobicity	Narrow formulation window; risk of cracking if thickness > 5 μm	[129]

whereas shorter CNTs typically require higher filler contents to achieve similar mechanical or electrical performance [147,148]. Hierarchical systems that combine CNTs with other tubular nanostructures, such as Au nanotubes, have also demonstrated improved stability under large deformations, thereby supporting the development of stretchable electronic platforms [149]. Therefore, 1D fillers maximize interfacial contact and directional transport, while simultaneously requiring careful dispersion control to avoid aggregation and ensure consistent behaviour within PDMS.

Two-dimensional fillers (2D), with AR < 1, introduce a distinct mode of interaction within PDMS composites. Lamellar nanomaterials, such as graphene [150], carbon nitride [151], hexagonal boron nitride (h-BN) or transition-metal dichalcogenides [152] present broad, planar interfaces that promote strong polymer–filler adhesion and enable in-plane phonon propagation across extended surface regions. Their sheet-like geometry favors the assembly of uneven but continuous networks, even when the incorporation method does not explicitly impose alignment. This behavior has been demonstrated in PDMS systems containing graphene- or BN-based aerogel frameworks, where the 2D scaffold acts as a large-area interfacial template that stabilizes the polymer matrix and enables efficient directional heat dissipation and load sharing. Within this morphological regime, graphene and related carbon-based sheets provide enhanced electrical conductivity and mechanical reinforcement, while also improving gas barrier properties and thermal stability by forcing diffusing species to traverse highly torturous paths [153]. Similarly, h-BN nanosheets contribute to high intrinsic thermal conductivity and ultraviolet shielding, improving the durability of PDMS-based coatings under photo-oxidative or environmental stress [154]. Graphitic carbon nitride (g-C_3N_4) nanosheets additionally introduce photocatalytic responsiveness when immobilized within PDMS matrices [151]. Transition metal dichalcogenides on PDMS enable flexible optoelectronic interfaces, leveraging their direct bandgaps and strong light–matter interactions for photodetection and energy harvesting [152]. Collectively, these 2D fillers operate through mechanistics dominated by interfacial area and surface continuity rather than by the point reinforcement typical of 0D fillers or the axial bridging characteristic of 1D structures, granting PDMS nanocomposites a multifunctionality unattainable with other geometries.

Thus, morphology selection, 0D for optical transparency and matrix stability, 1D for directional conductivity and mechanical reinforcement, 2D for photothermal response and barrier properties, must be guided by the balance between dispersion, interfacial interaction, and the intended multifunctionality of the composite. Whether a filler operates through interfacial scattering (0D), axial continuity (1D), or planar network formation (2D) defines not only how stress, heat or charge are transported through PDMS, but also the types of trade-offs that emerge when multiple properties are engineered simultaneously.

4. Effect of NPs on PDMS properties

4.1. Interfacial chemistry and property control in PDMS@NPs composites

The macroscopic performance of PDMS@NPs composites is governed by the chemistry and mechanics of the polymer–NP interphase. PDMS is apolar, flexible, and low-energy, whereas most inorganic fillers are polar, hydroxylated, or electronically delocalized. Thus, interfacial design is required to reconcile chemical mismatch and to tune functionality. Interfacial strategies fall into three classes: (i) strong covalent anchoring, for instance silanization and thiol-ene grafting, which maximizes stress transfer and reduces phonon scattering [155–157]; (ii) dynamic covalent or coordinative bonding, such as boronic esters, imine, disulfide and metal–ligand, which delivers intermediate strength with reversible rearrangement for toughness and self-healing [158–160]; and (iii) non-covalent interactions, such as van der Waals, π-π, hydrophobic and electrostatic, which favor chain mobility, particle sliding and network reconfiguration [161–165]. These regimes, either alone or combined, control mechanical, thermal, wetting, optical,

Table 4
Comparison of NP incorporation methods in PDMS.

Parameter	Addition of premade NPs in uncured PDMS	NPs synthesis in cured PDMS	*In situ* NPs synthesis in uncured PDMS	Ref.
Control over NP composition and size	High (pre-synthesis) but may change during mixing	Moderate; depends on reduction kinetics and surface activation	Moderate; nucleation/growth tied to PDMS chemistry; tuneable via precursors/catalysts	[90,103,116,138,139]
Dispersion quality	Dependent on the mixing method, improved by microfluidization or sonication	High surface uniformity; good coverage in foams and films	Often improved (particles nucleate in the matrix) but sensitive to cure conditions	[86,103,116]
Typical operating conditions reported	Solvent dispersion (ethanol), mixing, curing at ambient or elevated temperatures; some laser ablation methods avoid solvents	Surface activation (plasma, UV), immersion in metal salt solutions, chemical reduction	Sol-gel:PDMS:TEOS 15:1–5:1; particle concentration 5–15%; catalyst type (acidic/alkaline) influences size	[85,90,116,138]
Typical NP loadings	0.05–1.5 wt% for conductive fillers; up to 10–15 wt% for SiO_2 or porogens	Surface coverage tunable (0–70% in foams)	5–15% reported in solgel PDMS examples; controlled by precursor ratio	[84,94,103,116]
Advantages	Easy, modular, suitable for compositional screening	Excellent surface adhesion, good mechanical stability, ideal for flexible sensors	Better interfacial contact and one step processing options; tunable chemistry	[90,103,116,138,139]
Limitations	Aggregation, solvent residues, interfacial bonding issues	Requires surface activation, NP oxidation risk, scalability challenges	Coupled control of nucleation and cure; complex manipulation, possible byproducts altering PDMS	[86,116,138]

photoacoustic, and electrical properties.

Covalent anchoring of oxide or ceramic fillers, such as SiO_2 and TiO_2, to PDMS through silanes or sol–gel linkages leads to mechanical reinforcement due to the enhanced stiffness, effective bound-rubber fraction, and load transfer, besides improved mechanical performance and fatigue resistance [166,167]. This is more pronounced in polar oxide or ceramic NPs because strong chemical contacts suppress the interfacial debonding. Dynamic covalent or coordinative chemistries introduce sacrificial, rearrangeable bonds that are capable of energy dissipation and may allow for potential self-healing with much retention of the elastomeric compliance [168,169].

The thermal transport is constrained by phonon scattering at the polymer-NPs interface. Covalent bonding and intimate contact reduce the interfacial thermal resistance (Kapitza resistance) and, in turn, enhance heat conduction, especially in oxide or ceramic fillers [16,17]. Architectures using "hairy" filler surfaces or 3D continuous scaffolds can create percolating phonon channels and have been reported to yield substantial increases in thermal conductivity, in some cases several-fold over neat PDMS [170,171]. Poorly bonded or polymer-filled interfaces drastically reduce effective conductivity, demonstrating the critical importance of interfacial quality [172].

Surface wettability depends on interfacial chemistry and nanoscale roughness. Oxide NP coatings, silanization with low-energy tails, or hierarchical surface roughness enable tuning from hydrophilic to superhydrophobic surfaces, while dynamic or sacrificial interphases can impart self-healing or self-replenishing wetting states [82,173]. Covalent anchoring improves durability under abrasion without compromising optical transparency or elastomeric compliance [174,175].

Optical and plasmonic properties are sensitive to NPs chemistry/size and the interfacial design [176–178]. For transparent composites, low refractive-index contrast and surface coatings (core–shell silica or graded interphases) reduce scattering and preserve transmittance [179,180]. For plasmonic or photothermal NPs, sparse soft ligands favor near-field coupling and strong optical responses, while thick covalent shells stabilize dispersion and enhance device durability at the cost of reduced coupling [181–183].

Photoacoustic and photothermal generation couple optical absorption to fast thermal expansion [184,185]. Interface thickness and bonding type control heat transfer from absorbing NPs to the PDMS matrix, affecting acoustic amplitude and bandwidth. Thin covalent contacts or conductive bridges enhance conversion efficiency and high-frequency content, whereas polymeric ligand layers slow heat flow, lowering amplitude and broadening response [186–188].

Electrical performance is enhanced when interfaces preserve NPs connectivity and network rearrangement. Non-covalent embedding, soft ligands, or hierarchical filler networks facilitate high conductivity and strain-adaptive conduction in PDMS composites with carbon fillers or metal nanowires [189–191]. Covalent immobilization can improve contact stability and device lifetime but may reduce initial percolation efficiency [192,193].

In practice, the choice of interfacial strategy depends on both the chemical nature of the NPs and the desired property enhancement. Covalent anchoring enhances stiffness, thermal conduction, and overall mechanical integrity; dynamic covalent or coordinative bonds provide toughness, self-healing, and adaptable interphases; non-covalent or soft-ligand interfaces support electrical percolation, strain-adaptive conduction, and preservation of optical/plasmonic coupling. Hierarchical interphases combining a covalently anchored inner layer with a soft or dynamic outer layer often provide the best multifunctional performance. Table 5 summarizes common filler–interface combinations with reported property enhancements.

4.2. Mechanical and structural modifications

4.2.1. Fundamentals and mechanisms of mechanical performance in PDMS@NPs composites

PDMS is known for its high flexibility, optical transparency, biocompatibility and ease of processing. Nevertheless, is also characterized by low tensile strength, low hardness, and a modest elastic modulus resulting in an intrinsic mechanical weakness which limits its use in mechanically demanding applications [194]. These limitations are related with PDMS's molecular structure. The siloxane backbone is composed of repeating –Si–O–Si– units with pendant methyl groups. The low rotational energy barrier of the free siloxane gives high mobility to the polymer chains [195]. At the same time, the non-polar methyl groups minimize intermolecular forces such as hydrogen bonding or dipole–dipole interactions, leading to low chain–chain cohesion [196]. This combination results in a soft and extensible elastomer that cannot withstand extensive stresses or repeated mechanical cycling.

Addition of rigid nanofillers to the PDMS matrix restrains chain mobility, minimizes applied stresses and pore filling that otherwise act as sources of cracking. The effectiveness of the reinforcement is largely based on interfacial interaction in the form of covalent bonding, hydrogen bonding, or van der Waals forces that enhance adhesion and allow for effective transfer of stress [197,198]. For instance, uniform dispersion of nanodiamond or silicon nitride (Si_3N_4) resulted in clear increases in tensile modulus and strength [197], whereas functionalized nanodiamond exhibited even greater gains over untreated particles due to stronger interfacial bonding [198]. Poor dispersion, on the other hand, resulted in agglomeration, sheet fragmentation, and decreased reinforcement [199].

Thus, the mechanical fragility of PDMS can be optimally addressed by PDMS@NPs composites, which combine the elastomer's softness with the rigidity of nanofillers [197–204]. Similar reinforcement trends are reported in Fe@MWCNTs-based [205], GnF-based [206], and silane modified CNTs based [204] PDMS composites. In general, the maximum improvement was achieved where fillers were uniformly dispersed within the PDMS matrix, emphasizing the role of stable dispersion in mechanical reinforcement in PDMS. Fig. 6 provides a schematic overview of the main fabrication methods used in the preparation of PDMS@NPs composites (Fig. 6 A), the experimental configurations applied in mechanical characterization tests (Fig. 6 B), and a representative example of the typical stress strain behavior of these nanocomposites (Fig. 6 C (i, ii)).

4.2.2. Effects of PDMS@NPs composites on mechanical properties and applications

The addition of NPs to PDMS has proved experimentally the reinforcement mechanisms outlined above. Early experiments performed with multiwalled carbon nanotubes (MWCNTs) indicated that incremental addition to 7 wt% uniformly enhanced stiffness and Young's modulus [200–203], specifically addressing the low modulus inherent in pure PDMS. Subsequently, fillers such as boron nitride (BN), Si_3N_4, and nanodiamond have been found to increase tensile strength [197]. This becomes particularly pertinent when considering the effect of surface chemistry on filler performance. At 8 wt%, SiO_2 NPs increased tensile strength by approximately 80% and hardness to 8.34 kgf/mm^2, whereas TiO_2 NPs produced only a 20% strength improvement, accompanied by lower hardness (6.58 kgf/mm^2) and reduced ductility [167]. The better performance of SiO_2 results from its particle size and the presence of surface silanol groups to form hydrogen bonds with the PDMS matrix [167]. Hybrid filler systems can show synergistic behavior. For instance, a filler containing a combination of SiO_2 and ZnO NPs (2.5 wt% each) has shown the tensile strength of 16.5 MPa, elongation of 77%, and the modulus of 14 MPa, better than in single-filler systems [208]. Analogously, TiO_2 NPs supported on mesoporous silica (MCM-41) enhanced the modulus and strength and elongation at 10 wt%, while higher loadings resulted in agglomeration and decreased reinforcement efficiency [209].

Particle size also performs a highly significant role in mechanical properties. 15 wt% of nano-Al_2O_3 outperformed micro Al_2O_3 with a modulus of 2.45 MPa, tensile strength of 0.89 MPa, elongation of 260%, and Shore A hardness of 22.4. These improvements were due to enhanced interfacial interactions and the ability of NPs to fill microdefects, thus increasing matrix homogeneity [210].

Processing methods also strongly affect PDMS@NPs composites performance. Graphite nanoflakes (GnF)-reinforced PDMS has shown improved elastic modulus and strength up to a maximum of ~ 7.6 vol% filler, with spray lay-up outperforming solvent casting and hand lay-up through reduced porosity, bubble entrapment and residual solvent, resulting in a more homogeneous deposition (modulus 0.6 MPa, strength 1.96 MPa) [207].

Other than mechanical strengthening directly, nanofillers and structural modification can improve the durability of PDMS, with enhanced resistance to cyclic fatigue, frictional wear, and long term degradation [211]. To investigate the role of microstructure in PDMS composites with multi-walled carbon nanotubes (MWCNTs), two materials containing 4 wt% nanotubes were prepared by different methods: conventional mixing and processing via Coaxial Biaxial Extensional Rheometer (CBER). Electronic microscopy images revealed that the conventional method promotes agglomeration, while CBER produces a more refined and uniformly dispersed network. This structural difference results in higher reinforcement efficiency and more stable mechanical behavior in the CBER composite. The formation of agglomerates in conventional mixing reduces the effectiveness of reinforcement, as it limits the interaction between MWCNTs and the PDMS matrix, contributing to the loss of performance under mechanical loading. The composite obtained by CBER maintains a stable response under cyclic tension, withstanding 2000 cycles at 30% deformation, which enables its application in high-sensitivity wearable sensors for monitoring human movements (fingers, wrist, knee and swallowing) and in smart exoskeletons aimed at ergonomic support and injury prevention [211] become possible (Fig. 7 A). Similarly, ultra-soft PDMS composites filled with black carbon and dimethyl silicone oil exhibited low modulus (2.3–12 kPa), high elongation (~1500%), and rapid elastic recovery, with electrical stability maintained over 100,000 cycles at 100% strain [212] (Fig. 7 B).

Dynamic covalent networks also improve long term stability. Silyl ether cross linked PDMS has shown good tensile strength (~11 MPa), thermal stability ($T_5 \approx 322\,^{\circ}C$), and reprocessability (78% recovery after repeated cutting). Incorporation of 5–20 wt% MWCNTs improved strength without compromising structural integrity, where 15 wt% is an optimal composition for mechanical and electrical performance and resistance to handling under repeated loads (Fig. 7 C) [213]. Besides, surface wear can be prevented by structural design. Direct ink writing (DIW) printed PDMS@NPs composites incorporating nanometric SiO_2 were engineered with textured surfaces that reduced the coefficient of friction (COF) by 32.9%, trapped debris, and preserved structural integrity when subjected to ball on disc testing, with applications in wearable devices and soft robotics (Fig. 7 D) [214].

Reinforcement with advanced nanofillers like metal–organic frameworks (MOFs) and CNTs also yields exceptional performance. The covalent anchoring of methoxysilane-grafted UiO-66- (UiO-66-MS, a Zr-based MOF derived from UiO-66-NH_2) to the PDMS matrix results in a 2.8-fold increase in tensile strength and enhances fracture toughness from 0.655 to 1.013 MJ·m^{-3} [215]. The study shows that the stability of the composite is determined by the interface: unmodified particles (UiO-66-NH_2) aggregate and form voids, impairing stress transfer and reducing CO_2/N_2 selectivity, while the Si–O–Si bond resulting from the silanic treatment ensures homogeneous dispersion and avoids such degradation mechanisms. This difference is confirmed in continuous operation, where

Table 5
Summary of representative PDMS@NPs composite fillers, interfacial strategies, and the corresponding target properties. Covalent, dynamic covalent/coordination, and non-covalent approaches are highlighted for mechanical, thermal, electrical, optical, and wetting functionalities.

Filler type	Recommended interface	Target property
Oxide/Ceramic	Covalent anchoring (silanes, sol–gel)	Mechanical reinforcement, fatigue resistance, thermal conduction
Dynamic/Reversible fillers	Dynamic covalent or coordinative bonds (boronic esters, imine, metal–ligand)	Toughness, self-healing, adaptable interphase
Carbon/Metal nanowires	Non-covalent interactions, soft ligands, or hierarchical networks	Electrical conductivity, piezoresistive behaviour, stretchable sensors
Thermal fillers	Covalent bonding or conductive bridges	Enhanced thermal conductivity, phonon transport
Optical/Plasmonic NPs	Soft ligand shells, sparse coverage; or graded/core–shell for transparency	Plasmonic coupling, optical transmittance, photothermal/photoacoustic response
Surface-functional/Oxide NPs	Silanization, hierarchical roughness, dynamic layers	Tunable wettability, superhydrophobicity, self-healing surfaces

membranes with UiO-66-MS maintain stable permeability and selectivity for 100 h under 2–4 bar, whereas formulations without modification suffer progressive deterioration due to interfacial instability [215]. The incorporation of 10 wt% functionalized CNTs (OHCNT) into the PDMS@(OHCNT) dual-network (Fe^{3+}–Py/boronic-ester) double reversible network (Fig. 8 A (iii)) results in a mechanically robust and highly self-healing composite, as evidenced in Fig. 8 B (i). In this condition, the material has a toughness of ~ 7.2 $MJ{\cdot}m^{-3}$, elongation at break of ~ 882% and yield stress of ~ 1.1 MPa, recovering most of these properties after 12 h at 70 °C or approximately 40 s under near infrared (NIR) photothermal activation. This performance emerges from the cooperation between weak dynamic interactions, such as the boronic ester bonds (Fig. 8 A (i)), and the Fe^{3+}–pyridine coordination bonds, which provide support to mechanical strength (Fig. 8 A (ii)), together with PDMS/OHCNT interfacial interactions, responsible for energy dissipation and network reorganization. A moderate CNT content preserves the segmental mobility required for healing, while higher concentrations

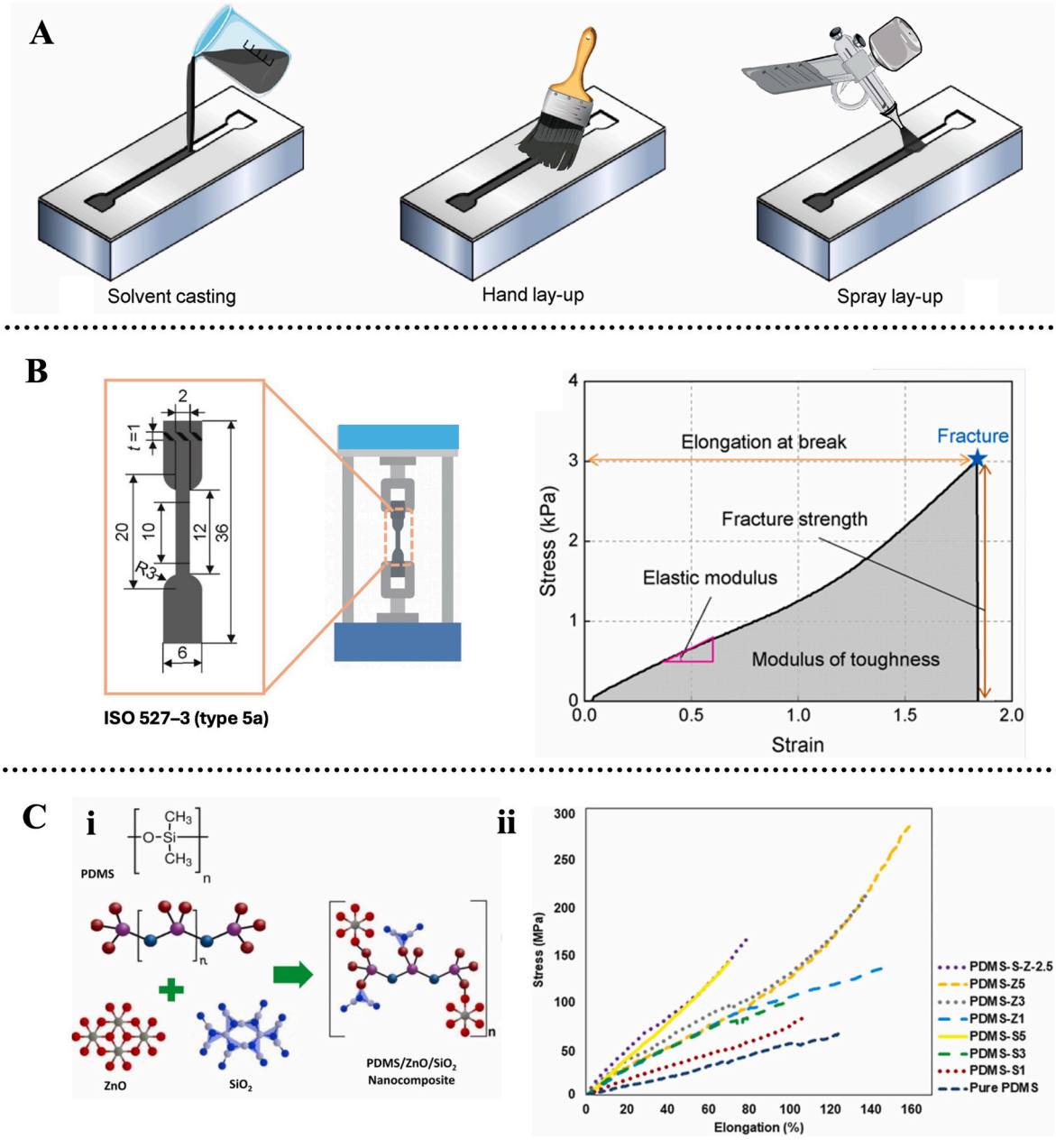

Fig. 6. Schematic representation of the fabrication processes, experimental configuration, and mechanical performance of PDMS-based nanocomposites. (A) Different fabrication methods for the specimens: solvent casting, hand lay-up, and spray lay-up [207]. (B) Schematic of the tensile testing setup and representative stress strain curve commonly used to illustrate the mechanical behavior of PDMS nanocomposites [207]. (C) (i) Schematic structure of the PDMS@ZnO/SiO_2 nanocomposite exhibiting enhanced mechanical and anti-corrosion properties; (ii) Typical stress strain curves of different specimens, highlighting the reinforcing effect of NPs [208].

increase the stress relaxation time and reduce the efficiency of the self-repair process (Fig. 8 B (ii, iii)). The scheme in Fig. 8 B (iv) summarizes this behavior, showing localized disruption followed by dynamic recombination of supramolecular interactions [216].

Self-repair plays an essential role in the durability of these nanocomposites, and the PDMS-COOH–Fe_3O_4 system features a distinct mechanism, governed by a dynamic supramolecular architecture, based solely on reversible hydrogen bonds between the carboxylic groups of the PDMS (Fig. 9 A). This network allows spontaneous structural reorganization at room temperature, resulting in

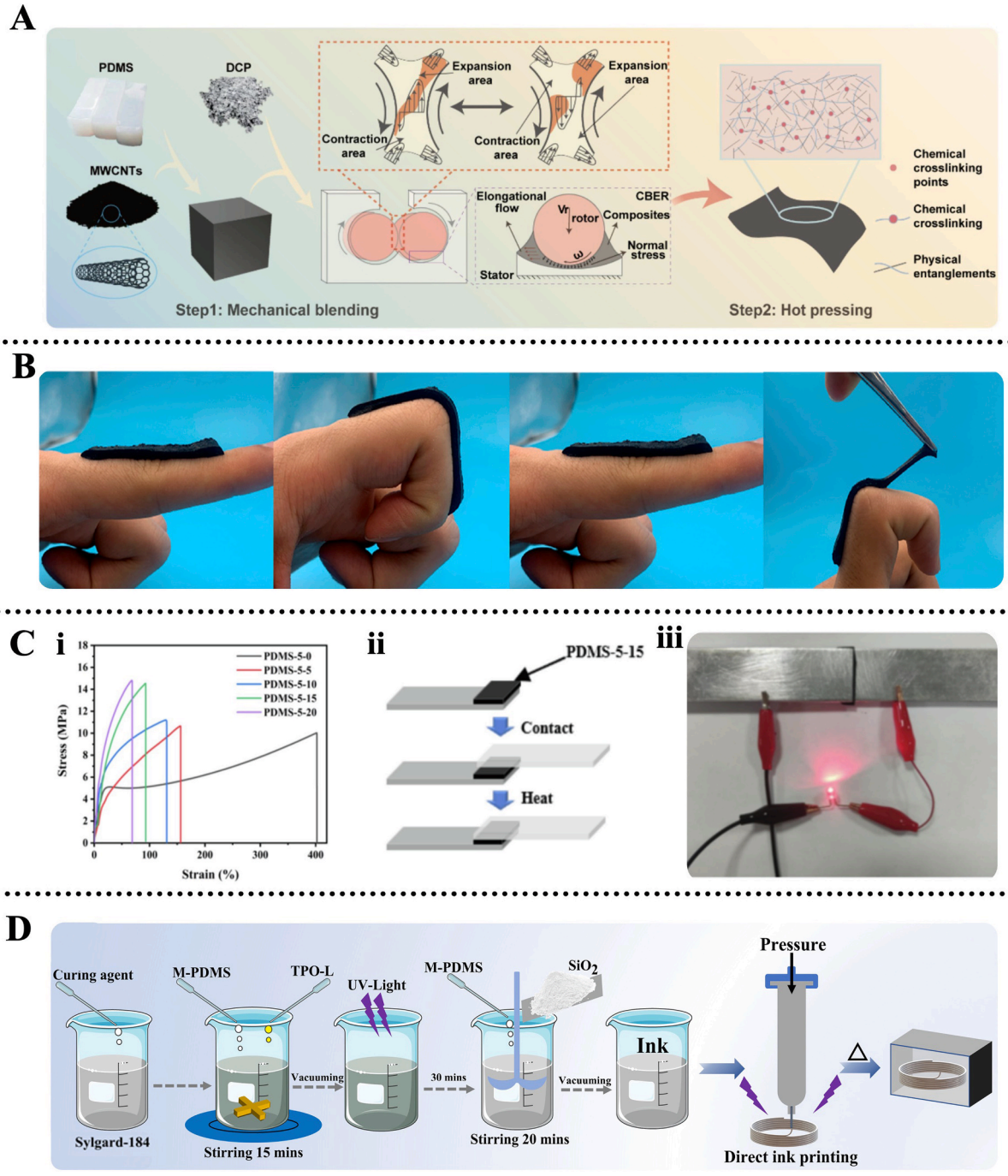

Fig. 7. (A) Schematic illustration of the preparation process of PDMS@MWCNTs composites involving mechanical blending and hot pressing. Adapted from [211]. (B) Demonstration of the performance of PDMS@silk fibroin (SF), showing superior softness, high elasticity, and self-adhesive behavior under deformation on finger skin. Adapted from [212]. (C) (i) Typical stress–strain curves of PDMS composites; (ii) schematic of test specimen preparation; (iii) digital image showing the electrical circuit of an adhered sample. Adapted from [213]. (D) Schematic illustration of the DIW process used for fabricating PDMS@SiO_2-based composite inks. Adapted from [214].

progressive mechanical recovery: the composite with 15 wt% of Fe_3O_4 restored 62.2% of the resistance in 30 min, reaching up to 97.7% after 8 h (Fig. 9 B (i–iv)). The magnetic response is also preserved after repeated damage–healing cycles (Fig. 9 B (v)). Among the evaluated compositions, 15 wt% Fe_3O_4 provided the most balanced combination of reinforcement, extensibility and healing performance, without compromising recovery after failure [217].

Thus, the two systems represent complementary approaches to overcome the traditional trade-off between mechanical strength and repairability in PDMS elastomers. While the Fe–Py–PDMS/PDMS–FBA system exploits the synergy between strong and dynamic bonds, enabling ultra-fast, light-activated curing, the PDMS-COOH–Fe_3O_4 system demonstrates efficient self-healing at room temperature with simpler molecular architecture governed solely by hydrogen bonds.

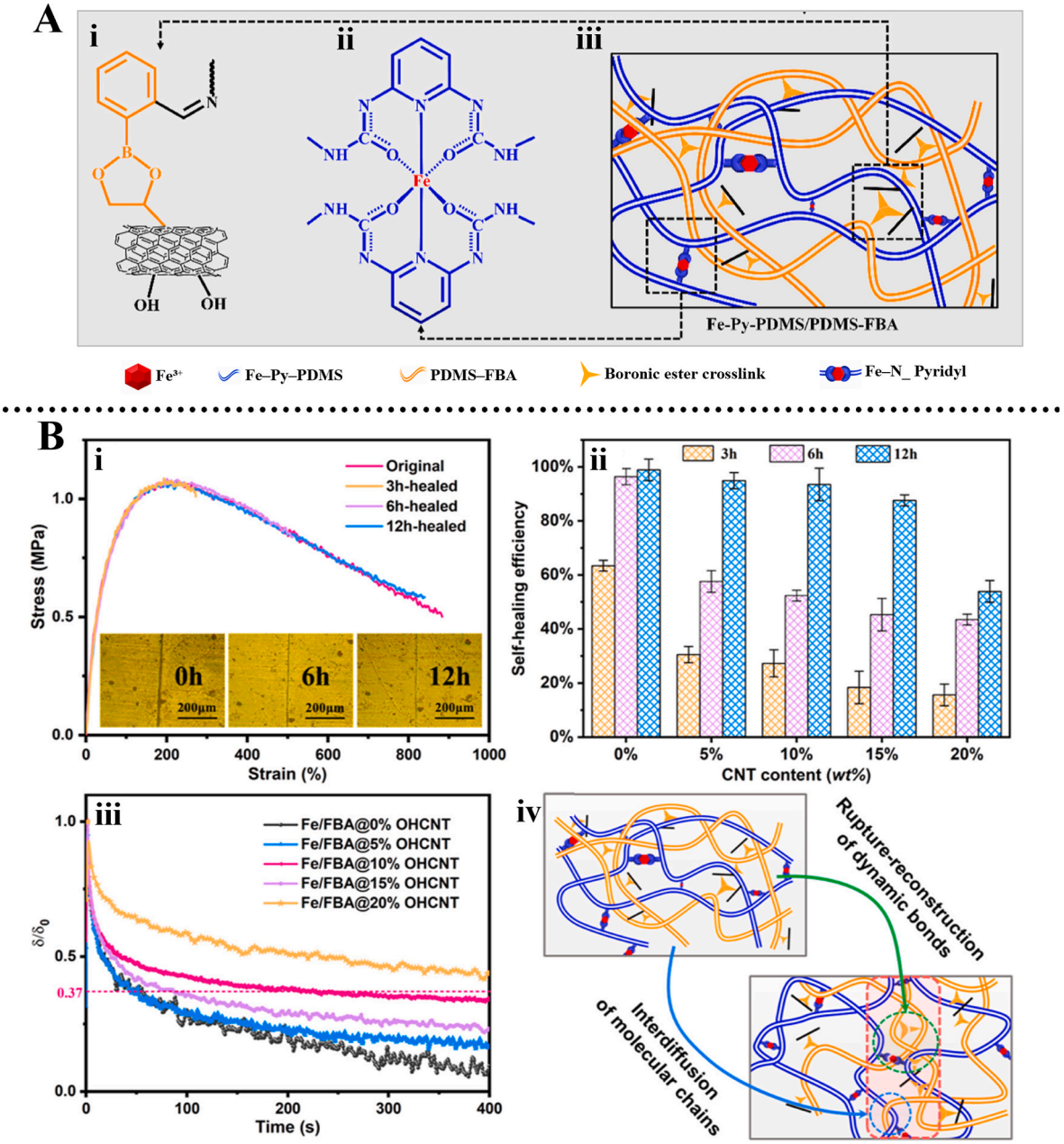

Fig. 8. (A) Scheme of the PDMS@(OHCNT) dual-network (Fe^{3+}–Py/boronic-ester) (A) Reversible dual network (i) Formation of dynamic boronic ester bonds between PDMS–FBA and functionalized OHCNTs. (II) Fe^{3+}–pyridine coordination complex. (iii) Resulting hybrid network (PDMS@(OHCNT) dual-network (Fe^{3+}–Py/boronic-ester). (B) (i) Stress–strain curves and optical microscopy images of the Fe/FBA@10% OHCNT elastomer before fracture and after healing at 70 °C. (ii) Self-healing efficiency of Fe/FBA@x% OHCNT samples after different healing times. (iii) Normalized stress-relaxation experiments for Fe/FBA@x% OHCNT. (iv) Schematic illustration of the self-healing mechanism.
Adapted from [216].

4.2.3. Durability, challenges, and future directions

The development of PDMS@NPs composites has evolved from early studies primarily focused on mechanical reinforcement through the simple incorporation of NPs [199] toward more advanced strategies emphasizing multifunctionality, durability, and application-oriented performance [212–215,217]. Research has moved into the analysis of interfacial engineering surface functionalization, particle size control, and the use of hybrid fillers to optimize stress transfer and reduce NPs agglomeration [197,199]. For instance, silanized nanodiamonds result in better mechanical enhancement than the unsilanized ones due to better interfacial adhesion [198], whereas SiO_2/ZnO hybrid fillers show a synergistic effect with an increased modulus and strength combined with good ductility [208]. The most important development has been the integration of multifunctional capabilities other than mechanical reinforcement. State of the art PDMS@NPs composites incorporate electrical conductivity (e.g., CNT networks for strain sensing [216]), magnetic actuation (e.g., Fe_3O_4 for soft robotics) and autonomous self-healing, often validated by cyclic fatigue testing and application focused simulations [217].

Despite these advances, several challenges make large scale application difficult. Firstly, more tests are needed under real conditions, including exposure to humidity, temperature variations and extended mechanical cycles, the reports of experiments are still

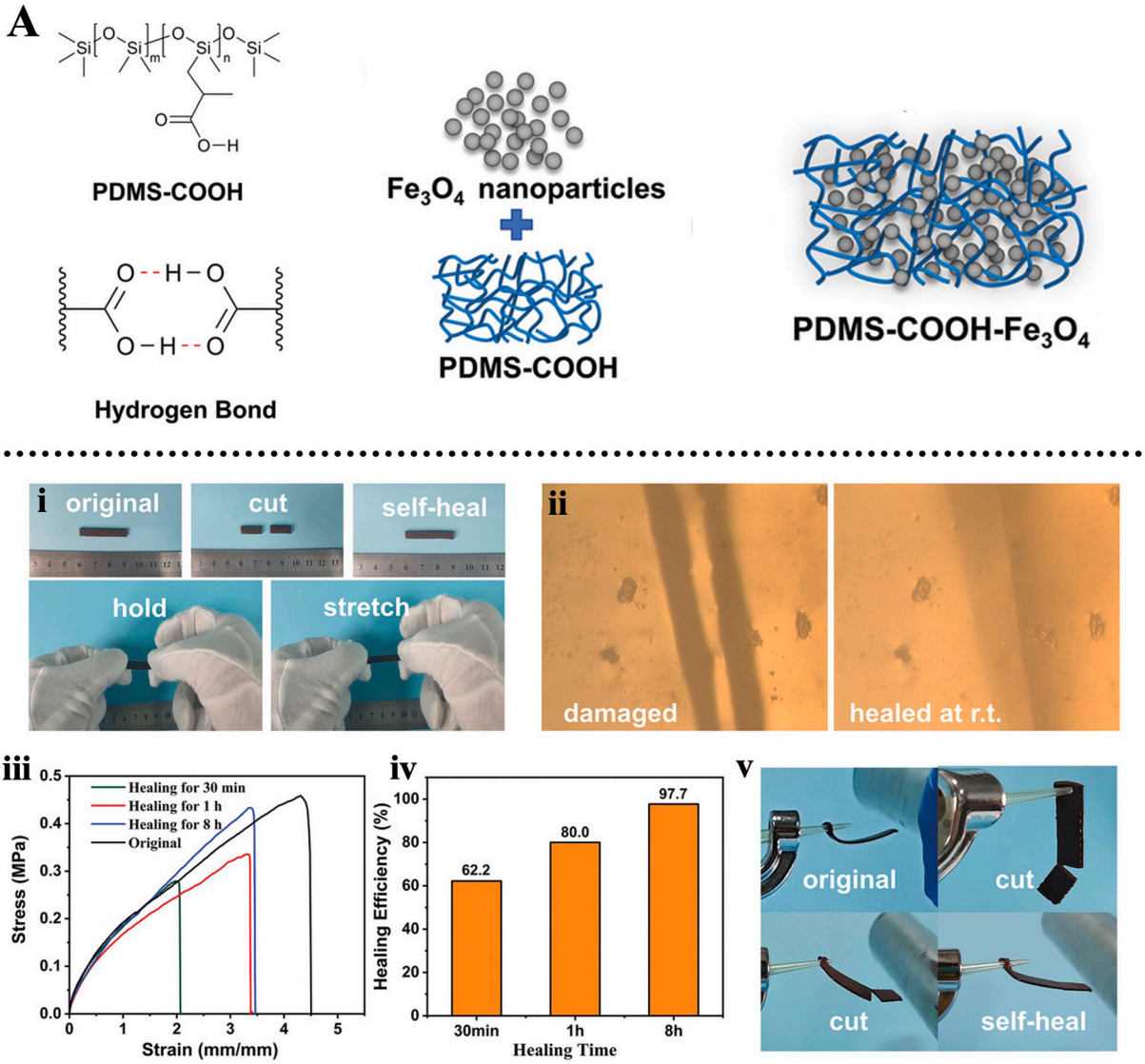

Fig. 9. (A) PDMS-COOH–Fe_3O_4 composite formation: PDMS functionalized with carboxylic groups forms reversible hydrogen bonds and allows the physical incorporation of Fe_3O_4 NPs into the network. (B) (i) Complete self-healing process of the PDMS-COOH-Fe_3O_4 (15%) film under ambient conditions. (ii) Optical microscopy images of the scratched sample and its healed state after 8 h at room temperature. (iii) Tensile tests of the cut and self-healed film at 25 °C. (iv) Self-healing efficiency. (v) Demonstration of self-healing of the polymer film (30 × 6 × 0.9 mm) under ambient conditions during magnetic actuation.
Adapted from [217].

optimized for idealized laboratory environments. Furthermore, high NPs loadings, although increasing stiffness, often induce agglomeration, reducing the effective interfacial area, favoring the formation of structural defects such as crack propagation and compromising mechanical, electrical, and optical properties, as well as hindering the processing of the material [199,204–206]. Also, scalability and sustainability are still an underexplored topic. Many high performance composites rely on synthesis methods that, although described as simple at the laboratory level, involve multiple steps and long processing times, as in the case of the functionalization of CNTs or the incorporation of MOFs [215,216]. These characteristics represent significant obstacles to scalability and to the transition from laboratory-scale fabrication to large-scale production. In addition, the environmental impact of NPs synthesis and the recyclability of PDMS elastomers at the end of their service life are rarely addressed in the literature. Together, these factors underscore the need for new strategies before PDMS@NPs composites can achieve widespread practical application.

Future research should focus on process simplification through dispersion techniques that allow for greater scalability, validation of robustness through material exposure to extreme conditions, and an integrated approach to material design that would balance, in a single step, mechanical resilience, multifunctionality (electrical, magnetic, sensory), and sustainability (e.g., biobased fillers, recyclable matrices). Achieving this balance will be critical to the transition of PDMS@NPs composites laboratory applications to reliable components in next generation technologies, including implantable biomedical devices, flexible electronics, and adaptive soft robots.

As summarized in Table 6, representative PDMS@NPs composites demonstrate how the NPs filler characteristics (type, size, concentration, and alignment) govern the mechanical behavior of the resulting PDMS composites, offering insights into their tunability for specific application requirements.

4.3. Thermal conductivity

4.3.1. Fundamentals and mechanisms of thermal transport in PDMS@NPs composites

PDMS is a low thermal conductivity polymer, whose representative values vary between 0.12–0.35 W/mK [70]. Heat transport occurs primarily via phonons, which are strongly scattered by the amorphous nature of the polymer. This limits directional conduction of heat and renders PDMS inherently insulating. Enhancement of thermal conductivity through the incorporation of NPs is a field of interest to thermal interface materials, wearable electronics, microchip cooling, and self-powered sensors, without sacrificing PDMS's flexibility and processability [218].

The degree of thermal improvement relies on the maximum filler loading in the PDMS matrix, which is widely dependent on NPs type and properties. Saturation values vary between as low as 4.4 vol% for carbon black to more than 50 vol% for silicon carbide (SiC) [219,220]. Surface area and porosity of NPs are particularly critical. For instance, NPs fillers with surface areas below 3.0 m^2/g and porosity below 0.003 cm^3/g favor efficient packing and continuous thermal pathways, while irregular pores trap polymer and hinder heat transfer [220]. The particle morphology presents a non-linearity regarding the enhancement of thermal properties: while it is possible to assert that large, irregularly shaped particles may yield superior results, specifically by facilitating phonon transport through the reduction of inter-particle interfaces, which introduce thermal contact resistance [219], spherical or near-spherical particles enable higher particle packing density, allowing for a denser composite and, consequently, enhanced thermal properties [220].

Interfacial thermal resistance at the filler–matrix interface is another controlling parameter, one employed strategy involves the use of coupling agent structures, such as aminosilane coupling agents (ATS, e.g., 3-aminopropyltrialkoxysilanes). These agents contain both hydrophobic and hydrophilic regions, facilitating bonding to hydrophobic PDMS and hydrophilic metals, while simultaneously enabling better dispersion within the material [221]. An alternative strategy is the decoration of particles with metallic NPs. This approach increases the specific surface area and creates bridges that expand the particle–matrix contact area. This is particularly effective for inert materials, such as Al_2O_3, as it facilitates bonding to the polymeric chain via van der Waals forces and hydrogen bonds, and improves particle–particle contact [222].

Predictive models have been widely employed to explain thermal conductivity in PDMS@NPs composites. The classical Maxwell's model of 1873 [223] addresses two-phase heterogenic solids with randomly distributed NPs and volume fractions between 10–50 wt%, but not particle shape or dispersion [218,224].

$$k_{eff} = k_m \cdot \frac{2k_m + k_p - 2\varphi(k_m - k_p)}{2k_m + k_p + \varphi(k_m - k_p)}$$

In equation 1, k_{eff} is the thermal conductivity of the composite, k_m is the thermal conductivity of the matrix, k_p is the thermal conductivity of the particle and φ are the volume fraction of the particles.

The Maxwell model is too simplistic and ignores several mixture parameters that affect the result. Refinements such as the Cheng–Vachon model of 1969 [225] and Okamoto–Ishida model [226] attempt to consider particle shape and dispersion. Other models of equations have been used, as shown in Table 7, in the attempt to help the prediction of the thermal properties. However, there are still significant deviations between experiments and predictions, especially at high concentrations or with oriented fillers [220]. The ideal contact between matrix and particles is considered in the effective medium theory (EMT), while particle–particle contact resistance is measured in the Foygel model [70,222].

Despite of analytical models fail as they cannot estimate, for instance, in structured or highly filled composites, tools involving Finite Element Methods have been reported for the verification of preferential heat paths, in which Liu et al. [222], for example, verified the greater heat flux caused by the addition of Ag NPs on the surfaces of BN flakes, since it was verified that the silver acted as a connecting agent for the particles. In another work, it was verified that NPs dispersed in a random manner encounter greater difficulty

since they are isolated by the PDMS matrix and that, when the particles are in a chain, the heat is better dissipated [218].

Due to the major limitations regarding especially the interaction of the different materials involved in the composite, these simulations ultimately provide a more qualitative analysis with limited results. Simulations by Molecular Dynamics, in turn, present a higher degree of complexity; Wang et al. [239] simulated the influence on the thermal conductivity of PDMS@molybdenum disulfide

Table 6
Representative PDMS@NPs composites for mechanical properties control, summarizing NPs filler characteristics (type, size, concentration, and alignment), their effects on PDMS properties, targeted applications, associated challenges and prospects and other relevant data.

Filler characteristics	Mechanical properties	Effects of NPs on PDMS properties	Applications	Challenges and prospects	Other data	Ref.
TiO_2 (~24 nm, 10 wt %) and SiO_2 (~11 nm, 8 wt%)	Higher hardness, elastic modulus and tensile strength; elongation maintained	Reinforcement without ductility loss; physical and chemical interaction with matrix	Insulating coatings for electrical applications	Agglomeration > 8–10 wt%; limited interaction between matrix and fillers	Contact angle ~ 93°; adhesion 4A; TiO_2 anatase, SiO_2 amorphous	[167]
ZnO (10–30 nm, 2.5 wt %) + SiO_2 (20–35 nm, 2.5 wt %)	Higher tensile strength and Young's modulus, increased stiffness; lower elongation	Mechanical reinforcement, better dispersion in the combination	Anticorrosion steel coatings	Aggregation > 5 wt%; need for long-term tests	Contact angle up to 120°; corrosion current 2×10^{-6} A/cm^2; potential − 0.55 V	[208]
GnF (~15 wt%; random alignment)	Higher modulus and strength at low loadings; drop at high; reduced elongation	Properties affected by process induced porosity; effective reinforcement up to optimal point Sensors, paint on coatings	Sensors, paint on coatings	Porosity; optimize spray lay-up	Surface roughness depends on process (spray, molding, brushing)	[207]
MWCNTs (4 wt%; refined dispersion via elongational flow field)	Good strength; flexible; high cyclic stability	Refined/ reconstructable conductive network; high sensitivity; wide strain detection range	Strain sensors for human motion monitoring and exoskeletons	Prevent aggregation at higher loadings (≥5 wt%); industrial scalability needed	Stable > 2000 cycles; GF up to 1151 (100–200% strain); MWCNTs: 9.5 nm × 1.5 μm	[211]
Carbon black + dimethyl silicone oil (0–50%; homogeneous dispersion)	Ultrasoft; highly stretchable; fast recovery; cyclic stability	Super softness; lubricating effect; self-adhesion (dry/ wet); stable electrical response	Motion sensors; flexible electronics; biomedical adhesives	Conductivity decreases with higher oil; optimization and scalability needed	Strong adhesion on glass, metal, biological tissues	[212]
Silyl ether linkages; MWCNTs (optimal ~ 15 wt %; 0–20 wt%)	Higher strength; good recovery	Thermal stability; hydrolysis resistance; electrical conductivity	Reprocessable elastomers; reusable conductive adhesives	Control of crosslink density; NP dispersion; scalability	High conductivity; reusable adhesion; MWCNTs: 10–20 nm × 5–30 μm	[213]
SiO_2 (~20 nm; 1:8–1:32; homogeneous dispersion; DIW printing at 0°, 60°, 90°)	COF reduction 32.9% (60°); lower wear	Adjusted rheology; textured surfaces reduce contact area	Flexible wearable devices; component protection	DIW scalability; tests under real use conditions	Contact angle ~ 99° (60°);	[214]
UiO-66-MS (UiO-66-NH_2 modified with methoxysilane; 40 wt%; homogeneous disp.)	Higher tensile strength; higher toughness	Improved interfacial compatibility; higher CO_2/N_2 selectivity; higher CO_2 permeability	CO_2/N_2 separation membranes	Scalability at high loadings; permeability–selectivity balance	100–200 nm; stable for 100 h	[215]
CNTs (dopamine-modified; 10 wt%; homogeneous dispersion)	Higher tensile strength; higher toughness	Mechanical reinforcement; ultrafast self-healing	Flexible electronics, anti-icing/deicing	Dispersion issues > 10 wt%; scalability	~9.5 nm dia.; ~1.5 μm length	[216]
Fe_3O_4 (20 nm; 15 wt%)	Higher tensile strength and toughness, high elongation, self-healing	Mechanical enhancement self-healing; magnetic response	Potential: magnetic actuators, soft robots, artificial muscles	Aggregation > 20%;	Glass transition 0.5 °C; thermal Decomposition 220 °C; Magnetization 35.9 emu/g	[217]

(MoS_2) and PDMS@boron nitride (BN/)MoS_2 composites simulated using reverse non-equilibrium molecular dynamics (RNEMD) in a simulation at the atomic level. Through the simulation, it was possible to observe factors of great relevance in the final thermal properties of the composite, such as the existence of voids in the PDMS@MoS_2 that were eliminated by the composites with the hybrid BN/MoS_2, in addition to the ideal concentrations of fillers in the matrix.

As seen, both the equations and the simulations highlight the importance of particle distribution and interfacial engineering, and it becomes clear that the way the NPs are distributed plays a fundamental role in improving thermal conductivity, since, as shown in Fig. 10, depending on the type of distribution, heat flow can be facilitated in systems that promote contact between the particles.

4.3.2. *Effects of PDMS@NPs composites on thermal properties and applications*

The incorporation of NPs into PDMS has yielded significant improvements in thermal transport, with results very dependent on the filler type, dispersion method, and composite architecture. Although random dispersion remains the most common practice (due to simplicity and cost), it only provides moderate improvements. For instance, boron nitride (BN) NPs (< 1 μm) achieved 0.29 W/mK at 6.6 vol% [219], while larger particles provided improved performance. Cu microparticles (45 μm) were up to 0.75 W/mK and Al microparticles (24.7 μm) were up to 1.20 W/mK for higher loadings [220]. These findings indicate the advantage of employing larger fillers in forming continuous thermal pathways.

In situ decoration of microparticles with NPs also offers a way to further enhance by reducing interfacial voids and improving particle matrix bonding. Huang et al. [240] decorated Al_2O_3 microparticles using Ag NPs, as shown in Fig. 10 A, increasing thermal conductivity from 0.54 W/mK to 0.67 W/mK. Later, Zhao et al. [241] demonstrated that h-BN (30 μm) decorated with Ag and Cu NPs (Fig. 10 B) achieved 1.56 W/mK at 25 vol%, whereas undecorated h-BN achieved 0.897 W/mK, highlighting the effectiveness of interface engineering. Moreover, external alignment methods (such as electric or magnetic fields) create anisotropic conductive networks. Gao et al. [218] observed conductivity increasing from 0.22 W/mK (random) to 0.31 W/mK when Ba–Ca–Ti–Zr oxide/copper nanorods were aligned by an AC field (Fig. 11 C). Hybrid filler systems also promote percolation: blends of BN flakes (5 μm) and Al_2O_3 spheres (800 nm) achieved 0.228 W/mK at 20 wt%, improving on composites with a single filler (Fig. 11 D) [242].

One of the most efficient alignment strategies is the creation of a 3D porous structure, known as a skeleton, which allows combining the particle alignment found in particles aligned by magnetic or electric fields, as previously seen, as well as the isotropic characteristics of random dispersion. BN@AgNP/rGO skeletons were reported to reach 2.34 W/mK at only 8 wt% [222], while expanded graphite skeletons achieved conductivities as high as 10.45 W/mK at 23.8 wt% [70]. These interconnected network architectures possess uninterrupted heat paths that surpass random or aligned dispersions. The potential of PDMS@NPs composites is further

Table 7
Equation models for prediction of the thermal conductivity of PDMS@NPs composites and their respective characteristics.

Model	Equation		Applied by	Observation
Cheng–Vachon[225] corrected by Okamoto–Ishida model [226]	$\frac{1}{k}=\frac{1}{\left\{4\left(\frac{3}{2}\varphi\right)^{-1/2}(k_p-k_m)\left[k_m+\left(\frac{3}{2}\varphi\right)^{1/2}(k_p-k_m)\right]\right\}^{1/2}}\times \ln\left[\frac{\left[k_m+\left(\frac{3}{2}\varphi\right)^{1/2}(k_p-k_m)\right]^{1/2}+\frac{1}{2}\left(\frac{3}{2}\varphi\right)^{1/2}\left[4\left(\frac{3}{2}\varphi\right)^{-1/2}(k_p-k_m)\right]^{1/2}}{\left[k_m+\left(\frac{3}{2}\varphi\right)^{1/2}(k_p-k_m)\right]^{1/2}-\frac{1}{2}\left(\frac{3}{2}\varphi\right)^{1/2}\left[4\left(\frac{3}{2}\varphi\right)^{-1/2}(k_p-k_m)\right]^{1/2}}\right]+\frac{1-\left(\frac{3}{2}\varphi\right)^{1/2}}{k_m}$	(2)	Various materials [220]	Attempt to consider particle shape and dispersion. Significant deviations at high concentrations or with oriented fillers
Maxwell-Eucken [227]	$k^{HS-}=k_m(2k_m+k_p-2V_f(k_m-k_p))/(2k_m+k_p+2\varphi(k_m-k_p))k^{HS+}=k_p(2k_p+k_m-2(1-V_f)(k_p-k_m))/(2k_p+k_m+(1-\varphi)(k_p-k_m))$	(3)	Au [228] GF/h-Fe_3O_4 [229] Ag [230]	Does not consider the formation of chains of particles
Hamilton-Crosser [231]	$k=k_m\left[\frac{k_p+(n-1)k_m+(n-1)\varphi(k_p-k_m)}{k_p+(n-1)k_m-\varphi(k_p-k_m)}\right]$	(4)	Al_2O_3 [232] TiN [233]	Modifying the Maxwell model to support non-spherical inclusions
Y. Agari [234,235]	$k=kp^{(C_2\varphi)}(C_1km)^{(1-\varphi)}$	(5)	Al_2O_3 [236]	Crystallinity, crystal size and formation of conductive networks taken into consideration
Hatta [237]	$k=[1+(\varphi)/(S(1-\varphi)+(k_m)/(k_p-k_m)))]k_m$	(6)	Ni [238]	Does not consider the formation of chains of particles

In equations 2 to 6 φ is the volume fraction of filler particles in the binder; $HS-$ is lower bound equation; $HS+$ is upper bound equation,n is related to the thermally conductive filler sphericity; $C1$ is the factor affecting the crystal size and the crystallinity; $C2$ is a factor of forming thermally conductive networks; S varies as a function of the direction and of the size of the filling.

demonstrated in practical applications. Cu NPs sponges functionalized with PDMS@GO exhibited improved conductivity from 0.52 to 1.38 W/mK via two networks of conduction (Fig. 11 E) [243]. Yan et al. [244] similarly functionalized carbon fibers using carboxyl groups (–COOH) in order to facilitate ZIF-67 crystal growth, which upon pyrolysis worked as catalysts for the formation of carbon nanotubes (CNTs) with encapsulated Co NPs. The CNTs formed connections between the fibers, enhancing the material's thermal conductivity by reducing the thermal resistance at interfaces (Fig. 11 F) creating a thermal pathway for the heat, up to 1.08 W/mK, 300% higher than in the untreated fibers case. Such hybrid systems are significantly promising for thermal interface materials, microchip cooling, flexible electronics, and microfluidic devices.

4.3.3. Durability, challenges, and future directions

PDMS is a material with high stability of its properties and, even in aging processes at temperatures of up to 175 °C, ultimately improve and stabilize its thermal properties [245]. The use of NPs in principle tends to improve thermal stability due particles hinder the movement of the Si-O chains of the PDMS matrix, presenting an significatively increase in the degradation temperature [49]. In more specific situations, In more specific situations, such as the PMDS composite with carbon felt and ACNTS studied by Yan et al. [244], the material was submitted to 10 thermal cycles between room temperature and 100 °C, and a decrease in thermal conductivity was observed with a slight reduction of 0.259 W/mK (in-plane) and of only 0.048 W/mK (out-of-plane), probably caused by minor damage due to temperature variations. Results regarding mechanical and magnetic properties after 1000 bending cycles remained satisfactory.

Even though thermal conductivity improvements are significant, several drawbacks must be considered. For instance, NPs addition eliminates PDMS intrinsic transparency. Complex methods such as field alignment or skeleton fabrication introduce scalability and processing challenges being harder to perform *in situ*. Alignment also induces anisotropy, constraining applications where isotropy must be maintained. Another concern is the durability of filler matrix interfaces under thermal cycling; mismatches in elastic modulus may cause debonding. This issue can be partly solved by varying prepolymer curing agent ratio to modify PDMS elasticity. Cost is another barrier. NPs are usually expensive to fabricate, and some composites require as much as 70 wt% of filler and can decrease flexibility properties [240].

Scaling, cost-efficient skeleton-based composites must be the target for future studies. Blending micro and NPs together to reduce interfacial resistance is particularly promising, as well the use of recycled particles from machining or laser cutting processes to reduce the cost of the NPs. Ag NPs deserve a special mention because they have good bonding with PDMS and high thermal conductivity improvements [240,241,246]. For industrial applications, in addition to the great advantage of meltability and ease of application, the simplicity of adding particles to the polymer matrix allows, for example, the addition of organic particles, such as Organic Thermochromic Materials (OTM), combined with the addition of NPs to improve thermal performance, enabling the material to change its color according to the temperature of the composite, allowing rapid visual inspections (Fig. 11 G) [188]. Finally, long term thermal cycling studies must be conducted to assess the reliability of these systems for practical, real-world applications.

As summarized in Table 8, representative PDMS@NPs composites demonstrate how the NPs filler characteristics (type, size, concentration, and alignment) govern the thermal conductivity behavior of the resulting PDMS composites, offering insights into their tunability for specific application requirements.

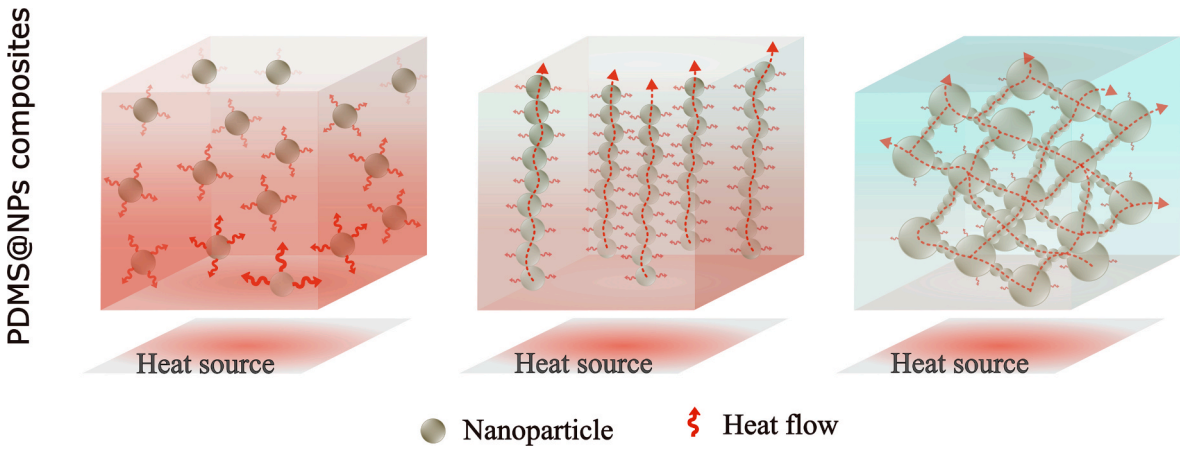

Fig. 10. Composite of PDMS with three different particle distributions: on the left, a random distribution, where thermal enhancements are not very significant due to the isolation of particles by the matrix material; in the centre, a chain-like distribution, where a preferential heat-transfer pathway is formed through the NPs, resulting in a material with anisotropic characteristics and improved thermal transport, particularly along the alignment direction; on the right, a 3D interconnected structure that allows for enhanced heat flow in all directions.

4.4. Wettability and surface energy control

4.4.1. Fundamentals and mechanisms of wettability control in PDMS@NPs composites

The intrinsic hydrophobicity of PDMS is characterized by water contact angles (CA) of 105° to 110° and surface energies of about 20 mN/m [249,250]. This behavior arises from the outward orientation of terminal methyl groups, which create a low energy interface. While this hydrophobicity can be advantageous for self-cleaning, anti-icing and drag reducing surfaces, it severely limits applications in microfluidics, biomedical devices and coatings that demand hydrophilicity or tunable wetting. Conventional treatments such as oxygen plasma or UV–ozone render hydrophilicity temporary by introducing silanol groups (Si–OH), while hydrophobic recovery is rapid due to the mobility of low molecular weight siloxane chains from bulk [62]. Beyond the well-known hydrophobic recovery of plasma-treated PDMS, the long-term stability of NP-based coatings is also influenced by particle migration, weakening of the interfacial bond, and surface chemical modifications. In NP-filled systems, the partial detachment or rearrangement of surface NPs can damage the hierarchical roughness that provides superhydrophobicity [251]. Furthermore, when photoactive NPs, such as TiO_2, are incorporated, prolonged exposure to UV rays can induce photocatalytic oxidation, which reduces hydrophobicity, as reported in TiO_2/PDMS coatings that transition to superhydrophilic states under irradiation [91,252]. Therefore, the need for studies that include time-dependent wettability data, tracked over days/months, is emphasized. This is particularly important because long-term mechanical, moisture, and UV stimuli often alter surface chemistry and roughness, rather than just observing initial CA values [253].

The incorporation of NPs offers an adjustable solution to overcome such limitations. Inorganic NPs, particularly SiO_2 and TiO_2, interact with PDMS chains through hydrogen bonding or covalent Si–O–Si bonds to facilitate increased NPs adhesion and interfacial stability [254,255]. Simultaneously, they produce micro and nanoscale roughness, which is beneficial for the Cassie–Baxter wetting regime where air bubbles trapped at the surface and as a result it reduces the liquid–solid contact area and lead to superhydrophobicity ($CA > 150°$, sliding angle $< 10°$) (Fig. 12) [256]. Aside from this spatial contribution, NPs also impact surface energy by chemical functionality: silanol or fluorinated groups decrease interfacial free energy further, while metal oxides or sulfides introduce polar sites that modify wettability toward higher hydrophilicity. Depending on the chemistry and illumination on the surface, it can promote a superhydrophilic surface. A clear example is a spray applied TiO_2 PDMS coating (ideally 3% TiO_2 with 50% PDMS) where exposed TiO_2 NPs and TiO_2 photoactivity produced pronounced photocatalysis (72–80% methylene blue degradation), superhydrophilicity (CA 8–9°) and antimicrobial activity, with irregular morphology (agglomerates) and sensitivity to illumination/substrate identified as critical performance factors. Hence, in this case it is produced a Wenzel type wetting regime (Fig. 12) [252].

In addition, NPs can introduce other properties to PDMS. For instance, TiO_2 NPs provides self-cleaning photocatalysis [255]; ZnO NPs gives mechanistically robust semirigid nanostructures that do not dissolve under mechanical stress [257]; Ag NPs provide antimicrobial characteristics [258]; and sulfide NPs (such as CuS) can provide local photothermal effects that facilitate droplet mobility [259,260]. Therefore, the NPs not only reverse the intrinsic limitations of PDMS but also promote its functionality beyond that the original polymer could not perform on its own.

4.4.2. Effects of PDMS@NPs composites on wettability and applications

The morphology (spherical, lamellar, porous, agglomerated) and chemical composition of NPs govern the scale and hierarchy of roughness and, consequently, the transition between wettability regimes. Si NPs are the most widely used fillers in PDMS due to the chemical compatibility and capacity for hierarchical structure formation. Core shell in-situ biosynthesized treated eco-friendly silica (IBTES)@SiO_2 NPs, for instance, were reported to form surfaces with water contact angles (WCAs) of 163° and sliding angles below 10°, while is extremely resistant to chemical degradation from pH 1–13 [254]. Their morphological control is also essential. Spiny SiO_2 NPs yielded transparent PDMS films with the WCA values of $165.4 \pm 1.0°$ and optical transmittance of 96.93%, demonstrating the potential for achieving such high hydrophobicity without sacrificing optical transparency [261]. Binary SiO_2–TiO_2 systems extended these properties by coupling high hydrophobicity (WCA $152° \pm 2°$) with photocatalytic oxidation of organic contaminants and chemical resistance under a broad pH range (2–12), demonstrating the multifunctionality accessible due to hybrid oxide fillers [255].

Other types of inorganic NPs can also modify PDMS composite performance. ZnO containing composites maintained superhydrophobicity under pressure due to the semi rigid nanostructures, which were resistant to compaction and still exhibited some surface roughness [257]. PDMS@Ag coatings introduced antimicrobiality alongside high CAs, extending the usefulness of these composites to textiles and biomedical applications [258]. Recently, porous fillers such as MOFs and sulfide-based NPs like copper sulfide (CuS) have introduced other functionalities. MOFs introduce inherent porosity and CuS NPs offer photothermal activity, both of which assist in providing an efficient oil water separation and irradiation induced self-cleaning [259,260]. PDMS acts as a flexible, low energy binder that anchors NPs and at the same time stabilizes the hierarchical topographies responsible for extreme wetting behavior. The interplay among morphology of NPs, surface chemistry, and matrix interactions will eventually determine whether the composite exhibits simple hydrophobicity, robust superhydrophobicity, or even multifunctional performance. PDMS@NPs composites allows the development of superhydrophobic coatings for the protection of cementitious materials [254], in an efficient oil water separation [251,261], photocatalytic self-cleaning [262], and anticorrosive protection [263,264]. The mechanical robustness is attained by strategies such as double cross linking [251] or functionalization with cyanoacrylate [174], while the optical transparency is preserved in coatings based on spiky SiO_2 NPs [261]. Slepička et al. [265] demonstrated that a single high-energy excimer laser pulse applied to Au/C films deposited on PDMS produces Au/C nanoclusters with high effective surface area that act as Surface-Enhanced Raman Scattering (SERS) hotspots while leaving PDMS wettability essentially unchanged.

Other applications of PDMS@NPs composites include their use in self-cleaning mechanisms (Fig. 13 **A**) [253], for oily wastewater remediation (Fig. 13 **B**) [266], in emulsion separations on porous surfaces with opposite affinities (Fig. 13 **C**) [267], as a PDMS@SiO_2@WS_2 super-hydrophobic sponge for oil/water separation in marine environments (Fig. 13 **D**) [34], and as a PDMS@ZnO

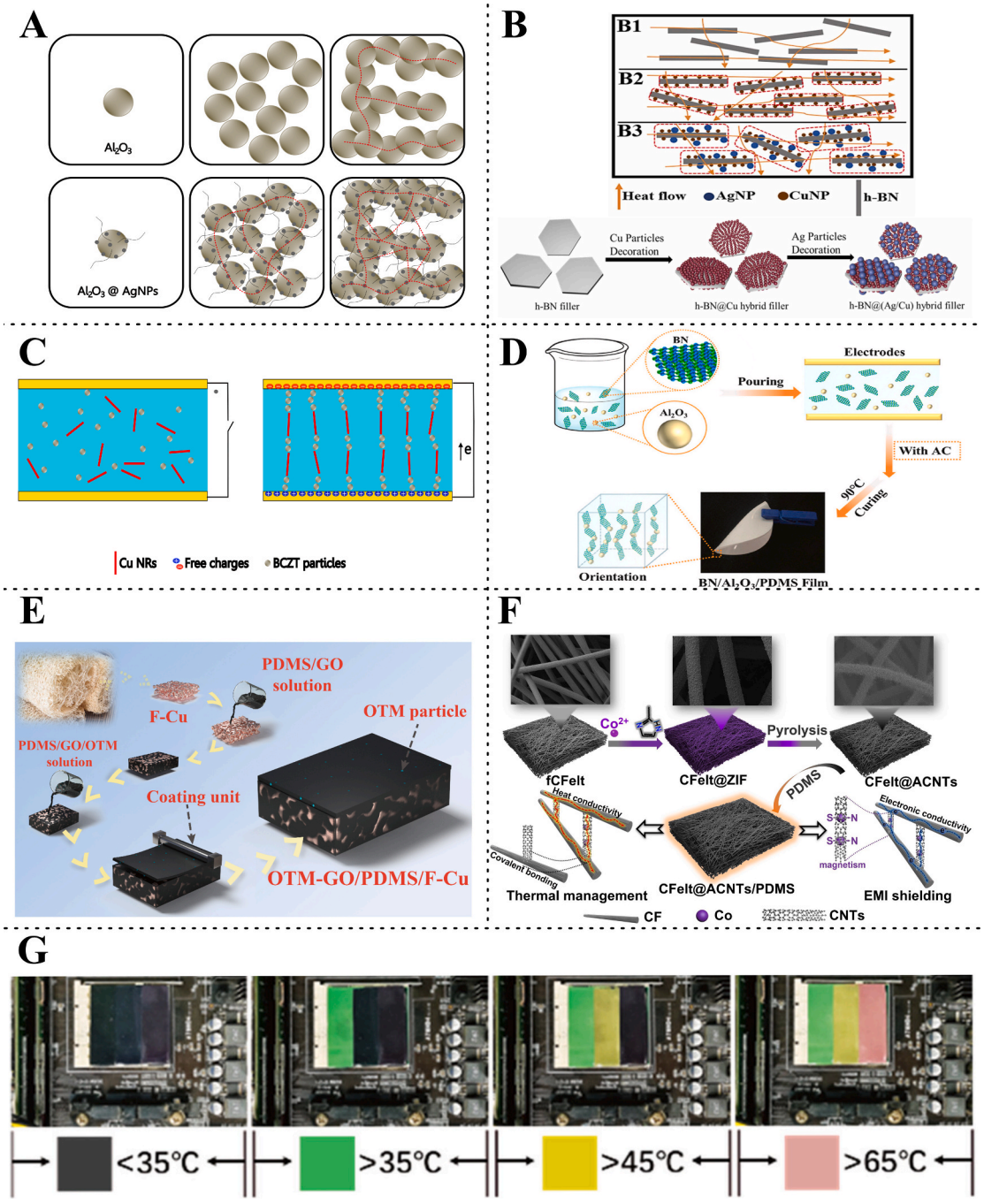

Fig. 11. (A) Differences in heat flux between pure Al_2O_3 NPs and Al_2O_3@AgNPs under random dispersion conditions with low and high NPs concentrations, demonstrating the higher efficiency of the decorated particles in facilitating phonon transport in both cases. Adapted from [240]. (B) h-BN particles decorated with Cu NPs and Ag NPs, with the heat flux of pure h-BN particles, h-BN particles decorated only with Cu NPs, and those decorated with both Cu and Ag NPs being compared under a random distribution. A visible improvement in heat flux is observed for the h-BN@Cu NPs compared to the pure h-BN particles, and an even more significant enhancement occurs when Ag NPs are also added, due to the improved interaction between the particle [241]. (C) Alignment process of barium calcium zirconium titanate (BCZT) NPs and Cu NRs within the PDMS matrix using an electric field that oriented the particles between the positive and negative electrodes. Adapted from [218]. (D) Mixing process of BN particles and Ag NPs within the PDMS matrix, followed by alignment through a direct-current–induced electric field. After curing, a flexible material is obtained, with the NPs aligned, resulting in enhanced thermal transfer compared to pure PDMS, particularly along the alignment direction [242]. (E) Cu sponge with a geometry inspired by natural plant sponges, filled with PDMS containing graphene oxide NPs to achieve improved thermal conductivity, both due to the three-dimensional structure of the sponge and the NPs-enhanced PDMS. On top, an additional layer of Organic Thermochromic Materials (OTM) is applied to enable visualization of colour changes according to the temperature of the composite [243]. (F) It

illustrates the formation process of CNTs with Co NPs within the carbon fiber network, demonstrating the mechanisms by which heat flux is enhanced through the connections between fibers created by the CNTs, which simultaneously allow for the passage of electrical current [244]. (G) Example of an application of a PDMS composite with OTM in a computer chip, where the visible colour patterns on the surface correspond to the temperature range of the composite [188].

Table 8
Representative PDMS@NPs composites for thermal conductivity properties control, summarizing NPs filler characteristics (type, size, concentration, and alignment), their effects on PDMS properties, targeted applications, associated challenges and prospects and other relevant data.

Filler characteristics	Thermal conductivity (W/mK)	Effect of NP on PDMS properties	Applications	Challenges and prospects	Other data	Ref.
$rGoCaCO_3$ (5%wt; random distribution)	0.44	Their shape and contact points improve thermal conductivity.	Heat dissipation in electronics; Flexible and wearable devices.	Uniformly dispersing the nanofillers in the polymer matrix is a complex task.	Direct dispersion and solution mixing; Simple/green synthesis method.	[49]
$(Ba_{0.85}Ca_{0.15})(Ti_{0.90}Zr_{0.10})O_3$/Cu nanorods (21%vol; chain like distribution)	0.31	Aligned NPs created a patch.	Low power wearable electronics; Self powered sensors; miniaturized and integrated electronic devices.	There is a physical limit to the design; Aligning two types of particles is extremely challenging.	Direct dispersion and solution mixing.	[218]
BN (150 nm; 6.6% vol; random distribution)	0.29	Their shape and contact points improve thermal conductivity	Thermal; Interface Materials (TIMs)	Low conductivity gain at low concentrations; Significantly lower impact than microparticles; Increase the concentration and add other particles	Direct dispersion and solution mixing	[219]
BN@Ag and rGo (23.8%wt; 3D network)	2.34	The AgNPs acted as thermal bridges between the BN flakes	TIMs	Maintenance material's electrical insulation; Use of AgNPs, which is expensive	*In situ* synthesis of AgNPs on BN NPs	[222]
Al_2O_3(5um) @AgNPs (70% wt; random distribution)	0.67	AgNPs chemically bonded to Al_2O_3 improved interfacial bonding	TIMs	Drastic increase in viscosity, Poor compatibility between the ceramic filler and the polymer matrix	Direct dispersion and solution mixing	[240]
BN (flaky,5 μm) and Al_2O_3 (spherical shape,800 nm) (20%wt; chain like distribution)	0.228	Inserting nano-Al between boron nitride sheets helps create easier paths	Thermal management in electronics	NPs orientation involves high energy costs; different NPs sizes improve thermal performance; Possibility of large-scale production.	Direct dispersion and solution mixing	[242]
CNT/Co (Fiber decorated)	1.08	Decreased contact resistance and created transfer paths between fibers	Precision electronic device	Immediate practical application; scability against mechanical stress; degradation due to thermal fatigue	*in situ* synthesis to create a bond between the fibers	[244]
h-BN@(Ag/Cu) (25%vol; random distribution)	1.5645	The NPs chemically bonded with h-BN and contributed to the creation of a spontaneous patch	Electrical Packaging	Low economic viability; difficult to produce on a large scale; loss of mechanical properties.	Direct dispersion and solution mixing; excellent results for random distribution	[241]
Graphite (20%wt; random distribution)	0.4370	Their shape and contact points improve thermal conductivity	Flexible and wearable electronics; sensors and actuators; biomedical devices	Agglomeration can degrade mechanical properties; low cost particles	Direct dispersion and solution mixing	[247]
CoNi (21%vol; chain like distribution)	2.44 (in plane) 0.75 (interplane)	Aligned NPs created a patch facilitating heat propagation in the preferred direction	5G communications; flexible Electronics	Heat buildup through microwave absorption degrades performance or damages devices.	Direct dispersion and solution mixing; "Three in one" multifunctional material	[248]

coating with antifouling properties (Fig. 13 **E**) [268]. Despite the successful applications of PDMS@NPs composites, challenges such as scalability, thermal stability, and UV degradation must be addressed through formulation optimization to meet industrial requirements.

4.4.3. Durability, challenges, and future directions

The long-term stability of wettability alteration depends on the robustness of the NPs PDMS interface and its hierarchical structure under environmental stress. Double crosslinking methods maintained CAs above 150° after 60 cycles of abrasion and 20 cycles of oil water separation [251], whereas PDMS–SiO_2–ethyl cyanoacrylate composites maintained CAs above 154° after 50 cycles of abrasion [174]. Mechanical durability tests (tape peeling and sandpaper abrasion) have shown films with retained CA > 150° after 300 tape peel cycles and have maintained superhydrophobicity (CA ~ 161°, SA < 9°) after 90 cm of abrasion, with CA still ~ 157° after 220 cm, evidencing a robust, thick PDMS@SiO_2 composite layer (Fig. 14). Thermal treatment, such as, rapid pyrolysis or flame scorching, generated *in situ* nanosilica within the PDMS backbone to form superhydrophobic surfaces with deformation, abrasion, and corrosive environment resistance [269]. Nevertheless, some problems may arise, including high NP loading that can compromise both transparency and mechanical flexibility [258,264]. Furthermore, while fluorinated surface modifications effectively reduce surface energy, they raise environmental and toxicological concerns [270].

Even in many PDMS@NPs systems, the immediate superhydrophobic character after preparation may not be maintained over long periods of time, unless facilitated by the stability of surface-bound nanoarchitectures and the absence of detrimental chemical reactions. The loss of wettability can be caused by PDMS chain mobility and oligomer diffusion, i.e., mechanisms relevant to hydrophobic recovery in plasma-treated PDMS [62], and by mechanical wear leading to the loss of micro/nano roughness, widely documented in cases of surface roughness damage [251]. Other wettability losses may be promoted by photocatalytic oxidation reactions induced by the presence of TiO_2 NPs after exposure to UV radiation [91,252], potentially leading to increased hydrophilicity following UV irradiation. In contrast, schemes employing more effective NPs binding approaches, such as dual crosslinking or PDMS-

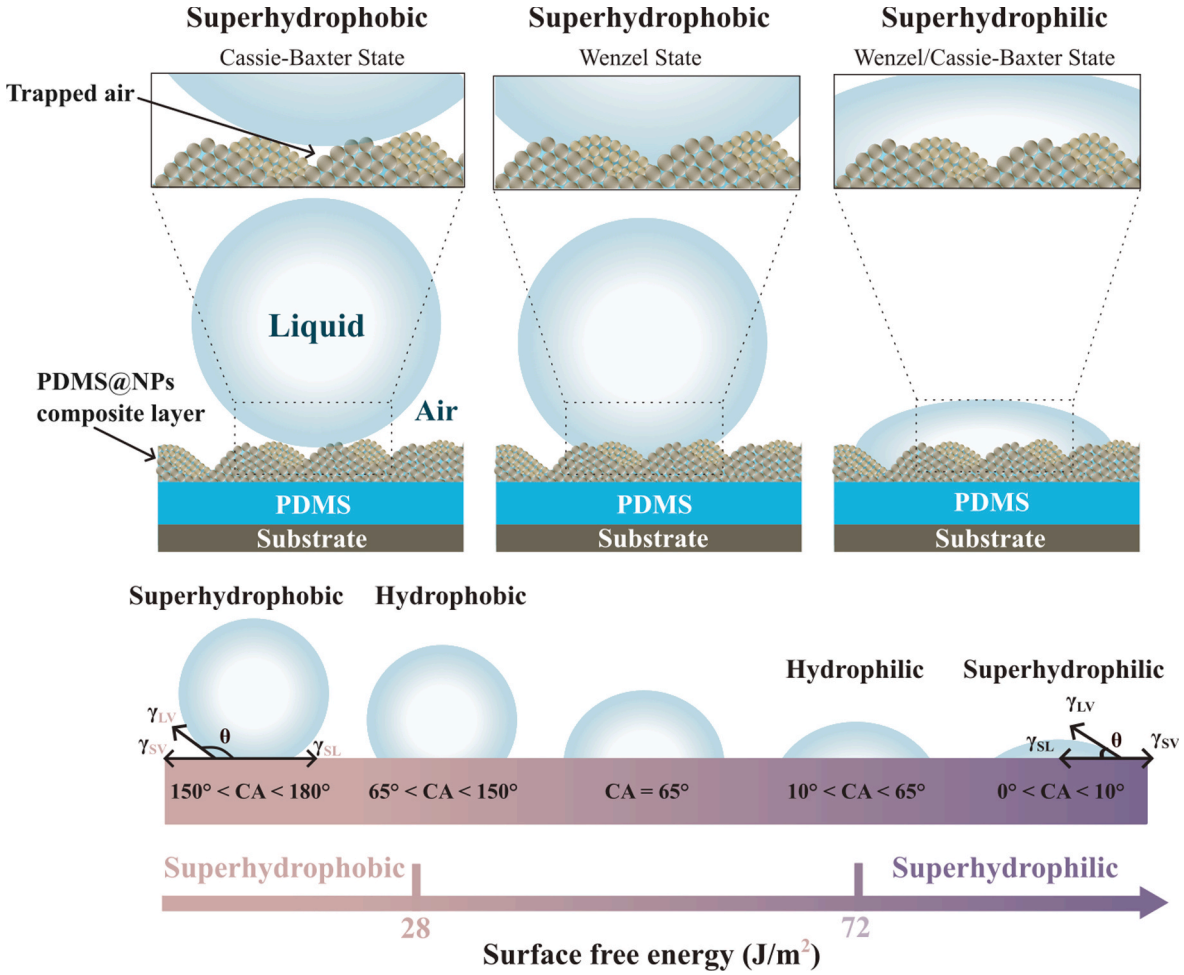

Fig. 12. Wetting behavior transition in PDMS@NPs composite surfaces demonstrating superhydrophobicity and superhydrophilicity. Superhydrophobic Cassie–Baxter state: trapped air pockets beneath the liquid droplet create a high contact angle (CA > 150°), minimizing solid liquid interaction; Wenzel state: partial liquid penetration into surface textures reduces the contact angle while maintaining hydrophobic character; and superhydrophilic Wenzel/Cassie–Baxter state: complete wetting of the textured PDMS@NPs surface leads to a very low contact angle (CA < 10°), enhancing liquid spreading. The bottom scale illustrates the correlation between contact angle and surface free energy, showing the transition from superhydrophobic (low surface energy, ~28 mJ m^{-2}) to superhydrophilic (high surface energy, ~72 mJ m^{-2}) regimes.

epoxy hybrids, have demonstrated significantly greater stability, including the integrity of superhydrophobicity under prolonged UV exposure and multiple abrasion cycles [253]. Collectively, such observations highlight the paramount need for common standards in evaluating the long-lasting functionality of PDMS@NP assemblies through terms such as temporal superhydrophobic stability after days or months and after exposure to UV radiation, mechanical wear cycles, and retention of the quantity or levels of nanoarchitecture.

Recent trends are pointing toward fluorine free alternatives such as PDMS@ZnO and bicontinuous PDMS@SiO_2 coatings, that combine high hydrophobicity with greater environmental sustainability [257]. At the same time, multifunctional coatings combining wettability engineering with antimicrobial, magnetic or photothermal properties are being explored for protective and biomedical uses [260,271,272]. In addition, up scalable deposition methods such as spraying and roll to roll coating are being devised to facilitate industrial translation [253,273]. A major current challenge is to combine high wettability with durability, scalability and environmental safety. The successful transition of PDMS@NPs composites from laboratory prototypes to large scale applications in protective coatings, microfluidics, biomedical systems, and environmental remediation will depend on the resolution of these challenges [207,208,210].

As summarized in Table 9, representative PDMS@NPs composites demonstrate how the NPs filler characteristics (type, size, concentration, and alignment) govern the wettability and surface energy properties of the resulting PDMS composites, offering insights into their tunability for specific application requirements.

4.5. Optical properties

4.5.1. Fundamentals and mechanisms of optical properties in PDMS@NPs composites

PDMS provides high transparency, low autofluorescence, and optical stability. However, the incorporation of NPs often alters these properties by introducing refractive-index mismatch and light-scattering effects (Fig. 15). The Si–O–Si backbone provides low electronic polarizability as well as low absorbance of its visible spectrum, leading to more than 90% transmittance between 400 and

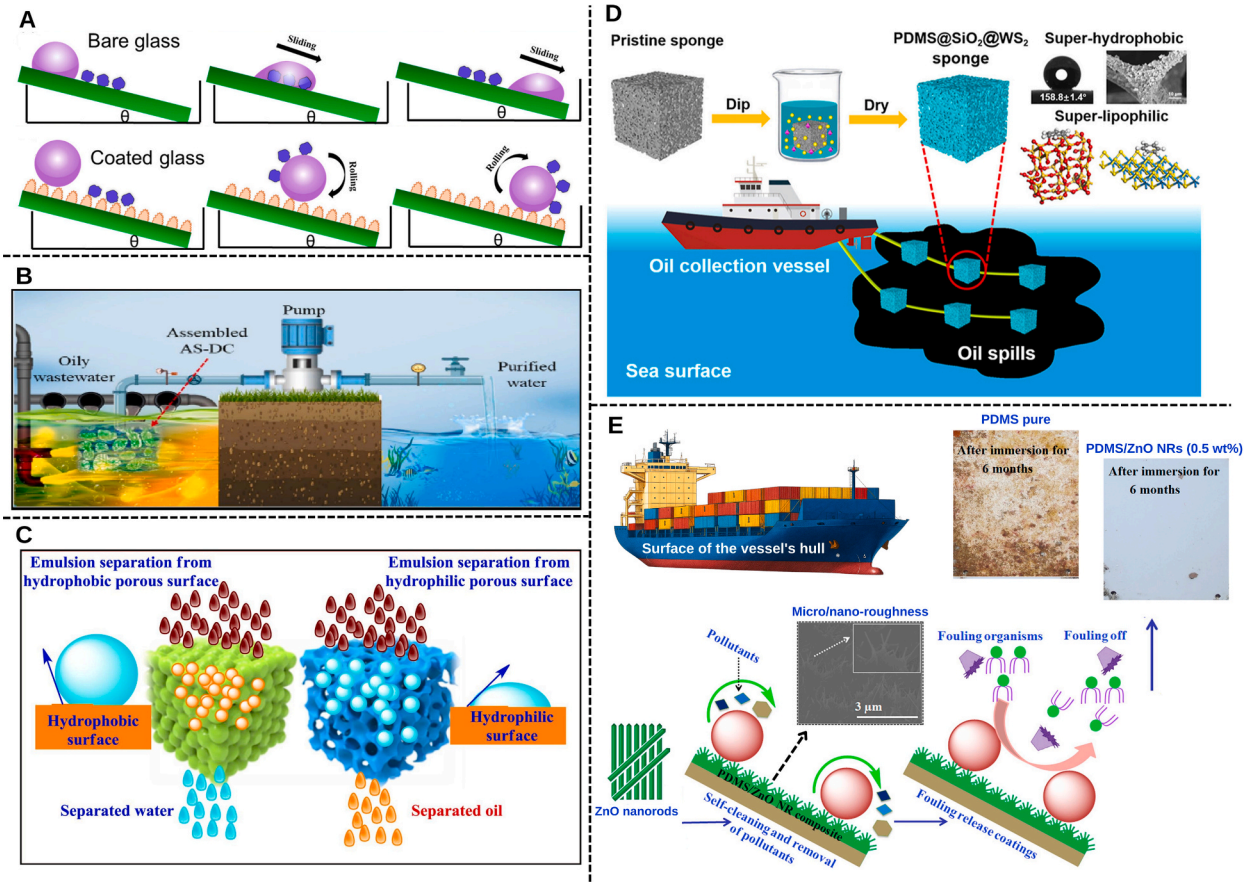

Fig. 13. (A) Comparison of the self-cleaning mechanism with bare glass and coated glass, adapted from [253]. (B) Schematic illustration for remediation of oily wastewater. Adapted from [266]. (C) Emulsion separations from hydrophobic (water) and hydrophilic (oil) porous surface. Adapted from [267]. (D) The durable and ecofriendly superhydrophobic PDMS@SiO_2@WS_2 sponge was fabricated by one step dipping method for efficient oil/water separation in complex marine environments. Adapted from [34]. (E) PDMS/ZnO nanorod composite coating as a marine anti-fouling surface. Adapted from [268].

1100 nm and a refractive index of 1.40–1.45 [275–278]. The amorphous structure and large Si–O–Si bond angle (120–180°) minimize variations of densities, suppress sing birefringence and light scattering. In addition, the absence of conjugated/chromophoric groups also guarantees low optical loss, making PDMS one of the clearest polymers used for photonic and biomedical devices [279,280].

The incorporation of NPs into PDMS offers an efficient way to modulate its optical response by changing the local dielectric environment through surface modification. High-index NPs like TiO_2, ZrO_2, Si, or ZnO raise the effective refractive index (n_eff) by increasing polarizability of the composite, as EMT theory predicts [281]. Maxwell–Garnett and Bruggeman models capture the monotonic increasing behavior of n_eff versus NPs volume fraction, if particles are highly dispersed. However, contrast of refractive index between PDMS and filler ($\Delta n = |n\_PDMS - n\_NP|$) also dominates scattering. If particle size reaches visible wavelengths, Mie scattering causes haze and loss of transparency [178].

The interfacial region between PDMS and NPs is therefore critical. Covalent Si–O–Si bonds, hydrogen bonding, or *van der Waals* interactions connect the polymer chains, influencing local dipole orientation and dielectric response. Controlled interfacial chemistry, via silane coupling, ligand engineering, or silica shell coating, tends to reduce refractive mismatch and aggregation, maintaining optical homogeneity [282–284]. In addition to the refractive index adjustment, NP inclusion adds unique optical mechanisms. For dielectric systems (e.g., TiO_2, ZrO_2, SiO_2), polarization and interfacial field effects prevail, which allow for stable, high transparency materials. For semiconducting or plasmonic systems (e.g., Au, Ag, Si, ZnO), other effects like exciton coupling or localized surface plasmon resonance (LSPR) come into play [282,285]. Plasmonic fillers enhance local electric field and refractive sensitivity but add wavelength selective absorption to diminish the transparency window. Semiconductor NPs, on the other hand, add quantum confinement induced luminescence or photoresponsivity.

The optical behavior of PDMS@NPs composites is due to four mutually related mechanisms: (i) refractive-index enhancement by stronger dielectric polarizability; (ii) scattering of light, depending on particle size, dispersion, and Δn; (iii) plasmonic absorption (metallic inclusions) or excitonic absorption (semiconducting inclusions); and (iv) interfacial polarization, depending on surface chemistry and NPs morphology. Fig. 15 presents a schematic comparison of the optical behavior of pure PDMS and PDMS@NPs composites under illumination within the 400–1100 nm wavelength range. Optimal optical performance is attained by balancing filler loading and shape through appropriately designed interfaces to optimize tunability while maintaining PDMS's intrinsic transparency.

NPs geometry plays a decisive role in shaping the optical response of PDMS@NPs composites. Size distribution governs how light is absorbed or scattered, with monodisperse nanoparticles supporting predictable, linear attenuation scaling, whereas polydisperse

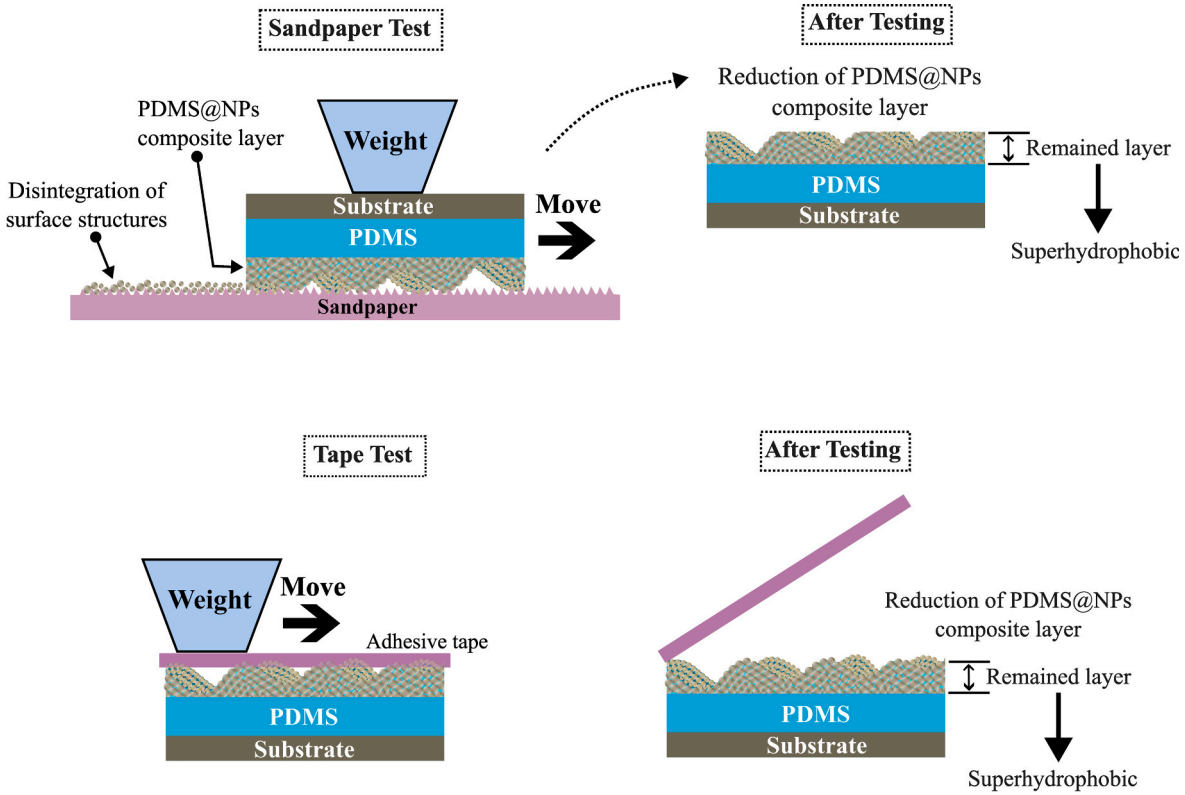

Fig. 14. Schematic representation of the mechanical durability tests performed on the superhydrophobic PDMS@NPs surface. In the sandpaper test, the sample is subjected to abrasion under load, resulting in partial removal of the surface structures while maintaining its superhydrophobicity. In the tape test, adhesive tape is pressed and peeled off from the surface, causing slight disintegration of the upper PDMS@NPs layer, which still preserves its superhydrophobic properties after the test.
Adapted from [274].

nanoparticles typically exhibit logarithmic attenuation behaviour due to broader morphological heterogeneity [286]. Spatial arrangement further contributes to optical performance: asymmetric nanoparticle distributions enhance overall attenuation, while reduced inter-particle spacing strengthens plasmonic coupling and field localization [286]. Particle size also matters, as smaller nanoparticles minimize scattering and help preserve transparency [287], whereas larger plasmonic particles enhance resonance selectivity and spectral tunability [286]. Consequently, the optimal geometric configuration depends on the application functionality, whether the priority is attenuation efficiency [286], plasmonic sensing sensitivity [285], tunable optical filtering [176], or maximizing optical transparency [287]. NPs morphology exerts also a influence on the optical behaviour of PDMS@NPs composites by dictating how light is absorbed, scattered, and locally amplified. Spherical NPs produce isotropic responses and can maintain high transparency when they are monodisperse, sub-wavelength, and well dispersed, as shown for silica-coated Au NPs in PDMS elastomer films and for ~10–20 nm ZrO_2@SiO_2 spheres uniformly dispersed in PDMS high-index nanocomposites [178,288]. In contrast, anisotropic shapes such as nanorods, nanoprisms, or nanoplates introduce geometry-dependent plasmon modes, enabling spectral tunability and enhanced field localization [289]. NPs with sharp features, including nanostars or branched morphologies, generate intense "hot spots" that greatly increase absorption and scattering, which benefits sensing but reduces optical clarity [290,291]. Irregular or polydisperse NPs (common in in-situ reduction inside PDMS) broaden extinction spectra and produce nonlinear attenuation due to heterogeneous size and shape distributions [292]. Overall, nanoparticle geometry determines the balance between transparency, resonance selectivity, and field enhancement, guiding the design of PDMS-based optical elastomers for photonic, sensing, and energy-conversion applications.

4.5.2. Effects of PDMS@NPs composites on optical properties and applications

The addition of NPs to PDMS enables refractive index, transparency, and photoluminescence to be systematically adjusted, extending its use from microfluidic optics to advanced photonic devices. One of the most reported achievements in PDMS@NPs composites is the refractive index modulation without significantly compromising transparency. The refractive index of pure PDMS (≈1.40) can be increased up to 1.65 with the incorporation of high-index NPs such as TiO_2 or ZrO_2 [178,281,283,293,294]. For instance, PDMS@ZrO_2/SiO_2 nanocomposites display roughly linear increase of refractive index from 1.42 to 1.60 at NPs loadings up to 50 wt%, with transmittance greater than 91% across the visible range [178]. Similarly, PDMS@ZrO_2 composites with diamine–siloxane ligand modification achieves homogeneous dispersion up to 20.8 vol%, with refractive indices 1.39–1.65 and transparency of around 93% [283]. PDMS@TiO_2 composites prepared by non-aqueous sol–gel processing also exhibit controlled index increases to values of approximately 1.56 (at 589 nm) at loadings of 0.2 to 15.5 wt% [281].

Transparency loss is mainly caused by NP aggregation induced light scattering and refractive index mismatch between phases. Transmittance decreases as NP aggregation occurs, particularly with high contrast TiO_2 fillers. SiO_2 NPs, whose refractive index contrast is lower than that of PDMS, however, maintain excellent transparency even under high loadings [282]. The interplay between Δn and dispersion defines an optimal region where the refractive index can be adjusted without compromising clarity. For PDMS@ZrO_2 and SiO_2 composites, the transmittance spectrum remains essentially constant throughout the visible range [178,293], whereas PDMS@TiO_2 systems show a gradual decrease toward shorter wavelengths due to Rayleigh scattering and intrinsic band edge absorption [281].

The incorporation of plasmonic or semiconductor NPs introduces additional optical functions beyond refractive index control. Au and Ag NPs in PDMS display LSPR to a maximum of about 520 nm and 450 nm, respectively [282,285]. The LSPR wavelength also increases with growing particle size or a higher surrounding refractive index, making the composites potential for refractive index sensing and optical strain sensing. Whereas metallic NPs increase the absorption but reduce the transparency. In addition, they offer valuable spectral selectivity and field enhancement, which are valuable for sensing and spectroscopy.

Semiconductor fillers such as Si, ZnO, CdSe, and perovskite nanocrystals, impart luminescent or photoresponsive character. As shown in Fig. 16 **A**, red and green color emitting perovskite nanocrystals ($CsPbBr_{0.75|2.\ 25}$ and $CsPbBr_3$, respectively) are alternately embedded in a UV-curable polymer matrix [279]. Light extraction is enhanced by the prismatic microtexture on the top red layer, while PDMS encapsulation guarantees passivation and long-term optical stability. The obtained multilayer stacked structure yields stable and high quality white emission upon excitation by a blue LED source [279]. Carbon dot and graphene quantum dot doped PDMS films emitting broad excitation dependent luminescence have been used for antimicrobial surfaces and flexible optoelectronic coatings [295]. Eu^{3+} or Tb^{3+} emitting lanthanide doped and MOF based PDMS hybrids have been used in ratiometric fluorescent devices and temperature sensors [296,297].

Mechanical flexibility is another significant feature of PDMS@NPs composites. The elastomeric nature of PDMS allows its optical properties to respond reversibly to deformation. Plasmonic PDMS films are stretchable with color change, due to interparticle spacing and local refractive field change [298]. In dielectric systems, refractive index and transparency are maintained even when curved, showing that the PDMS matrix maintains homogeneous NPs dispersion during mechanical stress [178,281,282]. This combination of elasticity and optical stability enables PDMS@NPs composites to find application in reconfigurable photonic devices, tunable coatings, and wearable optical sensors. Cho et al. [178] developed transparent nanocomposite films with adjustable refractive indices. Fig. 16 **B (i)** illustrates a schematic representation of the surface modification process, where ZrO_2 NPs are coated with a SiO_2 layer, involving TEOS and $NH_3{\cdot}H_2O$ and the resulting ZrO_2@SiO_2 NPs are dispersed in a PDMS matrix to create a transparent nanocomposite film. To confirm the presence of a SiO_2 layer on the surface of ZrO_2 NPs, the authors have performed TEM-EDX analysis of ZrO_2@SiO_2 NPs (Fig. 16 **B (ii)**). The results can be observed in Fig. 16 **B (iii)** where the images reveal the film's notable transparency, appearing almost invisible against the background.

The interconnection between morphology and optical behavior has been clarified by microscopy and surface topography investigations. Homogeneous, smooth morphologies with minimal roughness correspond to isotropic optical response and high

Table 9
Representative PDMS@NPs composites for wettability and surface energy properties control, summarizing NPs filler characteristics (type, size, concentration, and alignment), their effects on PDMS properties, targeted applications, associated challenges and prospects and other relevant data.

Filler characteristics	Wettability	Effects of NPs on PDMS properties	Applications	Challenges and prospects	Other data	Ref.
SiO_2 (core–shell IBTES@SiO_2;)	WCA 163°, SA < 10°.	Super hydrophobicity.; UV and chemical resistance (pH 1–13); Strong adhesion to mortar	Concrete protection against humidity and harmful ions (Cl-, SO_4^{2-}); Self-cleaning of urban surfaces.	Scalable NP synthesis; long term abrasion resistance.	Sol-gel + Surface functionalization	[254]
SiO_2 + TiO_2	CA 152° ± 2°	CA > 120° after 200 bending cycles; Chemical resistance (pH 2–12).	Wall protection; Reduced pollutant adhesion	Sensitivity to pH < 2 and > 13; Fragilization with excess TiO_2 (>15 wt%).	Sol-gel processing; Photocatalysis (~90% dye degradation)	[255]
SiO_2 ("spiky", ~120 nm; Mass ratio SiO_2:PDMS = 1:1.5)	WCA 165.4 ± 1.0°	Optical transparency 96.93%; Reusable for 20 oil/water cycles	Chlorine/water separation; suitable for multiple surfaces (glass, metal, wood, fabric, paper.	UV degradation after 360 h; Reduced transparency with excess NPs	Direct dispersion and solution mixing	[261]
SiO_2 (~20 nm; 23.3 wt%)	WCA > 150.5°	Stable after 60 abrasion cycles; Oil water separation efficiency of 95% in 20 cycles.	Treatment of industrial effluents; Separation of organic solvents (carbon disulfide, heptane and xylene).	Recycling after saturation; Outdoor durability testing.	Assisted deposition; Porous structure and double cross-linking.	[251]
SiO_2 (~3,37 μm) + TiO_2 (~20 nm). (NPs:PDMS → 4:1)	WCA 152.2°	Stable at 100 °C; Photocatalytic (59% MO in 60 min); UV/mechanical resistance	Self-cleaning; Repellency to acids (pH 2), bases (pH 11), solvents	Requires 400 °C annealing (limits heat sensitive substrates); degrades at high temperatures; economical and scalable synthesis methods	Direct dispersion and solution mixing; UV and heat resistance (<600 °C)	[262]
SiO_2 (60 wt% PDMS@SiO_2	WCA 156.29°, WSA 3°	Abrasion resistant; Dynamic droplet impact resistance	Anti biofouling; Self-cleaning coatings	>60% loading fragility; Adhesion to diverse substrates; Functionalization to increase chemical and thermal resistance	Surface functionalization; Spray coating; Thermal stability (<400 °C).	[263]
SiO_2 (~20 nm, 60 wt%)	CA > 154°	Stable after 50 abrasion cycles; CA > 150° after 2 months ambient + 250 h UV	Aluminum alloy protection; Self-cleaning of contaminated surfaces	Superhydrophobicity lost under severe abrasion	Direct dispersion and solution mixing	[174]
SiO_2 (~20 nm, 114 wt%)	CA = 163° and SA = 3.5°	Resistance to 20 abrasion cycles	High-speed water/sand impact; Corrosion resistance; Industrial scalability	−>28% SiO_2 reduces superhydrophobicity; Needs better thermal/chemical stability	Direct dispersion and solution mixing; Spray coating	[253]
NF-SiO_2 (5 wt%)	WCA = 158°	Stable after 150 tape peels, 100 steel wool rubs, 50 blade scrapes, 450 g sand impact; WCA 157.4° after 30 h at 100–300 °C.	Marine/industrial equipment; Self-cleaning; Laser structured metal surfaces	Long-term wear, extreme temperature, and NP retention need robust large-scale solutions.	Direct dispersion and solution mixing	[270]

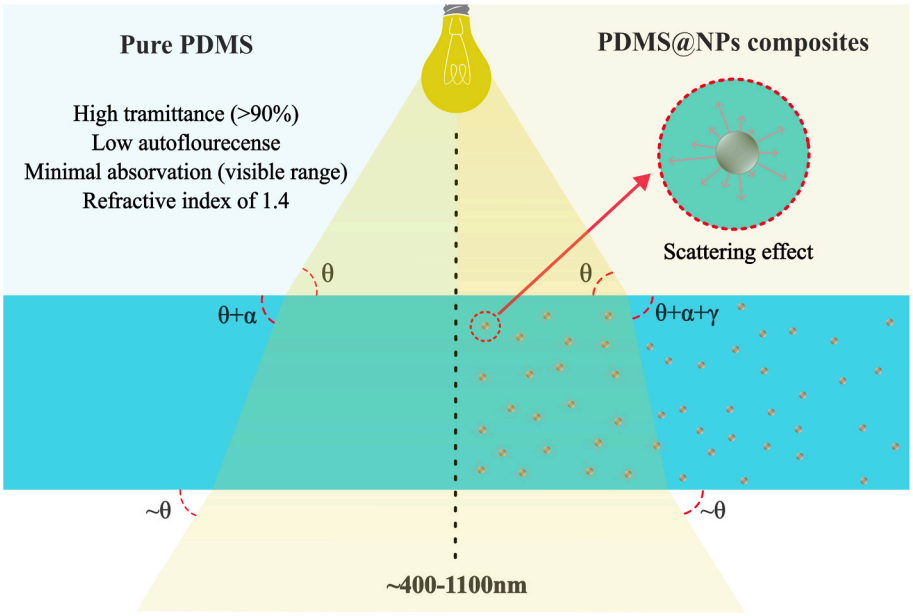

Fig. 15. Optical behaviour of pure PDMS compared with PDMS@NPs composites where it is observed that the light enters with angle θ of incidence in both composites and afterward, due to the change of the index of refraction, bends θ + α due to the index of refraction of the PDMS and leaving in evidence the influence of the NPs by the term γ in the other composite side. The scattering effect of the light on the NPs is also demonstrated through the detailed image. After passing through the PDMS, it is observed that it is possible to maintain the transparency with the transmission of the passage of light in the range between ~ 400–1100 nm and with the exit angle being similar to the angle of entrance.

transmittance, whereas aggregation gives rise to scattering centers that degrade clarity [178,179,283,284,293]. *In situ* sol–gel synthesis and surface functionalization improve NPs dispersion and interfacial compatibility. For instance, silane coupling agents or SiO_2 shells improve intimate adhesion to the PDMS network and reduce local refractive discontinuities [282,284,293]. The methods lead to reproducible optical performances of the composites and have enhanced stability. The versatility of PDMS@NPs composites has led to their applications in different optical devices. PDMS is an optically transparent encapsulant, and it protects luminescent NPs in LEDs and photovoltaics from oxidation and water and maintains optical emission over time [279,280,299,300].

PDMS@NPs composites are also employed as high index substrates for lenses, waveguides, and photonic coatings in flexible photonic devices. Luminescent PDMS composites incorporating perovskites or quantum dots are applied as color conversion layers and luminescent solar concentrators [299,301,302]. Mechanochromic and thermochromic PDMS systems that change color or emission upon mechanical strain or temperature are promising for sensing and anti-counterfeiting uses [298,303,304]. The PDMS@NPs composites have also been employed in biomedical diagnostics that take advantage of their optical and photothermal properties. Han et al. [305] have developed a PDMS@TiO_2 nanocomposite-photonic polymerase chain reaction (PCR) reactor for portable quantitative polymerase chain reaction (qPCR) analysis. PDMS@TiO_2 film integrated with a carbon graphene mixture enhances the absorption and scattering of the light and as result it enhance the thermal cycling (Fig. 17 **A**). Fig. 17 **B** and **C** demonstrate the most significant mechanisms: increased heating cooling rates due to photon scattering and increased fluorescence intensity through TiO_2 driven light reflection, amplifying the dye DNA complex signal. This design demonstrates the potential of PDMS@NPs composites to integrate optical enhancement and thermal management into compact molecular diagnostic platforms.

4.5.3. Durability, challenges, and future directions

Despite the extensive developments, optical stability over the long term and reproducibility are challenging in PDMS based nanocomposites. Photo oxidation, aggregation, and thermal mismatch can progressively degenerate transparency and luminescence [178,279–281,283]. Plasmonic structures, being highly sensitive, are particularly prone to chemical instability and absorption losses upon prolonged exposure to illumination [282,285]. Cycling temperature or humidity exposure may trigger interfacial debonding, altering local refractive indices and scattering behavior.

Another limitation is the lack of standardized optical characterization protocols. Reported refractive index or transparency data can be inconsistent due to variations in film thickness, wavelength range, or measurement geometry. Having comparable results of the wavelength resolved transmittance, haze, and n and k spectra, will allow quantitative cross studies comparison.

To meet these challenges, many strategies are emerging. Controlled surface modification (e.g., silica shelling [282], ligand engineering [293]) homogenizes interfaces and minimizes scattering. In metal systems, particle size, shape, and operating off the plasmon resonance optimize to minimize absorption losses [281,285]. Self-healing PDMS networks (already demonstrated in mechanical systems) holds out an appealing way to preserve optical clarity under strain or environmental stress.

Scalability and sustainability are further issues. Most high-performance composites are based on laboratory sol–gel or sputtering

methods, which are challenging to scale up to a large area fabrication. Green, solvent free methods and recoverable PDMS matrices should be the focus of future development to ensure industrial applicability.

Looking forward, the field is shifting toward adaptive and multi-functional optical elastomers. Dynamic refractive index modification via responsive fillers, hybrid metasurfaces combining elasticity with plasmonic or dielectric nanostructures [306], and bio-inspired structures mimicking anisotropic tissue optics are promising research frontiers. Achieving stable dispersion, standardized evaluation, and scalable synthesis will be decisive to realize PDMS@NPs composites as reliable components in flexible displays, smart sensors, and soft photonic systems operating across visible and near infrared regimes.

Long-term optical degradation in PDMS@NPs composites results from physical-chemical degradation, environmental influence and

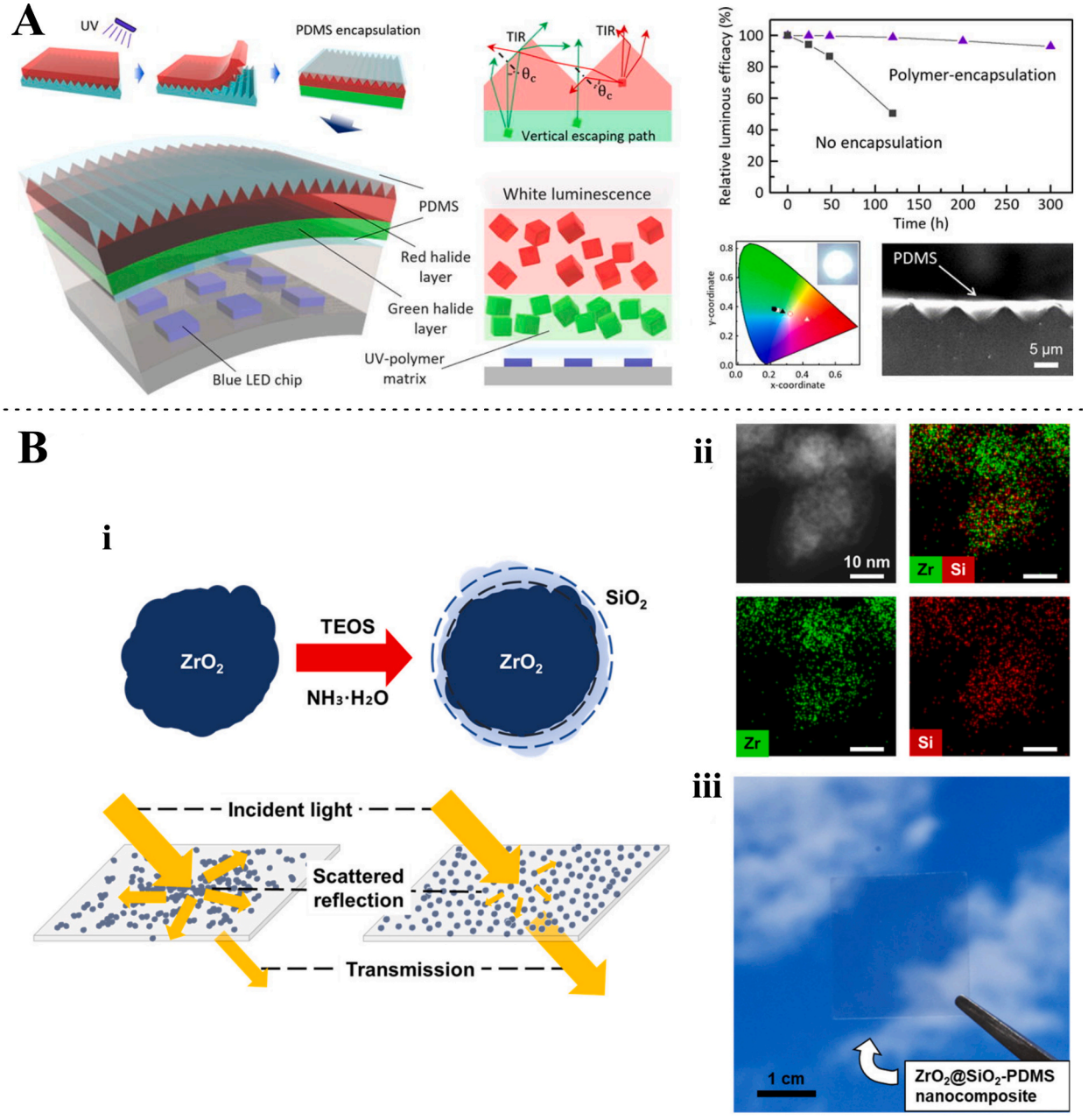

Fig. 16. (A) Fabrication of PDMS-encapsulated stacked prismatic layers of red and green halide nanocrystals dispersed in a UV-curable polymer, forming a white emitting composite with enhanced luminous efficacy and stability under blue LED excitation. Adapted from [279]; (B) i. Schematic representation of the surface modification of ZrO_2 NPs using TEOS for producing a transparent nanocomposite film with a configurable refractive index; ii. TEM-EDX images of ZrO_2@SiO_2 NPs demonstrate that a SiO_2 layer has changed the surface of the ZrO_2 NPs; iii. ZrO_2@SiO_2-PDMS nanocomposite film with a thickness of 100 nm, comprising 50 wt% ZrO_2@SiO_2 NPs. Adapted from [178,281,282].

photochemical pathways. The primary chemical degradation pathways include oxidation [307], hydrolysis of Si-O-Si backbone bonds [308], and pH-mediated changes affecting both matrix and embedded particles [309]. Physical degradation manifests as cracking under radiation exposure [310], NPs aggregation [311], and structural transformations at particle–matrix interfaces [312]. Environmental conditions often act synergistically, and the combination of elevated temperatures (85–100 °C) and high humidity (85% RH) produces the most severe degradation [311]. Photochemical pathways are particularly significant when photocatalytically active nanoparticles such as uncoated TiO_2 or Cu_2-xS generate reactive oxygen species that oxidize the PDMS matrix [313]. Critically, NPs play a dual role in optical degradation. Surface-modified nanoparticles with silica shells [313] or organosilicon coatings [314] provide protective barrier effects and suppress radical generation, while uncoated photocatalytic nanoparticles accelerate matrix degradation [313]. Concentration-dependent light scattering also reduces transparency with increasing NPs loading [287]. Degradation timelines range from hours under accelerated conditions (64.1% efficiency loss in 160 h for unprotected PDMS@QDs) [315] to years of stability with appropriate protective architectures [307], indicating that degradation rates are highly dependent on composite design and

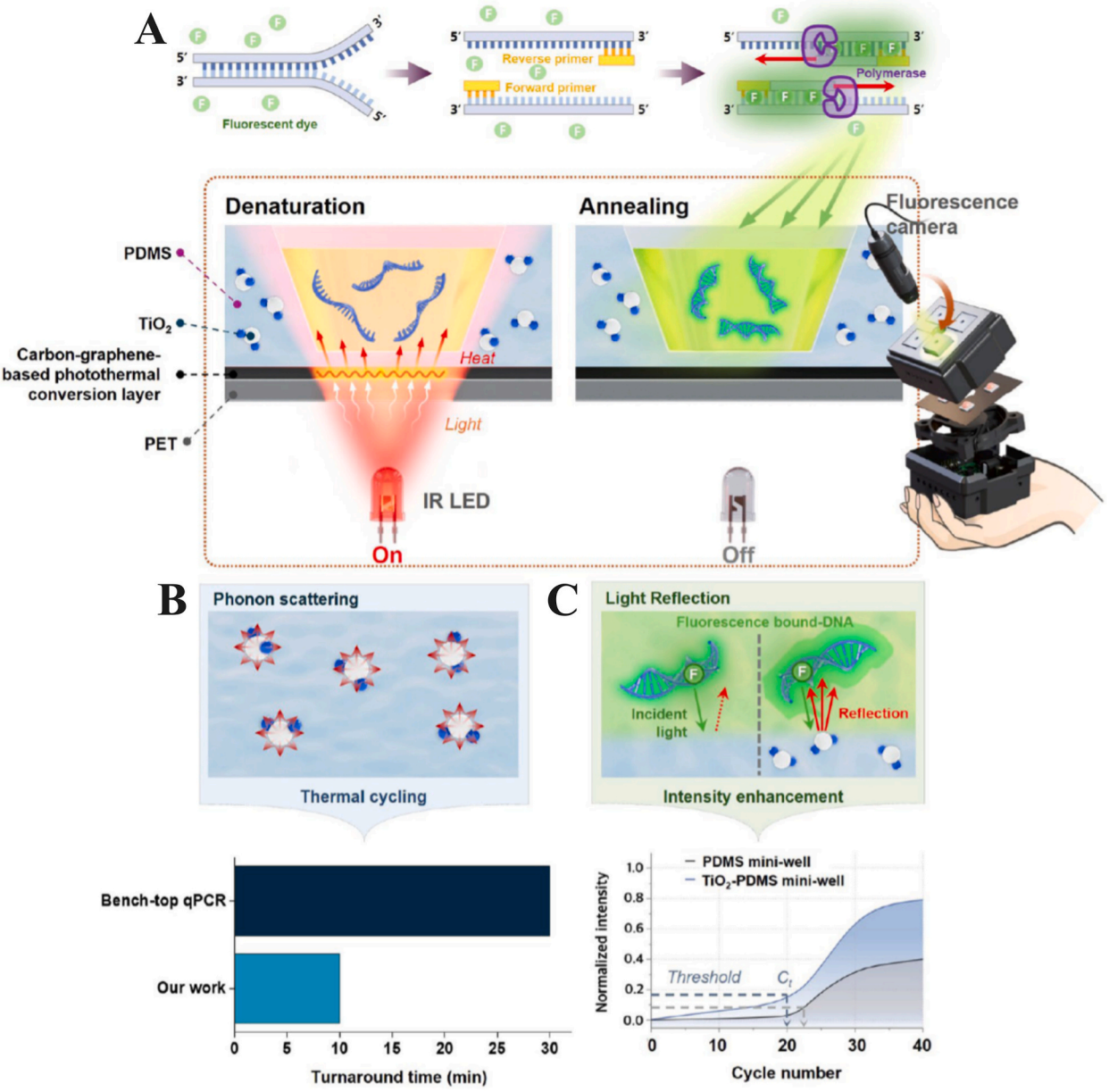

Fig. 17. Schematic representation of the (A) photonic qPCR system and data acquisition setup. The near-infrared LED (940 nm) runs photothermal cycling, while fluorescence is recorded by a detection camera. (B) Enhanced heat transfer through PDMS@TiO_2 improves cooling efficiency, and (C) reflected light increases fluorescence intensity, reducing Ct values in the qPCR analysis.
Adapted from [305].

exposure conditions rather than being intrinsic to PDMS@NPs systems.

As summarized in Table 10, representative PDMS@NPs composites demonstrate how the NPs filler characteristics (type, size, concentration, and alignment) govern the optical behavior of the resulting PDMS composites, offering insights into their tunability for specific application requirements.

4.6. Acoustic and photoacoustic properties

4.6.1. Fundamentals and mechanisms of photoacoustic generation in PDMS@NPs composites

PDMS is frequently used as a flexible matrix for photoacoustic (PA) and optoacoustic transducers due to its mechanical compliance, low acoustic impedance, and thermally expandable property [318]. However, the intrinsic optical transparency of PDMS requires the presence of light absorbing NPs to efficiently convert incident laser energy into heat and subsequently into acoustic pressure waves. The photoacoustic phenomenon occurs upon excitation of NPs in the PDMS by incident laser pulses, followed by the conversion of optical to thermal energy. The thermal energy produces local temperature rise, initiating thermoelastic expansion, and leading to transient acoustic pressure waves propagating PA signals and being picked up by ultrasound sensors. At the end, the acquired data are processed to obtain the PA signal and form high resolution PA images (Fig. 18) [319,320].

Different types of nanofillers have been explored to enhance the conversion of the incoming laser energy to heat. Plasmonic NPs (e.g. Au NPs) possess high plasmonic absorption in the visible spectrum (~540 nm), directly increasing PA conversion [321]. Carbon based nanomaterials such as CNPs [322], multiwalled carbon nanotubes MWCNTs [323], and graphene nanoflakes [324] provide a synergy of broadband optical absorption as well as high thermal diffusivity and permit high amplitude and high frequency generation of ultrasound. Semiconductor or oxide NPs, such as lead zirconate titanate (PZT) [325] and $BiMgFeCeO_6$ (BMFCO) [326], have introduced piezoelectric or multiferroic properties, for gas detection and sound detection respectively. The dependence of photothermal conversion efficiency on geometry has been studied through both numerical simulations and experiments. For instance, asymmetric plasmonic NPs tend to generate and concentrate stronger plasmonic heating at sharp tips, corners and edges due to highly enhanced electromagnetic fields [327]. A numerical work performed by Baffou et al. [328] has investigated the influence of Au morphology by quantifying the heat generation through mapping the heating power density within Au nanostructures. Additionally, experimental studies have shown geometry dependent effects in a wide range of nanostructures, including nanoplates, nanorods, nanocubes and branched nanostructures [327,329,330]. Overall, highly symmetric nanospheres and nanocubes typically exhibit strong absorption resonances, whereas low symmetry polyhedral NPs show broader and reduced absorption with multiple plasmon resonance peaks [327,331,332]. It is worth mentioning that the blackbody nanostructure proposed by Huang et al. [333] consisting of an Au nanorod coupled to an Au nanosphere, exhibits nearly perfect absorption (98–99%) %) across a wide spectral range from 400 to 1400 nm. Several fundamental equations related to photoacoustics including the thermal energy remaining in the absorber, pressure rise generated from the thermal expansion, and the photothermal conversion efficiency can be found at Vella et al. [324], Hosseinaee et al. [334] and Cui et al, respectively.

4.6.2. PDMS@NPs composites effects on acoustic properties and applications

The amplitude, frequency content, and stability of generated ultrasound are strongly influenced by NP type, concentration, morphology, dispersion quality and synthesis procedure. PDMS@Au NPs composites synthesized in alcohols exhibited high optical absorption and an improvement of 20% in PA amplitude compared to those made using acetone or water [321]. PDMS@CNP NPs coatings on optical fibers have reached a maximum pressure of 1.04 MPa with a bandwidth of 54.2 MHz, exhibiting high uniformity over probes made by means of a spin coating method [322]. Similarly, graphene nanoflake PDMS films exhibited optical absorption up to 11 MPa at laser fluences of 228 mJ cm^{-2}, with spatial confinement bigger than 40 MPa outputs which enables acoustic cavitation microbubbles in water and in tissue mimicking material such as agar phantoms [324]. Additionally, it is well known that NPs affect the generation of ultrasound frequency. For instance, graphene decorated with Au NPs dispersed in PDMS leads to a better dispersibility of the flake into the polymer matrix, which leads to an increase in a bandwidth at 6 dB up to 85 MHz and an enhanced interfacial heat transfer. Hence, the generation of high frequency and high pressure ultrasound waves enables enhanced permeabilization of biological membranes and improved imaging resolution (Fig. 19) [335].

CNT combined with self-healing PDMS (PDMS@FeHpdca), has shown the ability of achieving ultrasound pressures exceeding 25 MPa with high conversion efficiency (10.66×10^{-3}), while maintaining self-healing properties under laser or mechanical damage (Fig. 20) [336]. Piezoelectric composites (PDMS@PZT) integrated into acoustic wave resonators exhibited enhanced sensitivity for gas sensing due to their high piezoelectric charge coefficients [325]. Beyond PA generation, PDMS@NPs composites also enable multifunctional strain and acoustic sensing: PDMS@ MWCNT strain sensors detected sound waves up to 3 kHz [323], PDMS@PPyAg NPs hybrid films were able to detect changes in acoustic vibrations during normal speech [337], and PDMS@graphene–cellulose nanocrystal elastomers have the ability to recognize different subtle acoustic vibrations of syllables, such as “good” and “delight” [338]. These advances shows that the incorporation of NPs into the PDMS not only enhance the intensity and spectral control of ultrasound but also enable multifunctional applications ranging from fatigue crack detection [318], optoacoustic flow [336], invasive biomedical imaging [322], and thrombolysis [336], to human machine interfacing and wearable acoustic sensors [337,338].

4.6.3. Durability, challenges, and future directions

Despite significant advances, several challenges remain in translating PDMS@NPs acoustic composites into practical devices. Uniform dispersion of nanofillers is critical, as metal and carbon NPs have the tendency to form agglomerates. Furthermore, agglomeration increases solution viscosity due to the high concentration of the absorbers in the polymer matrix. Apart from

influencing the uniformity of the composite, it also reduces control over its thickness. As a result, the film occasionally exceeds the light penetration depth, affecting the photoacoustic signal. It is particularly difficult to attain stable water solution dispersions of carbon based materials because of their hydrophobic nature and inherent tendency to agglomerate [335,339]. High NP loading can be positive for absorption but often compromises the transparency of the PDMS matrix [338,340]. Acoustic stability upon repeated use is another constraint, since thermal degradation or nonlinear thermal effects may degrade the transducer's performance [324,341,342]. Yao et al. [323] have proposed a flexible strain sensor, based on a PDMS@MWCNTs composite film, that can detect sound waves over a wide frequency range (0–3000 Hz), recognize speech at different volume levels, and sense finger and arm bending motions, while remaining resistant to sweat and rain during various human movements. However, cyclic strains of 20% tend to cause wear at the ends of the conductive film, which can reduce conductivity and potentially degrade the sensor performance.

Table 10
Representative PDMS@NPs composites for optical properties control, summarizing NPs filler characteristics (type, size, concentration, and alignment), their effects on PDMS properties, targeted applications, associated challenges and prospects and other relevant data.

Filler characteristics	Optical properties	Effects on PDMS properties	Applications	Challenges and prospects	Other data	Ref.
ZrO_2 (13.7 nm;50 wt %, isotropic dispersion)	n increases 1.42 → 1.60; > 91% transmittance	Variation in refractive index without compromising transparency	High-index optical elastomers, coatings	Aggregation at > 50 wt% depending on the reaction time; simple synthesis and fabrication	Sol–gel incorporation with Si–O–Si linkage	[178]
ZrO_2 (3–10 nm; 20.8 vol%, homogenously, isotropic dispersion)	n up to 1.65; >93% Transmittance	Variation in refractive index without compromising transparency	Optical devices	Difficulty of large scale production	NPs functionalized with Di-amine head group and Siloxane double tail structure	[293]
TiO_2 (43 wt%; randomly distributed, isotropic dispersion)	n 1.40 → 1.56	Decrease in contact angle. Significant loss of transparency	Waveguides, led encapsulation and coating	Increasing the concentration of NPs makes the material more fragile; processing uniformity	NPs prepared *in situ* non aqueous method	[281]
Ag (dispersed on the surface)	Plasmonic dips in transmittance at 430–510 nm, corresponding to LSPR peaks	Significant color change depending on DC voltage and PDMS composition; Decrease in contact angle	Metal enhanced fluorescence to microfluidic devices or flexible tunable plasmonic substrates for SERS	Ag NPs are expensive	NPs deposited on the surface by sputtering	[282,285]
Au 3D conglomerates (distributed on surface)	Sensitivity of ~ 250 nm/RIU	Color tuning	Colorimetric sensors, SERS, LSPR based (bio)sensing	The thickness of PDMS influences the growth behavior of Au NPs and affects their optical properties	*In situ* NP reduction in PDMS	[285]
Au (0.1–0.2 wt%, isotropic dispersion)	Luminescence peak at 425 nm under UV excitation at 280 nm.	Enhanced light trapping, scattering and luminescence properties	Optical devices, light guides, scintillation detectors	Uniform dispersion, bubble formation, and scalability. improving the stability of the material	When irradiated with 2.9 MeV proton beams, PDMS with AuNPs emits blue luminescence.	[316]
$CsPbX_3$@glass	PLQY of ~ 95% and FWHM of ~ 16 nm ($CsPbBr_3$) PLQY of ~80% and FWHM of ~ 33 nm ($CsPbBr_{1.5}I_{1.5}$)	Color converter	High quality white backlight for LCD screens	Excellent resistance against water/heating	$CsPbX_3$ *in situ* nucleation/growth inside the glass matrix	[299,302]
B_2O_3/ $CsPbBr_3$@K_2SiF_6:Mn^{4+} 2,78%	Photoluminescent emission (green 521 nm)	The composite turns yellow	optoelectronics industry	Excellent resistance against water/heating	–	[299,302]
Nitrogen doped carbon quantum dots (isotropic dispersion)	Efficiently convert UV light (365 nm) emitted by an LED chip into visible light of various colors (blue, green, yellow and red)	Maintained transparency with the particles without altering the amorphous nature of the polymer	Color converting LEDs and adjustable white lighting.	Aggregation induced quenching;	Synthesis by microwaves and purification	[295,317]

PDMS@NPs composites are emerging as versatile materials as next generation multifunctional acoustic and photoacoustic materials. Emerging applications will combine plasmonic, carbon based, and piezoelectric fillers to optimize light absorption, heat transfer, and electromechanical conversion [326,343]. The development of self-healing optoacoustic materials offers a promising way to create robust and flexible ultrasound devices for biomedical applications. Merging self-healing PDMS matrices with efficient absorbers of NPs, such as CNT, can enable flexible, long term transducers to withstand high laser fluence and mechanical load, paving the way for next generation implantable, wearable, and therapeutic ultrasound technology [336]. In a study performed by Zhang et al. [336], it was observed that when the CNT concentration was below 6.7 wt%, the surface damage on the device was almost completely eliminated. In contrast, at CNT concentrations exceeding 6.7 wt%, the self-healing capability gradually weakened, resulting in only partial recovery and visible residual marks. This behavior was attributed to the availability of binding sites between internal metal ions and ligands within the self-healing PDMS. At low CNT concentrations, a greater number of binding sites between internal metal ions and ligands were preserved in the self-healing PDMS, facilitating the reformation of metal ligand coordination bonds. In contrast, excessive CNT tend to reduce the number of dynamic metal–ligand bonds, thereby compromising the self-healing process. The study further demonstrated that after physical damage, such as cutting, the self-healing PDMS patch exhibited no significant changes in both output sound pressure and signal waveform. Even after repeated cutting cycles, the patch has maintained a stable performance, provided that the damage intensity remained below the irreversible threshold of the material. In such cases, metal ions in the damaged regions remained near the ligands due to strong interactions, enabling rapid bond formation and effective self-healing. However, it was found that the patch performance tends to deteriorate under repeated thermal damage and nearly failed after 20 thermal cycles at an intensity of 50 mJ $pulse^{-1}$ for 5 min. In contrast to cutting damage, thermal breakdown has introduced both physical disruption and irreversible chemical degradation. Irreversible chemical damage accumulated with increasing damage cycles, tends to weak the patch performance by impeding the formation of metal–ligand coordinate covalent bonds. Further details on this self-healing optoacoustic material and its precursor system can be found in Zhang et al. [336] and Li et al. [344] respectively.

Scalable fabrication methods such as spin coating [322], roll to roll printing [325], and freestanding NP films [337] are being reconfigured to allow affordable bulk production. All these developments will contribute to new technological advancements in high resolution imaging, drug delivery, wearable electronics, human machine interfaces, and energy harvesting devices. Table 11, summarizes representative PDMS@NPs composites demonstrate how the NPs filler characteristics (type, size, concentration, and alignment) govern the acoustic and photoacoustic behavior of the resulting PDMS composites, offering insights into their tunability for specific application requirements.

4.7. Electrical and dielectric properties

4.7.1. Fundamentals and mechanisms of electrical and dielectric properties control in PDMS@NPs composites

PDMS is intrinsically an insulating polymer that exhibits high volume resistivity (~3.9×10^{14} Ω·cm) and a high dielectric breakdown strength (~32.2 kV/mm) [345]. This low conductivity results from its non-polar, amorphous structure, which restricts

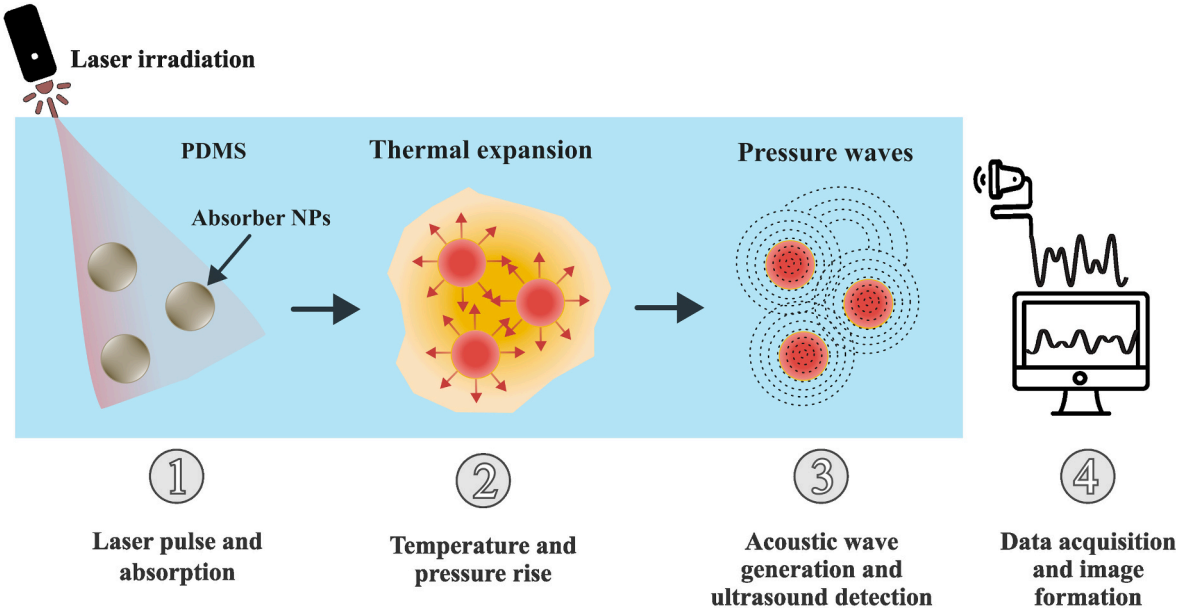

Fig. 18. Photoacoustic principle: (1) Pulsed light applied to PDMS@NPs composites and NPs absorb the light's energy; (2) Absorbed optical energy is converted into heat, resulting in a localized temperature increase, then the surrounding pressure rises through thermal expansion; (3) The generated pressure propagates as photoacoustic waves from the location of interest toward the surface and are recorded by ultrasound detectors; and (4) The acquired data are processed the PA signals are reconstructed into images.

charge mobility and prevents a long range electron transport [346,347]. Its dielectric properties are dominated by electronic and atomic polarization with minimal contribution from dipolar and interfacial polarization due to the low chain polarity [348,349]. The introduction of conductive NPs into PDMS through the preparation of PDMS@NPs composites has emerged as an active approach to promote electric conductivity and charge storage. As illustrated in Fig. 21, two main mechanisms support such improvements, namely: (a) the formation of percolating networks that establish a continuous electrical pathway between adjacent NPs, reducing the percolation threshold, thus allowing a large range conduction [350–352]; and (b) interfacial polarisation, which arises from the accumulation of charge at polymer NP interfaces, significantly enhancing the dielectric constant [353,354]. Conductive carbon fillers and metallic NPs further enhance these phenomena owing to the promotion of electron delocalization [355,356], while liquid metals (LMs) act as dynamic fillers, preserving the conductive connectivity under mechanical deformation conditions [357,358].

Other mechanisms exist, including space charge accumulation, whereby trapped or immobile charges at the filler matrix interface create local electric fields that influence bulk conductivity and dielectric properties [359]. PDMS@NPs composites overcome the intrinsic insulating nature of PDMS by providing multiple, mutually complementary charge transport and polarization mechanisms such that electrical and dielectric performance can be improved.

4.7.2. Effects of PDMS@NPs on electrical and dielectric properties and applications

The incorporation of NPs into PDMS transforms the polymer from an electrical insulator into a multifunctional material. The inherent mechanisms improve bulk electrical and dielectric properties, enabling PDMS@NPs composites to surpass pure PDMS in several applications, for instance, in energy harvesting, thermal management, and flexible energy storage.

PDMS@NPs composites are highly beneficial in energy harvesting and thermal management applications. Flexibility, translucency, and electronegativity of PDMS allow simple integration with NPs to fabricate high performance triboelectric nanogenerators (TENGs) (Fig. 22 **A**) [360]. The operational mechanisms of TENG based on the integration of triboelectric effects and electrostatic induction can be found in the review by Zhou et al. [361]. In addition to TENGs, PDMS is used in passive daytime radiative cooling. In nanoporous polyethylene (nanoPE)/bilayer PDMS textiles, infrared emissivity within the 8–13 μm atmospheric transparency window is enhanced by the transparent PDMS top layer to enable sub ambient cooling under non input of external energy [361,362]. This results from the intrinsic Si–O–Si and Si–C vibrational modes of PDMS, and scalability and automatability of the fabrication process ensure industrial feasibility [361].

Metal NPs, such as Ag NPs, highly enhance dielectric behavior of pure PDMS. The incorporation of 20 wt% Ag NPs increases PDMS dielectric permittivity from 5.3 to 16.9 at 1 kHz with triboelectric performance of short circuit currents of 5.1 μA, open circuit voltages of 33.6 V, and peak power outputs of 72.2 μW at 8 MΩ load, compared to negligible responses in the case of the pure PDMS [356]. LMs

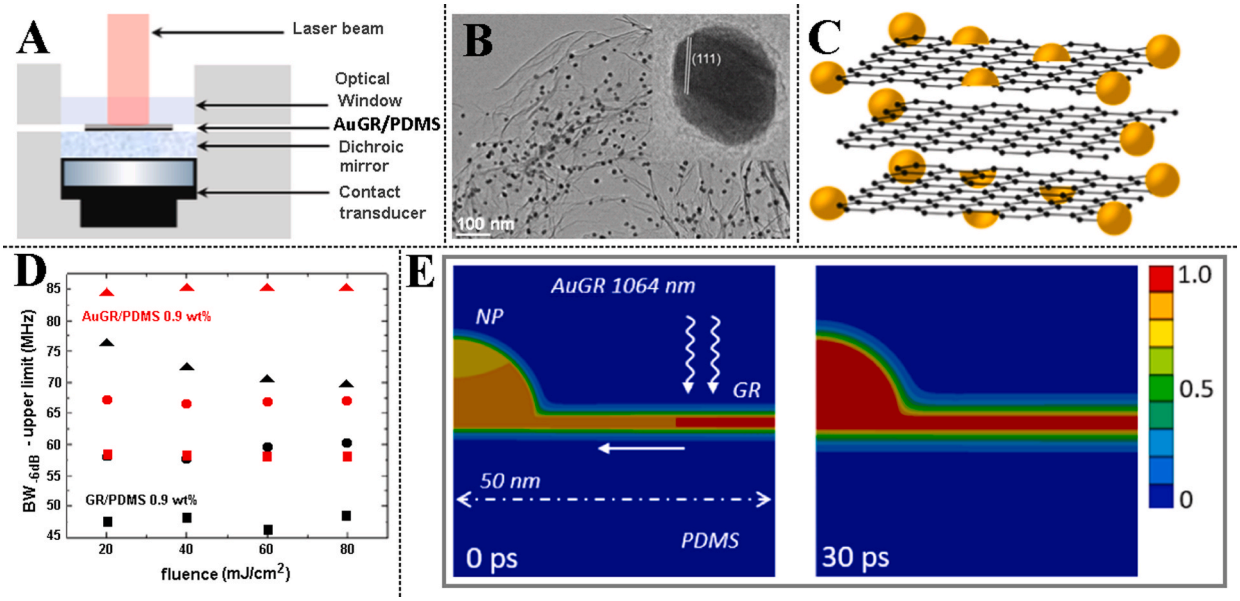

Fig. 19. Photoacoustic generation of ultrasound using graphene (GR) nanoflake composites decorated with gold NPs (Au NPs): (A) Illustration of the experimental setup used to detect high frequency ultrasound signals generated by laser irradiation; (B) TEM image showing graphene flakes decorated with Au NPs; (C) Illustration showing the surface decoration of a few layers of graphene, where polymer chains are intercalated between the flakes; (D) Bandwidth at 6 dB upper limit as a function of the laser fluence for GR (black) and AuGR (red) 0.9 wt%, and for four different film thicknesses: 17 μm (square), 11 μm (circle) and 9.5 μm (triangle). (E) Computational simulations showing a few graphene layers (1.65 nm thick) with an embedded gold NP (radius 12.5 nm) surrounded by PDMS (50 × 50 nm), where at a time of 0 ps the laser irradiates GR and at 30 ps the absorber is almost fully thermalized.
Adapted from [335].

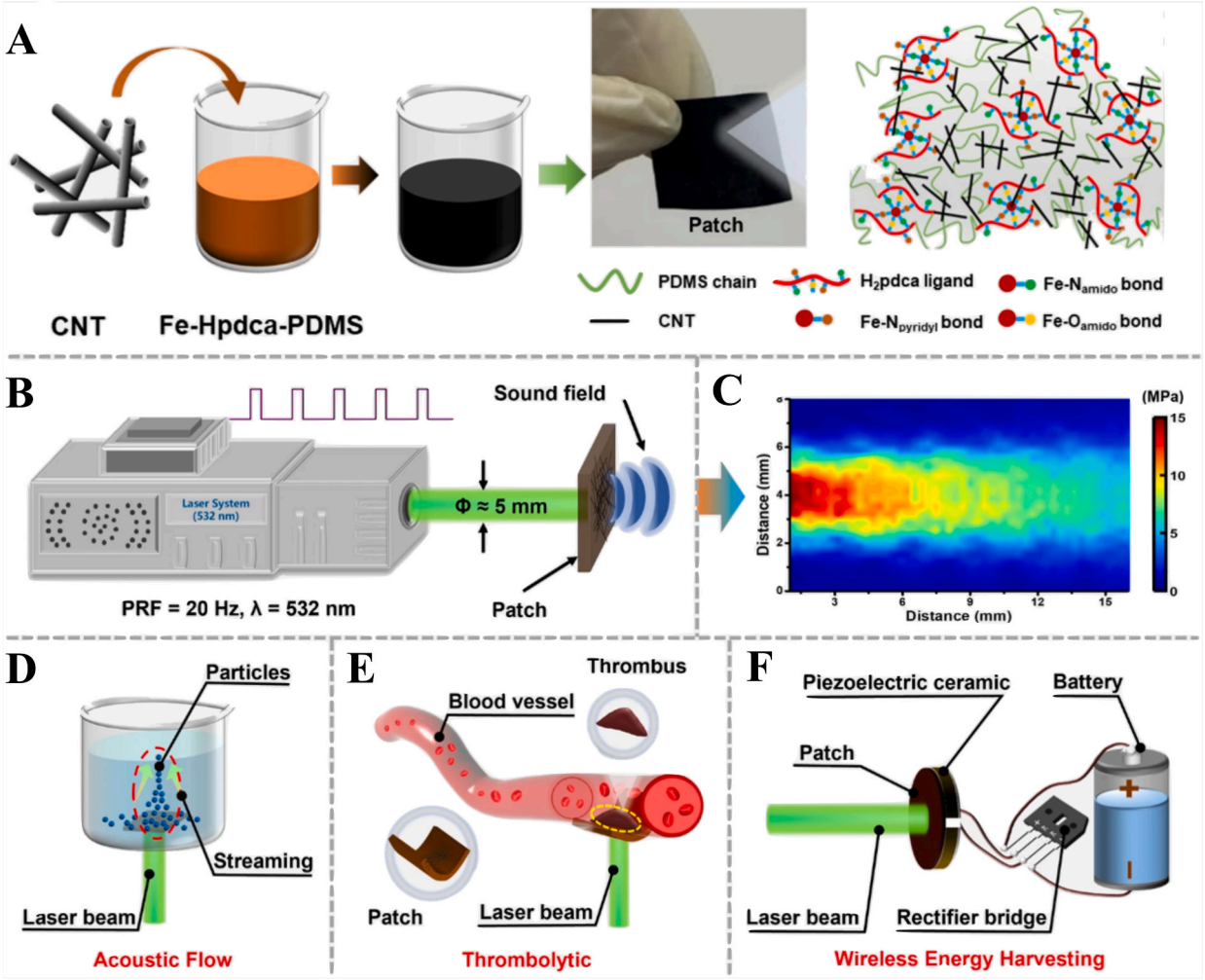

Fig. 20. (A) Fabrication of a self-healing optoacoustic flexible patch by mixing light absorbing material (CNTs) with thermally expandable PDMS@FeHpdca matrix. (B) Optoacoustic patch under pulsed laser irradiation (532 nm). (C) Effective acoustic energy output generated by the patch. The practical applicability of the patch was evaluated through the performance of several experiments, including acoustic flow (D), thrombolysis (E), and wireless energy harvesting (F) [336].

Table 11
Representative PDMS@NPs composites for acoustic and photoacoustic properties control, summarizing NPs filler characteristics (type, size, concentration, and alignment), their effects on PDMS properties, targeted applications, associated challenges and prospects and other relevant data.

Filler properties	Acoustic and photoacoustic properties	Effects on PDMS properties	Applications	Challenges and prospects	Other data	Ref.
Lead zirconate titanate (PZT) NPs (~560 nm; random)	Piezoelectric FPW response; frequency shift with gas absorption	Enables piezoelectric effect in PDMS; improved acoustic response	CO_2 gas sensors; acoustic transducers	Frequency drift due to humidity and gas absorption	Mechanically mixed and dispersed in PDMS prepolymer; cured to flexible piezoelectric film	[325]
Graphene nanoflakes with Au NPs (~25 nm Au; 20 wt% on GR)	Bandwidth 85 MHz (−6 dB); enhanced PA signal strength	Improved thermal interface and PA efficiency; higher heat dissipation in PDMS	High resolution PA imaging; biological membrane permeabilization	Complex fabrication; cost of AuNPs	AuNPs decorated on graphene, then mixed into PDMS; vacuum degassed and cured	[335]
Polypyrrole (PPy)/Ag NPs (~50 nm; uniformly dispersed)	Sensitive acoustic detection of vocal vibrations (qualitative)	Ag NPs increased electrical conductivity, cycling stability and mechanical compliance; improved strain sensing	Flexible sensors; wearable electronics; human machine interfaces; recover speech from vocal damage	Complex fabrication; potential oxidation of AgNPs, bending tolerance of about 1050 cycles	*In situ* polymerization of PPy/AgNPs in PDMS matrix to form conductive film, high reproducibility and stability for the stretching and recovering tests, monitor respiration and real time pulse wave (0 to 60 mA)	[337]
CNTs (0–3.03 wt%; size n/s; random)	Grüneisen coefficient ≈0.72; acoustic impedance 1.02–1.13 MRayl	Enhanced acoustic impedance matching and optical attenuation	Dual mode optical/ ultrasound imaging, *in vivo* imaging	High cost; dispersion uniformity limits reproducibility	Ultrasonic/mechanical mixing of CNTs in uncured PDMS; highest performance at 1.52% CNTs-PDMS coating	[343]
Candle soot NPs (Size n/s; random alignment)	Nonlinear surface acoustic wave (SAW) generation; light absorption	Improved SAW intensity and SNR; promotes efficient wave propagation through PDMS	Non-destructive crack detection	Requires precise laser alignment; limited to microscale fatigue detection	CSNPs dispersed directly in PDMS prepolymer and thermally cured	[318]
CNPs (30 nm; 15 wt%; uniform distribution)	PA output 1.04 MPa; bandwidth 54.2 MHz	High light absorption; stable PA response	Optical fiber PA probes, high resolution ultrasound imaging	Limited scalability; dependent on spin coating precision	CNPs mixed in PDMS base with solvent assisted dispersion and degassing	[322]
Au NPs (<100 nm; random distribution)	Optical absorption peak ≈540 nm; PA amplitude + 20% vs. pure PDMS	Enhanced optical absorption and PA conversion efficiency	Fiber optic PA transducers; microfluidic devices	Risk of agglomeration; reduced uniformity at high loading	Au NPs ultrasonically dispersed in PDMS prepolymer; cured via spin coating	[321]
MWCNTs (10–20 nm dia., 0.5–2 μm length) + magnetic NPs (~1 μm); aligned under magnetic field	Acoustic detection range 0–3000 Hz	Enhanced sensitivity, linearity and stretchability; Superhydrophobic and self-cleaning ability	Flexible stretchable sensor; sound and human motion detection, electronic skin of bionic robots.	Complex fabrication; Repeated stretching wears the film and reduces the film's conductivity.	Magnetic field assisted alignment of CNTs within PDMS during curing	[323]
Graphene nanoflakes (0.6–1.2 nm; 0.7–1.1 wt%; random distribution)	PA amplitude 11 MPa; confined ultrasound of high amplitude (> 40 MPa); bandwidth 21.5 MHz	Improved PA amplitude and optical absorption;	Cavitation therapy; sonophoresis-based NPs drug delivery, photoacoustic medical devices	Saturation at high fluence due to Grüneisen parameter decrease	Controlled protocol to obtain well dispersed layers of graphene nanoflakes in the PDMS matrix	[324]
CNTs (8 nm dia., 20 μm length); Fe–Hpdca self healing PDMS	Ultrasound output > 25 MPa; efficiency 10.66×10^{-3}	Self-healing at room temperature; enhanced mechanical strength and PA output	Biomedical ultrasound; thrombolysis; acoustic flow; wireless energy harvesting	High cost; thermal and mechanical degradation limits performance	CNTs blended into PDMS@FeHpdca via dynamic covalent bonds; physical or thermal damage does not significantly degrade both output sound pressure and signal waveform	[336]

also offer a different alternative, with high inherent conductivity (~3.4×10^6 S·m^{-1} in eutectic gallium–indium) and mechanical deformability, with dielectric enhancement under strain and stretchable electronic devices (Fig. 22 **B**) [358,363].

Carbon based nanofillers, including graphene nanoplatelets (GNPs) and reduced graphene oxide (RGO), establish extended conductive networks within PDMS. The use of GNP foams was reported to improve conductivity from 13.5 S·m^{-1} at 0.15 vol% to 30.4 S·m^{-1} at 0.24 vol%, while the hybridization with LMs even strengthened the networks with sustained mechanical integrity [33]. Similarly, RGO coated fibers on polyurethane/polyester scaffolds have demonstrated conductivity improvements from 0.012 to 0.136 S·m^{-1} with multiple dip coating cycles [364]. These findings indicate the effectiveness of carbon-based fillers in developing light, high conductivity composites.

Crucially, NPs morphology plays a decisive role in governing charge percolation, as it dictates the efficiency with which conductive networks are established. This structural parameter is intrinsically linked to the overall performance profile of the composite, particularly in terms of thermal conductivity enhancement and mechanical robustness. 1D fillers, (such as CNTs, nanofibres, or metallic nanowires) are widely recognised for their effectiveness in achieving electrical percolation [365,366], significantly reducing the percolation threshold (p_c), defined as the minimum concentration required for the transition from insulating to conductive behaviour. Their inherent waviness or tortuosity further promotes three–dimensional contact and facilitates electron tunnelling across narrow gaps [365], thereby ensuring continuity within the conductive network. In terms of thermal transport, 1D fillers consistently outperform plate–like or brick–like counterparts, with reported thermal conductivity enhancement (TCE) ratios approaching 4.5 compared to approximately 1 for lower–aspect–ratio morphologies [367]. Nevertheless, these advantages come with processing challenges: high filler loadings increase matrix viscosity, hinder uniform dispersion, and may induce aggregation, creating structural defects that compromise tensile strength and reduce film integrity [365].

At the opposite end, 0D fillers (e.g., carbon black or spherical SiO_2) are generally less efficient percolators [368,369] and therefore require higher volume fractions to reach a continuous charge-transport network [365,366]. Their elevated surface area and surface energy promote agglomeration, which disrupts homogeneity and diminishes thermal conductivity enhancement compared to well–dispersed systems [369]. Moreover, clustered 0D particles act poorly as rigid reinforcements, often reducing overall mechanical strength and toughness relative to composites in which fillers are uniformly distributed.

2D sheet–like morphologies—such as graphene platelets or nanosheets—occupy an intermediate position between these extremes. Characterised by one nanoscale dimension and two extended lateral dimensions, they offer large interfacial areas and readily form extensive network structures, achieving relatively low p_c values compared to spherical fillers, though typically higher than those observed for high–AR 1D materials [368]. Regarding thermal performance, platelet-like or sheet-like morphologies exhibit comparatively lower TCE than rod-like 1D structures [367]. For instance, the enhancement factor for platelet, brick, or polygonal shapes is approximated at a ratio of 1 compared to the 4.5 factor observed for CNTs/nanowires [367]. However, the incorporation of 2D fillers introduces its own complexities: achieving optimal dispersion and alignment within the polymer matrix remains a significant challenge, and poor control over these parameters can result in fillers acting as mechanical weaknesses [368].

Moreover, attempts to enhance electrical conductivity by elevating filler content sometimes lead to compromises that could undermine the overall mechanical integrity of the nanocomposite. These trade-offs are extensively established in effective medium theories like as Maxwell-Garnett and Bruggeman, which describe how filler shape and volume fraction influence the composite's dielectric and conductive properties [370]. While these models provide useful predictive frameworks, they also emphasize the drawbacks of pushing systems towards percolation thresholds, where conductivity increases are accompanied by higher dielectric

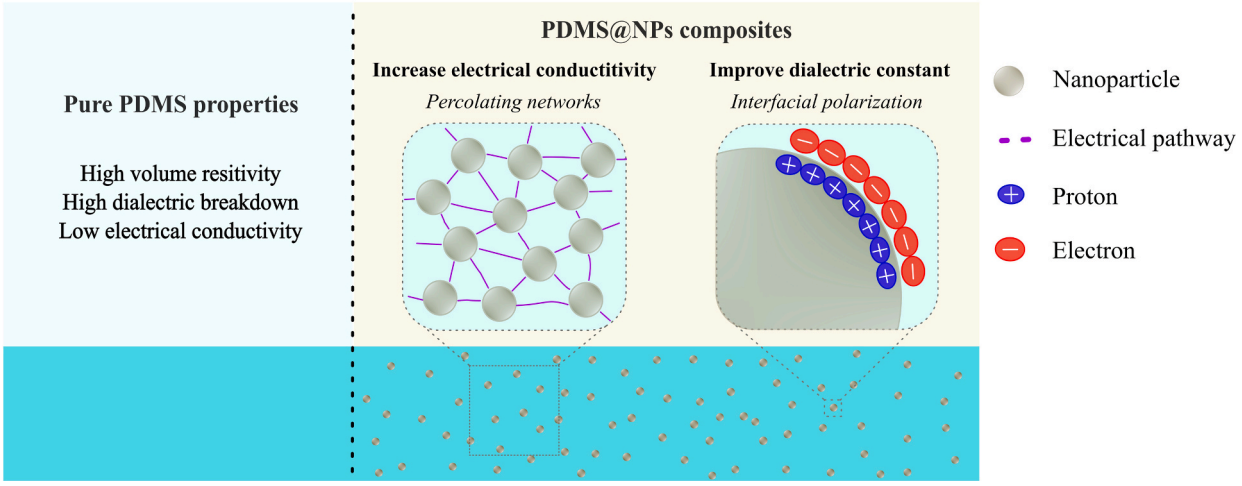

Fig. 21. Schematic representation comparing the intrinsic electrical properties of pure PDMS with the mechanisms responsible for enhanced performance in PDMS@NPs composites. On the left, pure PDMS exhibits high volume resistivity, high dielectric breakdown strength, and low electrical conductivity due to its non-polar, amorphous structure. On the right, PDMS@NPs composites demonstrate two key improvements: formation of percolating networks, which establish continuous electrical pathways between NPs, thereby increasing electrical conductivity; and interfacial polarisation, resulting from charge accumulation at polymer NP interfaces, which contributes to an increased dielectric constant.

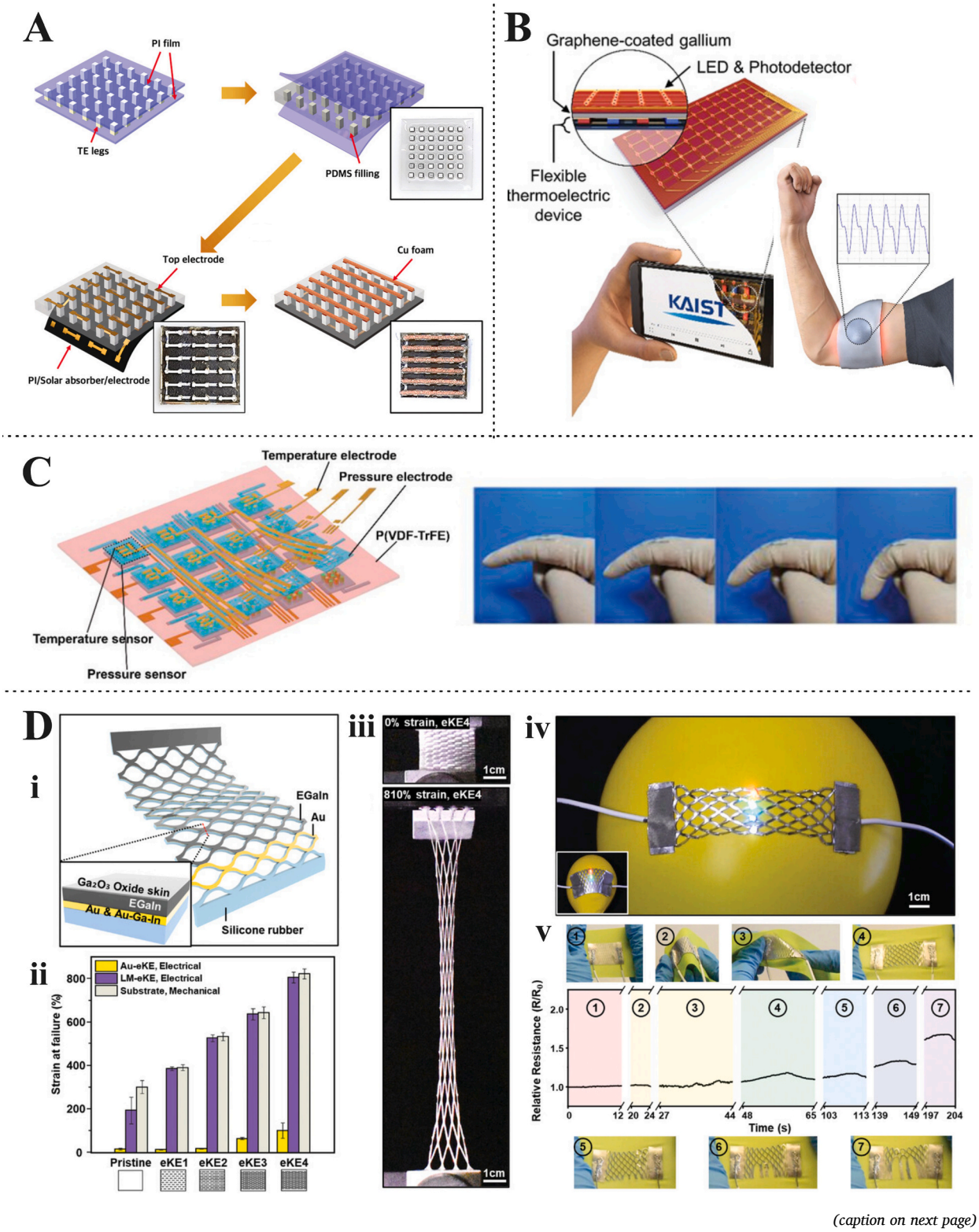

(caption on next page)

Fig. 22. Interdisciplinary research on F-TEDs. (A) Schematic and optical images showing the fabrication process of sunlight assisted F-TEDs. Adapted from [289]. (B) Schematic representation of a wearable, three dimensional piezoelectric/thermoelectric dual-mode tactile sensor array designed for electronic skin (e-skin) applications. Adapted from [290]. (C) Interface engineering between graphene and F-TEDs for developing an innovative adaptive electronic system capable of fast, bidirectional stiffness modulation. Adapted from [291]. (D) i. Schematic of the liquid metal based elastic kirigami electrode (LM-eKE) and its cross sectional view; ii. Comparison of the electrical and mechanical failure thresholds between the gold coated electrode (Au-eKE) and LM-eKE; iii. Images of LM-eKE under 0% strain and 810% strain; iv. Image of the LM-eKE attached to both an uninflated balloon (inset) and a fully inflated balloon powering interconnected LEDs; v. Changes in resistance of the LM-eKE on natural rubber under various mechanical deformation and damage conditions. Adapted from [292].

losses and structural instability.

Pure PDMS is an ideal base for sensors used in smart textiles, soft robotics, and monitoring systems. For instance, a wearable 3D architecture piezo/thermoelectric bimodal tactile sensor array for electronic skin (e-skin) applications has been developed, designed to empower robots with tactile capabilities and for human health monitoring (Fig. 22 **C**) [360]. Stretchable conductors are fabricated by coating and encapsulating graphene platelets (GnPs) with PDMS, allowing them to be bent and stretched robustly (Fig. 22 **D (iii, iv)**) [371]. PDMS based flexible resistive strain sensors exhibit varying elasticity based on their microstructure and sensing components [372]. Composites with Ag nanowire PDMS@networks, carbon black PDMS@NPs, and PDMS@EGaIn can achieve stretch abilities of 60–100%, while CNT films can reach up to a strain of 280% [372]. Biodegradable and breathable leaf vein based tactile sensors with adjustable sensitivity have also been explored [362]. LM based flexible/stretchable mechanical and motion sensors include ultra-sensitive strain sensors with a brick and mortar architecture, highly sensitive pressure sensors with knotting structures, and LM based elastic kirigami electrodes **(**Fig. 22 **D (i))** [373].

PDMS@NPs composites improve stretchable and flexible energy storage devices too. Incorporating tungsten oxide coated Ag nanowires (WO_3@AgNW) into PDMS increases adhesion, mechanical stability, and resistance to repeated bending and stretching induced delamination [374]. PDMS is also used as a substrate, encapsulant, and protective matrix for current collectors such as PDMS@Au/AgNW [33,374], while LM polymer composites embedded in polyacrylamide-hemicellulose matrices serve as flexible zinc ion battery anodes with performance being maintained under mechanical stress and extended cycling [33]. LM particle containing PDMS based hydrogels are also being investigated for use in flexible supercapacitors, providing electrochemical performance along with mechanical flexibility [33,375].

4.7.3. Durability, Challenges, and future directions

PDMS@NPs composites are mechanically flexible and retain electrical and dielectric performance after repeated pressing, bending, and stretching cycles [33,362,371,372]. These features support their use in wearable and flexible devices. Nonetheless, long term stability remains an issue, particularly in wearable electrochromic energy storage devices and thermoelectric devices, where delamination, filler dissociation, and one dimensional metallic nanowire oxidation can destabilize performance, and liquid electrolytes can evaporate or leak upon bending [374]. By using core shell materials such as Au/Ag nanowires and self-healing polymer matrices have been reported to recover structural integrity, enhance durability, and extend device lifetimes [12,362,374]. Thermoelectric devices made from sponge and textiles indicate that properly designed composites can withstand hundreds of bending or flex cycles and thousands of compression cycles to support wearable systems with good robustness [360].

Moreover, low cost, scalable fabrication is an ongoing issue. Metallic nanowire weak adhesion, filler agglomeration, and surface buckling may compromise uniformity [356,376]. Inkjet and screen printing are scalable methods to produce flexible films but usually are limited to single function devices and are based on high cost, specially nanofluids [374,375,377]. Electrostatic spray deposition, additive manufacturing, and hierarchical assembly are alternative methods for multifunctional composites with modulated microstructure, but further optimization is needed [361,374].

Environmental and biocompatibility considerations are critical for wearable and implantable applications. PDMS provides inherent biocompatibility, while organic and hybrid thermoelectric materials offer low toxicity and lightweight alternatives [12,360]. New directions include integration of smart sensing, self reporting, and ionic thermoelectric capability in PDMS composites [12,360,362], under computational design and machine learning for electrical, thermal, and mechanical property optimization [361]. Additional progress toward nanofluid design, surfactant engineering, and hierarchical filler structures should enhance performance and reliability further [377]. Combined, these developments will overcome current constraints to render PDMS@NPs composites as a strong platform for next generation flexible electronics, energy harvesters, and wearable bioelectronics.

As summarized in Table 12, representative PDMS@NPs composites demonstrate how the NPs filler characteristics (type, size, concentration, and alignment) govern the electrical and dielectric behavior of the resulting PDMS composites, offering insights into their tunability for specific application requirements.

5. Tunable structure–property relationships in PDMS@NPs composites

The previous sections have shown how NPs can be incorporated into PDMS to enhance specific physicochemical properties. However, when these materials are designed for practical applications, improvements in each property are rarely isolated. Changes in filler morphology, loading or interfacial interactions that enhance one functionality often influence others, sometimes in an unfavorable way. In this section, these interdependencies are discussed to deepen the understanding of durable structure–property relationships in PDMS@NPs composites, focusing on comparative trends, intrinsic trade-offs, and strategies commonly employed to balance multifunctional requirements. Table 13 summarizes representative examples that illustrate how the enhancement of a target

property in PDMS@NPs composites is often accompanied by secondary effects on other functionalities.

As shown in Table 13, a single design parameter rarely affects only one material property and usually influences multiple properties simultaneously. Once fillers begin forming pathways, anchoring the network, or restructuring the surface, the composite response shifts across transport, mechanics, optics, and wettability in ways that are difficult to separate.

5.1. Mechanical nanoreinforcement

Single-walled carbon nanotubes (SWCNTs) can be effective mechanical reinforcements in PDMS, even at ultra-low loadings, increasing elastic modulus, hardness, and contact stiffness while also reducing spatial variability in surface mechanics. In the reported study, silane-functionalized SWCNTs form Si–O–Si linkages with the PDMS network, improve dispersion and interfacial adhesion and reduce point-to-point variance [388]. The same 1D networks that carry stress can also support electromechanical function. SWCNT films transferred onto PDMS can be tuned to behave either as strain insensitive stretchable electrodes ($\Delta R/R_0$ ~0.05–0.07 up to 40% strain) or as highly sensitive strain gauges (gauge factor ~ 20 at 100% strain), depending on the prestretching/transfer protocol [389]. In this work, the trade-off is the optical property, as SWCNT networks become more continuous, light scattering/absorption increases and transparency decreases, as visible both in the thin-film conductor study [389] and in nanoindentation driven reinforcement, making optical transparency the most consistent penalty when mechanical and electrical gains are pursued simultaneously [388].

5.2. Thermal conductivity

A recurring trend across PDMS@NPs systems is that increasing filler concentration raises thermal conductivity but also increases Young's modulus, resulting in higher rigidity and reduced elongation capacity [219]. NPs, especially those with elongated geometries (e.g., dendritic structures), can facilitate heat conduction by enabling phonon transport along the major direction and improving the probability of forming connected pathways. By contrast, spherical particles do not provide preferential transport directions and typically exhibit minimal interparticle contact area, which limits phonon transfer between fillers. These same characteristics, however, may result in losses in mechanical performance, particularly as loading and connectivity increase. By creating more continuous pathways, alignment can also increase the dielectric permittivity while maintaining low dielectric loss when insulating fillers such as Al_2O_3 and BN are used [242]. h-BN and related 2D morphologies are therefore attractive for thermal management in PDMS, but improvements in heat dissipation are typically accompanied by reduced deformability as stiffness increases with network formation. An interesting case of interfacial synergy is vinyl-grafted h-BN, where the grafted vinyl groups participate in PDMS hydrosilylation, so the filler can simultaneously densify the network (anchoring sites that raise tensile and compressive strength) while enhancing heat dissipation and delaying thermal decomposition [167]. The trade-off remains consistent, as BN loading rises, elongation at break and tensile compliance decline. Similar alignment strategies in mixed ceramic systems (e.g., Al_2O_3 combined with BN to control dielectric properties while enhancing thermal conduction) confirm the principle that directed pathways amplify heat flow but progressively tax flexibility as the volumetric fraction and connectivity increase [242]. If the aim is to increase both thermal and electrical conductivity, conductive fillers can further improve thermal transport by enabling electron transport through percolated pathways, in addition to phonon-mediated contributions [218]. Specific filler attributes can also be exploited to access additional functions. For example, Co-based NPs can induce magnetic losses, enabling composites that, in addition to improved thermal performance, also serve as EMI shields [244].

5.3. Wettability

SiO_2 NPs can deliver synergistic surface effects in PDMS by combining low surface energy with hierarchical roughness, promoting a Cassie–Baxter wetting state and durable water repellency. At the same time, rigid inclusions can increase hardness and modulus and reinforce tensile strength when dispersion and coupling to the silicone matrix are adequate. For instance, in the work performed by Cordoba et al. [167], the incorporation of 8 and 10 wt% SiO_2 have increased the Vickers hardness, elastic modulus, and tensile strength while maintaining surface hydrophobicity virtually unchanged. The NPs act as rigid reinforcements that transfer mechanical stresses and reduce plastic deformation, while the in-situ sol–gel approach supports dispersion quality and helps to preserve surface properties. In multifunctional coatings, the same architecture has also been reported to support self-cleaning, corrosion resistance, antifouling, and antibacterial performance [387]. A regular trade-off is the optical property. For instance, in the study by Lu et al., wettability increased significantly for larger diameters of particles at low concentrations, but optical transmittance dropped dramatically at higher loadings due to light scattering [386]. Overall, SiO_2 PDMS coatings can combine wettability control, chemical stability, and mechanical reinforcement, balanced against a transmittance penalty that is strongly size- and structure-dependent.

5.4. Optical performance

In PDMS@NPs composites, improving optical performance often introduces trade-offs with thermal and mechanical properties. High-index or plasmonic NPs enhance refractive-index modulation and optical absorption but can increase photon and phonon scattering, thereby reducing transparency and modifying heat transport pathways [293]. Metallic NPs can further promote photothermal conversion via plasmonic heating, yet local temperature rises under prolonged illumination, and can induce localized heating, which raises practical constraints for mechanical integrity and long-term stability [284]. Increasing filler loading also constrains polymer chain mobility, raising stiffness at the expense of elasticity. Consistent with this, ZrO_2 is reported to be a high-index route but

Table 12
Representative PDMS@NPs composites for electrical and dielectric properties control, summarizing NPs filler characteristics (type, size, concentration, and alignment), their effects on PDMS properties, targeted applications, associated challenges and prospects and other relevant data.

Filler characteristics	Electrical and dielectric properties	Effects on PDMS properties	Applications	Challenges and prospects	Other data	Ref.
Ag NWs (Aligned network Embedded thin film between PDMS layers)	Sheet resistance ≈ 18 Ω·sq^{-1}; GF 2–14	Improves strength, elasticity; resists oxidation when embedded	Stretchable strain sensors, EESD electrodes	Oxidation, delamination under bending	Durable: 14% ΔR after 1000 cycles @70% strain	[374,376]
GnP (Random planar Coated/encapsulated with PDMS)	High conductivity; sheet R ≈ 1100 Ω·sq^{-1} at 25% strain	Enhances elasticity, sensitivity, fast recovery	Wearable/stretchable sensors and conductors	Sharp resistance increase past ~17.5% strain	Stable up to 550 cycles	[371]
CNTs (variable conc. Random/partial alignment Direct dispersion or patterned deposition)	Thermoelectric $S^2\sigma$ ≈ 2.85–250 μW·m^{-1}·K^{-2} reported	Adds strength, conformability; durable on skin	Flexible electronics, thermoelectric/strain devices	Variability from defects/ geometry	Serpentine interconnects via photoresist patterning	[360,361,372,374]
Ag, Cu, Al, Zn, Sn (~30–50 nm; 20 wt %; Random dispersion)	Ag/PDMS (20 wt%) showed Isc 5.1 μA, Voc 33.6 V	Increases permittivity (5.3 → 16.9 @1 kHz)	TENGs, energy harvesting sensors	Agglomeration at high loadings (≥20 wt%)	Probe sonication + RT curing; Power ≈72 μW @10Hz	[356,361]
CuNWs (AR≈100–1000; ≤4.1 vol%; Random network)	> 3 × thermal k at 4.1 vol% (vs PDMS)	Improves heat spreading and thermal management	TIMs, flexible electronics substrates	Surface oxide, interfacial thermal resistance	Direct mixing + curing @85 °C; Linear k–loading relation	[378]
LMNPs (22.1 vol%; Random network)	σ ≈ 35.15 S·m^{-1}; thermal k + 1133% (foam)	Flexible dual network; strong EMI shielding (~40.8 dB)	EMI shielding, stretchable electrodes	Leakage (fluidity) needs binders/encapsulation	PVA assisted anchoring (salt template; Lightweight porous foam	[33,373]
Au, Ag, alloys (conc. n/s; confined film)	High connectivity (no σ given)	PDMS confinement → smaller NPs, narrow size dispersity	LSPR / SERS optical sensors	High T dewetting, complex patterning	Thermal dewetting under PDMS; Particle size ↓ with PDMS thickness	[379]
AuNPs/AgNPs (conc. n/s)	Rapid photothermal heating (> 100 °C under LED)	Enables *in situ* NP formation; photothermal effects	Photothermal microfluidic pumps, sensors	Solvent control and NP surface modification needed	Deposition in uncured PDMS; optimal solvents: 2-butanone (Au), IPA (Ag). Cure~80 °C,30 min	[380]
$BiMgFeCeO_6$ multiferroic particles (size n/s; wt % varied; random distribution)	Highest electrical output of 17 V and 38 nA; 3.8 V and 10 nA (wrist exercise); 4.9 V and 19.3 nA (clapping motion); sound detection (qualitative)	Electrical output of the piezoelectric is enhanced by the oriented polarization of the particles	Biomechanical energy harvesting, sound detection;	Complex fabrication, Undefined particle size; difficult to eliminate stress-induced magnetic anisotropy	Particles were blended into the polymer to form a flexible PDMS composite film; capacitor charging over several cycles has shown long-term stable and durable electrical output	[326]
Gold NPs (Au NPs), Spherical, 10 nm diameter. Loadings typically 0.1 wt% to 0.3 wt%	Conductivity up to 1.0 × 10 $^{-9}$ S·cm^{-1}. Dielectric constant (ϵ_1) between 1.6 and 2.6. Resistivity drops by > 3 orders under 90% strain	Increased radiation resistance. Drastic stiffness reduction (Young's modulus in kPa range). Optical shift to violet via LSPR	Capacitive/resistive pressure sensors. Optical waveguides. Selective thermal ablation of tumours	Thermal aggregation alters plasmonic peaks. Shrinkage saturation in lithography. Microbubbles (10–80 μm)	Fabricated via sugar-template leaching. Porosity levels of 65–79%	[381–383]
Ni–PDMS (Ni^{2+} complex) (conc. n/s; No alignment; Metal–ligand coordination)	Insulating matrix; self-healing electrical damage	Intrinsic self-healing of electrical breakdown (EB)	Self-healing insulation & packaging	Slow healing (~5 days); limited studies	Healing based on Ni^{2+} coordination; can repair holes/cracks and electrical trees	[12]

Table 13
Synergistic and trade-off effects observed in PDMS@NPs composites.

NP and morphology	Target property enhancement	Secondary property effects (trade-offs)	Functional role and structural features	Main applications	Ref
Al_2O_3 (800 nm, spherical) (0D) + BN (5um, flaky) (2D)	↑ Thermal conductivity	↑Dielectric permittivity; ↓ Optical transparency	Alignment/organization increases dielectric permittivity; low dielectric loss due to ceramic fillers	Thermal management for miniaturized electronic equipment	[242]
Au Spherical (0D)	↑ Optical absorption	↓ Wettability	Au NPs exhibit surface plasmon resonance (SPR), which enhances the optical absorption of the PDMS matrix	Optics; electronics; biomedicine; material science	[284]
Au-nanostars (0D)	↑ Thermal conductivity	↓ Optical transparency and mechanical robustness	Au nanostar (5–6 sharp branches), which lead to the absorption of NIR light, enables rapid temperature increase, and prevents biofilm formation.	Antibacterial and anti-biofilm surfaces for medical devices	[384]
(Ba,Ca) $(Ti,Zr)O_3$ + Cu nanorods (1D)	↑ Thermal conductivity	↑Current density; ↓ Optical transparency	Alignment enables the transfer of both thermal phonons and electric current	Low-power wearables; self-powered sensors	[218]
$BiMgFeCeO_6$ multiferroic particles (0D)	↑ Electrical and dielectric	↑ Flexibility	Electrical output enhanced by oriented polarization of particles	Biomechanical energy harvesting; sound detection	[326]
CNT (1D) / Co (0D) (Fiber decorated)	↑ Thermal conductivity	↑EMI shielding	Co magnetic properties and combined architecture support heat transport and EM attenuation	Humanized and precision electronic device	[244]
CNTs (1D)	↑ Photoacoustic image	↑ Optical image	Optimized CNTs-PDMS (~1.52%) balances low ultrasound loss with high light sensitivity	Dual mode microscopy; *in vivo* imaging	[210]
CNTs with Fe–Hpdca self-healing PDMS (1D)	↑ Photoacoustic	↑ Mechanical and electrical	CNT absorption and thermoelastic expansion enhances optoacoustic conversion; Fe-Hpdca crosslinked network yields high strength/ tensile properties	Ultrasound biomedical devices; acoustic flow; wireless energy harvesting	[336,344]
Cu (10–25 μm spheroidal; <45 μm dendritic) + Ni (3–7 μm; <45 μm) (0D) + BN (150 nm)	↑ Thermal conductivity	↓ Optical transparency; ↓Mechanical properties	Increasing particle volume fraction strengthens thermal pathways but also stiffens PDMS	TIM	[219,317]
Graphene / Nanoplates (GNPs) (Platelet/ Sheet, 2D)	↑ Electrical conductivity; ↑dielectric constant	↑Enhances rigidity ↑ Young's modulus; ↑ ultra-high thermal conductivity	The high aspect ratio, combined with high intrinsic conductivity, facilitates the formation of conductive pathways	Shielding against Electromagnetic Interference; 3D electrochemical biosensors and energy storage devices; flexible & recyclable conductive composites with self-healing capacity.	[368,385]
GOQDs/Si-GOQDs (0D)	↑ Water Barrier Properties	↑ Fluorescence	Compact/dense Si-GOQD layer reduces accessible diffusion sites for water	Food packaging; biomedical devices; bioimaging; optoelectronics	
h-BN (2D)	↑ Thermal conductivity	↓ Flexibility	Vinyl groups on h-BN undergo hydrosilylation with PDMS, thereby increasing crosslink density. Acts as an anchoring site, improving tensile and compressive strength. Delays thermal decomposition and improves heat dissipation.	Protective coatings for cement-based substrates (e.g., mortar and concrete) in harsh environments	[154]
MWCNTs (1D) + Fe_3O_4 (0D)	↑ Flexibility (via PDMS ratio optimization)	↑ Hydrophobic capability; ↑ acoustic detection	PDMS ratio 13:1 optimizes flexibility; micro-nano bulges enable superhydrophobic and self-cleaning; microcracks improve sensitivity, linearity and stretchability	Sound and motion sensors; e-skin; sweat/rain resistant	[323]
MWCNTs (tubular; ~9.5 nm × ~1.5 μm) (1D)	↑ Electrical conductivity and sensitivity	↑ Elastic modulus; ↓ Extensibility; ↓ Sensitivity at high loadings; ↑ Local aggregation;	Percolative conductive network; elongational flow (CBER) refines/ reconstructs network and mitigates aggregation.	Strain sensors	[211]

(*continued on next page*)

Table 13 (*continued*)

NP and morphology	Target property enhancement	Secondary property effects (trade-offs)	Functional role and structural features	Main applications	Ref
PPy (2D) / Ag NPs films (0D)	↑ Acoustic detection of vocal vibrations	↑ Electrical conductivity	PPy provides a uniform and large area to immobilize Ag NPs, enhancing electrical conduction	Flexible sensors; wearable electronics; human–machine interfaces; speech recovery	[337]
SiO_2 (0D)	↑ Wettability	↓ Optical transmittance	Larger NP favors Cassie–Baxter; high roughness scatters light (worse transmittance)	Self-cleaning; glass/ functional films	[386]
SiO_2 (0D)	↑ Wettability	↑ Mechanical (Vickers hardness, elastic modulus, and tensile strength)	Rigid NPs act as reinforcements within PDMS	Robust insulating coatings	[167]
SiO_2 (0D)	↑ Wettability	↑ Mechanical; ↑ Chemical stability; ≈ Optical Transparency	Low surface energy and adhesion and reinforced structure improve strength and chemical stability	Self-cleaning; corrosion resistance; anti-fouling; antibacterial	[387]
SWCNT (1D)	↑ Mechanical stiffness and hardness	↓ Optical transparency	Functionalized SWCNT improves elastic modulus, hardness and contact stiffness of PDMS; enhances localized stiffness and reduces variance in mechanical properties	Wearable electronics and flexible Sensors; biomedical devices; electromechanical systems	[388]
SWCNT (1D)	↑ Thermal conductivity	↓ Optical transparency	SWCNT films (~40 nm thick) provide high electrical conductivity and mechanical flexibility	Stretchable and transparent electronics; strain sensors; stable stretchable electrodes	[389]
ZnO nanotubes (1D)	↑ Electrical conductivity	↓ Flexibility	Enhance triboelectric effect and modify PDMS permittivity; contribute to charge generation during friction and deformation	High output nanogenerator for energy harvesting from mechanical motions	[142]
ZrO_2 (0D)	↑ Refractive index	↓ Transparency (if agglomerated)	High n (~2.2) increases PDMS refractive index (1.39 → 1.65)	High-index optical elastomers; lenses; coatings, light-guiding	[293]

with transparency loss if agglomeration occurs, whereas spherical Au increases optical absorption via SPR while reducing wettability [284,293]. Embedding Au-nanostars in PDMS illustrates how optical absorption can be translated into thermal functionality for medical surfaces, i. e., the reported morphology enables near-infrared absorption, rapid temperature increase, and antibiofilm performance [384]. At the same time, increasing nanostar loading to maximize the photothermal effect typically reduces optical transmittance and may compromise mechanical robustness.

5.5. Photoacoustic performance

In PDMS@NPs composites, enhancement of photoacoustic performance is closely linked to secondary effects on optical, thermal, mechanical, and electrical properties. Photoacoustic efficiency relies on strong optical absorption and efficient thermoelastic expansion; therefore, carbon based and plasmonic nanofillers such as CNTs or Au NPs are commonly used to increase the optoacoustic conversion efficiency [324,336]. Optical absorption and acoustic output are frequently improved by increasing nanofiller loading. However, it also introduces trade-offs, such as decreased optical transparency, increased viscosity, and limited control over film thickness, which can limit light penetration and degrade signal uniformity [324,338,340]. Thermal effects introduce additional trade-offs, i.e., efficient photothermal conversion enhances acoustic pressure generation, but the local temperature that rises under high laser fluence can induce nonlinear thermal behavior, attenuate the Grüneisen coefficient of PDMS, and reduce long-term acoustic stability during repeated operation [324,336,341,342]. Approaches to mitigate these trade-offs include optimizing nanofiller morphology and concentration, as well as incorporating multifunctional polymer networks. For instance, Xu et al. [343] have optimized the PDMS@CNT composite in order to enhance the sensitivity to the optical signals without compromising the sensitivity of the ultrasound detection. The incorporation of self-healing PDMS matrices further exemplifies how photoacoustic enhancement can be improved without sacrificing mechanical and electrical properties. While CNTs improve optical absorption and acoustic pressure generation, dynamic metal–ligand coordination networks preserve mechanical integrity and allow the material to recover after damage, as long as the nanofiller concentrations remain below a critical level [336,344]. Overall, these examples highlight that maximizing photoacoustic performance in PDMS@NPs composites requires balancing absorption, thermal stability, and mechanical reliability through careful control of nanofiller morphology and loading.

5.6. Electrical conductivity

Several examples in Table 13 show that electrical conductivity in PDMS@NPs composites is closely linked to the network formation. It therefore tends to couple strongly with stiffness, extensibility, and often optical transparency. For instance, ZnO nanotubes increase electrical output in triboelectric systems by improving the triboelectric effect and changing PDMS permittivity. This

contributes to charge generation during friction and deformation. However, the reported trade-off involves reduced flexibility [142]. Similarly, aligned (Ba,Ca)(Ti,Zr)O_3–Cu nanorods systems promote both phonon and electron transport. This results in better thermal conduction and current density, while reducing optical transparency [218]. CNT–Co fillers show an additional functional relationship, as related magnetic losses enable EMI shielding while the composite structure supports thermal transport. However, excessive filler loading and connectivity can compromise the mechanical compliance [244]. In CNT-filled PDMS, electrical conductivity typically increases sharply once the percolation threshold is reached. This is accompanied by high piezoresistive sensitivity due to the formation of continuous conductive networks. At moderate loadings, good nanotube dispersion helps network formation and increases physical entanglement between nanotubes (MWCNTs) and PDMS chains. This leads to higher elastic modulus and mechanical strength. However, at high concentrations, severe local aggregation changes network topology, reduces extensibility, and compromises electrical sensitivity. This change is attributed to the competing rupture and reconnection mechanisms of the conductive network under strain [211]. The multiferroic compound $BiMgFeCeO_6$ uses elongational flow processing as an important strategy to effectively address the trade-off between conductivity and extensibility. This method supports a uniform dispersion and helps to create strong conductive networks with multiple parallel pathways. As a result, it allows for efficient biomechanical energy harvesting in a device made with 10 wt% BMFCO and PDMS (PENG10). This device can maintain a high electrical output of 17 V while still being fully rollable and mechanically flexible. In this way, the composite can maintain high conductivity and sensitivity, a wide detection range, and limit aggregation at high loadings, while maintaining superior mechanical performance and cyclic stability [211]. Therefore, elongational flow processing is considered a critical design variable in several studies.

5.7. General considerations

Overall, these examples indicate that multifunctionality in PDMS@NPs composites is constrained by coupled transport and interfacial mechanisms and cannot be achieved by increasing filler loading alone. Across PDMS@NPs systems, increasing NP concentration is associated with concurrent increases in mechanical rigidity and thermal conductivity, so a balance becomes necessary when high elongation and high mechanical properties are both required [219]. In this context, hybrid filler strategies (combined particles rather than a single filler type) are often proposed to improve thermal transport while attenuating mechanical losses [208,361].

Beyond composition, Table 13 also highlights three practical levers that repeatedly shape whether synergies can be retained or trade-offs become dominant. First, interfacial coupling can alter the efficiency of load transfer, phonon transport, or charge transfer; for example, silane-functionalized SWCNTs improve adhesion and mechanical uniformity [388], and vinyl-functionalized h-BN participates in PDMS hydrosilylation, increasing crosslink density while enhancing heat dissipation [154]. Second, shape and connectivity govern pathway formation, i.e., percolated 1D carbon networks permit electromechanical functioning but diminish optical transparency [389], while 2D ceramic fillers promote thermal transfer but penalize deformability [154]. Third, alignment serves as a multifaceted technique, facilitating concurrent enhancements in heat transport and dielectric permittivity within ceramic systems [242] and promoting integrated phonon/electron transport in aligned hybrids [218]. Finally, the optical parameters impose stringent limitations on numerous applications. Adding metallic fillers to enhance thermal performance (e.g., Au morphologies) often compromises high optical transparency, making optical transparency a frequently critical design criterion [284].

6. Conclusions and outlook

The continuous evolution of PDMS@NPs composites through nanoscale engineering has transformed silicone elastomers from passive encapsulants into adaptive, multifunctional materials that combine flexibility, optical transparency, and responsive functionality. Recent advances further demonstrate that this transformation is not only chemistry-driven but also critically governed by NPs morphology and interfacial architecture. The macroscopic performance of these composite systems arises mainly from the interplay between PDMS chemistry, NPs identity, particle geometry (0D, 1D, and 2D aspect ratios), and incorporation strategy, which collectively govern dispersion homogeneity, interfacial adhesion, and structure property relationships.

The direct mixing process to incorporate NPs into PDMS remains the simplest and most scalable method for composite fabrication, yet agglomeration and limited interface strength restrict property uniformity. In contrast, *in situ* synthesis within cured or uncured PDMS matrices provides stronger chemical anchoring and morphological control, offering enhanced mechanical and functional stability but often at the cost of process complexity and limited to scale up. Recent studies further highlight that filler aspect ratio and alignment during processing can partially mitigate these limitations by enabling percolated networks at lower loadings. Developing advanced fabrication methods that couple interfacial engineering with scalable processing will be essential to the successful transition of PDMS@NPs composites from laboratory prototypes to large scale applications. A key outcome of this review is that interfacial chemistry is the fundamental control variable correlating NPs morphology, processing, and macroscopic performance in PDMS@NPs composites. The inherent chemical mismatch between apolar PDMS and polar or electronically active NPs demands careful interphase engineering involving covalent anchoring, dynamic or coordinative bonding, and non-covalent interactions. The interphase character dominates stress transfer, phonon transport, surface energy, optical and plasmonic coupling, photoacoustic conversion, and electrical percolation, often imposing trade-offs between robustness and adaptability. Additionally, in this review, we have focused on elucidating the structure property relationships in PDMS@NPs composites and the interaction mechanisms between NPs and polymer chains that enable the tunable enhancement of several properties, as outlined below.

(1) Mechanical behavior

The incorporation of NPs improves significantly the mechanical integrity of PDMS, helping to overcome its inherent softness and limited fracture strength. The surface modification by SiO_2, Al_2O_3, or carbon-based fillers promote stronger polymer filler coupling through covalent or hydrogen bonded interfaces, improving both stress transfer efficiency and fatigue life. Several studies have shown that high-aspect-ratio 1D and 2D fillers tend to achieve reinforcement more efficiently than spherical fillers by forming load-bearing networks at lower volume fractions. Recent strategies using dynamic bonds and polydentate ligands further introduce reprocessability and autonomous self-healing under mild conditions. However, the complex relationship between filler content, crosslink density, and viscoelastic relaxation highlights the need for predictive models to optimize toughness without sacrificing elasticity.

(2) Thermal conductivity

The intrinsic low thermal conductivity of PDMS (0.12 to 0.35 W/m K) can be increased by over an order of magnitude through the introduction of high conductivity fillers such as Al_2O_3, BN, graphene, or hybrid carbon ceramic networks. Furthermore, the incorporation of 3D fillers also results in superior thermal conductivity when compared to one- and two-dimensional fillers. Additionally, making continuous phonon pathways via 3D porous or aligned architectures minimizes interfacial thermal resistance and enables efficient heat dissipation. The interface of NPs also has a great influence, with its functionalization allowing for a decrease in the thermal contact resistance as well as facilitating the formation of percolation networks. The high thermal performance of the PDMS@NPs composites presents great potentials in a wide variety of fields including thermal management and storage in electronic and biomedical devices. However, excessive filler loading, or rigid percolation networks often compromise transparency and stretchability. Advanced surface functionalization and gradient architectures are therefore critical to balance phonon transport with mechanical compliance.

(3) Wettability and surface energy

Nanostructuring the PDMS surface with oxide NPs, (SiO_2, TiO_2, or mixed SiO_2–TiO_2), enables the wettability to be tuned from superhydrophilic to superhydrophobic. These materials effectively manipulate surface properties, with controlled roughness and energy modification producing contact angles exceeding 160° while maintaining high transparency (~97%). Recent durability-focused studies have shown that long-term wettability retention depends strongly on NP anchoring and resistance to UV-induced or mechanical degradation. It was reported, a maximum contact angle above 150° even after numerous abrasion cycles and stability across a wide pH range. These features enable applications such as self-cleaning, anti-fogging, and drag reduction. However, high NP loadings or high temperature treatments are often used, and as a result it can deteriorate both flexibility and optical transparency. Emerging approaches based on low energy plasma activation, layer by layer assembly, or fluorine free coatings show promise for more sustainable and durable wettability control.

(4) Optical functionality

Optical functionality can be optimized through NPs incorporation while maintaining PDMS flexibility and transparency. The incorporation of high index (ZrO_2, TiO_2) or plasmonic (Au, Ag) NPs allows a precise adjust of refractive index values and develop new capabilities for luminescence, color manipulation and refractive index detection. Several studies have shown that NPs geometry and size distribution critically govern scattering, plasmonic coupling, and long-term optical stability. The key design challenge lies in suppressing Mie scattering that arises when the particle dimensions approach the wavelength of incident light. Precise dispersion and refractive index matching between filler and matrix remain crucial to preserve $>$ 90% transmittance. Standardized film thickness, wavelength range, and haze is still needed to compare optical data reliably. Multifunctional composites integrating mechanical elasticity with optical responsiveness can offer a pathway toward stretchable lenses, adaptive coatings, and flexible waveguides. Overall, the optical performance and durability of PDMS@NPs composites are governed not by the presence of NP alone but by the deliberate control of their geometry, dispersion, surface chemistry, and loading, which together determine the balance between transparency, field enhancement, and long-term stability under environmental and photochemical stresses.

(5) Acoustic and photoacoustic functionality

PDMS composites have revealed a huge potential for efficient light to sound conversion through the incorporation of optically absorbing NPs. The most effective fillers include Au NPs, CNT, and graphene nanoflakes, achieving photoacoustic pressures bigger than 40 MPa and bandwidths up to 85 MHz and as a result enhances interfacial heat transfer. Several studies indicate that NP morphology and interfacial thickness directly regulate heat-to-pressure conversion efficiency and signal bandwidth. Beyond opto-acoustic efficiency, the integration of self-healing PDMS matrices enables robust and flexible ultrasound devices. CNT filled self-healing PDMS has been shown to maintain stable acoustic output after repeated mechanical damage when CNT concentrations remain below 6.7 wt%, due to preserved dynamic metal–ligand coordination bonds. Higher CNT loadings reduce available binding sites and weaken the self-healing response. Despite challenges such as NPs aggregation and dispersion uniformity, PDMS@NPs composites have shown potential in applications such as biomedical imaging, therapeutic ultrasound, acoustic flow control, thrombolysis, wearable sensors, and energy harvesting. The NPs composition optimization, dispersion methods, and scalable fabrication techniques will further enhance their performance and will lead to the successful translation of the next generation of optoacoustic devices.

(6) Electrical and dielectric performance

The addition of conductive and semiconductive fillers has transformed PDMS from a simple insulating elastomer into a genuinely functional material for flexible and stretchable electronics. Networks built from CNTs, graphene, silver nanowires, or mixed metal oxide structures allow charge to move efficiently while the elastomer still stretches far beyond its original shape. At the same time, dielectric fillers such as $BaTiO_3$, TiO_2, and AlN increase permittivity and lower dielectric losses, making PDMS suitable for high output triboelectric and piezoelectric generators. The dielectric response of PDMS composites depends on their structure and processing. Increases in permittivity with low dielectric losses are typically linked to interfacial polarisation, while processing conditions and filler morphology can introduce non-linear responses that are useful for sensing and energy applications but remain difficult to reproduce without standardised protocols. Recent studies have shown that filler aspect ratio governs percolation thresholds, dielectric nonlinearity, and electromechanical coupling. Current work is moving toward the development of PDMS@NPs composites with integrated smart sensing, self-reporting and ionic thermoelectric functions, optimized by computational and machine learning approaches. In addition, progress in surfactant engineering and hierarchical fillers will enhance PDMS@NPs composite performance, positioning them as a robust materials platform for the next generation of soft electronic and energy harvesting technologies.

Although PDMS@NP composites have advanced substantially in recent years, several challenges still limit their practical use. Interfacial stability under repeated mechanical or thermal stress remains insufficiently understood and achieving uniform NP dispersion on an industrial scale continues to be difficult due to viscosity and mixing issues. The need to balance stiffness, transparency, and conductivity often forces arrangements that restrict multifunctional optimization. In addition, most processing methods still depend on solvents and non-recyclable matrices, causing environmental concerns. PDMS@NP composites also lack common characterization protocols, which makes it difficult to compare results between laboratories and to build reliable structure property databases.

Moving forward, progress will depend on environmentally friendly, solvent free fabrication methods and on recyclable PDMS matrices that reduce environmental impact. Combining multiscale modeling with knowledge-based design could help link molecular structure, interfacial chemistry, and overall performance. Experimental techniques, such as spectroscopy, microscopy, and scattering under mechanical or thermal load, should be more widely used to reveal how interfaces evolve in real time. Establishing standardized testing frameworks will also be vital for significant comparison of mechanical, thermal, electrical, and optical data. Taken together, these directions point to a future where PDMS@NPs composites become reliable, reconfigurable, and sustainable materials linking to polymer chemistry, nanoscience, and soft matter mechanics. Their continued progress is likely to redesign flexible electronics, soft robotics, biomedical systems, and adaptive photonic technologies, approaching silicone-based materials well beyond their traditional limits.

CRediT authorship contribution statement

B.D. Cardoso: Writing – original draft, Methodology, Data curation, Conceptualization. **G. Nobrega:** Writing – original draft, Investigation, Data curation, Conceptualization. **I.S. Afonso:** Writing – original draft, Data curation. **A. Souza:** Writing – original draft, Data curation, Conceptualization. **L.B. Neves:** Writing – original draft. **C.L. Faria:** Writing – original draft. **J.L. Diaz de Tuesta:** Writing – original draft, Validation. **J.E. Ribeiro:** Writing – review & editing, Supervision, Funding acquisition, Conceptualization. **R. A. Lima:** Writing – review & editing, Validation, Supervision, Resources, Project administration, Funding acquisition, Conceptualization.

Declaration of competing interest

The authors declare that they have no known competing financial interests or personal relationships that could have appeared to influence the work reported in this paper.

Acknowledgments

The authors acknowledge the partial financial support of the project 2022.06207.PTDC (https://doi.org/10.54499/2022.06207.PTDC), COMPETE2030-FEDER-00771500 and COMPETE2030-FEDER-00689800 through national funds (OE), within the scope of the Scientific Research and Technological Development Projects (IC&DT) program in all scientific domains (PTDC), through Fundação para a Ciência e Tecnologia (FCT). The authors also acknowledge the partial financial support by national funds through FCT/MECI/MCTES (PIDDAC): MEtRICs, UID/04077/2025; CEFT, UID/00532/2025; CMEMS, UID/04436/2025; CIMO, UID/00690/2025, UID/PRR/00690/2025, SusTEC LA/P/0007/2020 and LA/P/0045/2020. Glauco Nobrega acknowledges the financial support by the doctoral grant PRT/BD/153088/2021 (https://doi.org/10.54499/PRT/BD/153088/2021), financed by FCT, and with funds from MCTES/República Portuguesa, under the MIT Portugal Program. Inês Afonso and Lucas Neves acknowledge the financial support by FCT, of the doctoral grant 2024.05919.BDANA and 2025.00900.BDANA, respectively. Andrews Souza acknowledges financial support from FCT, under grant reference 2021.07961.BD (DOI: https://doi.org/10.54499/2021.07961.BD). J.L. Diaz de Tuesta acknowledges the financial support through the program of Atracción al Talento of Comunidad de Madrid (Spain) and Consolidación Investigadora 2024 of Agencial Estatal de Investigación for the individual research grants 2022-T1/AMB-23946 and CNS2024-154264, respectively.

Data availability

Data will be made available on request.

References

[1] Brook M. The chemistry and physical properties of biomedical silicones. Biomaterials in Plastic Surgery 2012:52–67.
[2] Strohle G, Tan C, Li H, Mohanty AK, Misra M. Classification of Biomaterials and Surface Strategies. Surface Engineering of Biomaterials: CRC Press. p. 105-33.
[3] Kharwade R. Polymers in implant medical devices. Materials Research Foundations 2025;172.
[4] Owen MJ. Silicone surface fundamentals. Macromol Rapid Commun 2021;42:2000360.
[5] Katsoulis DE, Schmidt RG, Zank GA. Siloxanes and silicones (advances in silicone technologies 2000–15). organosilicon compounds. Elsevier; 2017. p. 301–22.
[6] Kowalewska A, Majewska-Smolarek K. Self-healing antimicrobial silicones—mechanisms and applications. Polymers 2023;15:3945.
[7] Zare M, Ghomi ER, Venkatraman PD, Ramakrishna S. Silicone-based biomaterials for biomedical applications: antimicrobial strategies and 3D printing technologies. J Appl Polym Sci 2021;138:50969.
[8] Zhu Q, Wang Z, Zeng H, Yang T, Wang X. Effects of graphene on various properties and applications of silicone rubber and silicone resin. Compos A Appl Sci Manuf 2021;142:106240.
[9] Bian P, Wang Y, McCarthy TJ. Rediscovering Silicones: the anomalous water permeability of “hydrophobic” PDMS suggests nanostructure and applications in water purification and anti-icing. Macromol Rapid Commun 2021;42:2000682.
[10] Liu S, Liu S, Wang Q, Zuo Z, Wei L, Chen Z, et al. Improving surface performance of silicone rubber for composite insulators by multifunctional Nano-coating. Chem Eng J 2023;451:138679.
[11] Šesták J, Duša F, Týčová A, Přikryl J, Foret F. Miniaturization and microchips. liquid chromatography. Elsevier; 2023. p. 647–77.
[12] Yang X, Huang W, Dong H, Zha JW. Smart polydimethylsiloxane materials: versatility for electrical and electronic devices applications. Adv Mater 2025;37:2500472.
[13] Warrick E, Lauterbur P. Filler phenomena in silicone rubber. Industrial & Engineering Chemistry 1955;47:486–91.
[14] Bueche A. Filler reinforcement of silicone rubber. J Polym Sci 1957;25:139–49.
[15] Boonstra B, Cochrane H, Dannenberg E. Reinforcement of silicone rubber by particulate silica. Rubber Chem Technol 1975;48:558–76.
[16] Xia Y, Whitesides GM. Soft lithography. Angew Chem Int Ed 1998;37:550–75.
[17] Giri K, Tsao C-W. Recent advances in thermoplastic microfluidic bonding. Micromachines 2022;13:486.
[18] Paul J, Sindhu S, Nurmawati M, Valiyaveettil S. Mechanics of prestressed polydimethylsiloxane-carbon nanotube composite. Appl Phys Lett 2006;89.
[19] Khosla A, Gray B. Fabrication of multiwalled carbon nanotube polydimethylsiloxne nanocomposite polymer flexible microelectrodes for microfluidics and MEMS. SPIE 2010.
[20] Goyal A, Kumar A, Patra PK, Mahendra S, Tabatabaei S, Alvarez PJ, et al. In situ synthesis of metal nanoparticle embedded free standing multifunctional PDMS films. Macromol Rapid Commun 2009;30:1116–22.
[21] Lima RA. The impact of polydimethylsiloxane (PDMS) in engineering: recent advances and applications. Fluids 2025;10:41.
[22] Takayama S, McDonald JC, Ostuni E, Liang MN, Kenis PJ, Ismagilov RF, et al. Patterning cells and their environments using multiple laminar fluid flows in capillary networks. Proc Natl Acad Sci 1999;96:5545–8.
[23] Shevkoplyas SS, Yoshida T, Gifford SC, Bitensky MW. Direct measurement of the impact of impaired erythrocyte deformability on microvascular network perfusion in a microfluidic device. Lab Chip 2006;6:914–20.
[24] Faivre M, Abkarian M, Bickraj K, Stone HA. Geometrical focusing of cells in a microfluidic device: an approach to separate blood plasma. Biorheology 2006;43:147–59.
[25] Lima R, Wada S, Tanaka S, Takeda M, Ishikawa T, Tsubota K-i, et al. In vitro blood flow in a rectangular PDMS microchannel: experimental observations using a confocal micro-PIV system. Biomed Microdevices 2008;10:153–67.
[26] Zhang Q, Xu J-J, Liu Y, Chen H-Y. In-situ synthesis of poly (dimethylsiloxane)–gold nanoparticles composite films and its application in microfluidic systems. Lab Chip 2008;8:352–7.
[27] Scott A, Gupta R, Kulkarni GU. A simple water-based synthesis of Au nanoparticle/PDMS composites for water purification and targeted drug release. Macromol Chem Phys 2010;211:1640–7.
[28] Kim HJ, Huh D, Hamilton G, Ingber DE. Human gut-on-a-chip inhabited by microbial flora that experiences intestinal peristalsis-like motions and flow. Lab Chip 2012;12:2165–74.
[29] Rafeie M, Zhang J, Asadnia M, Li W, Warkiani ME. Multiplexing slanted spiral microchannels for ultra-fast blood plasma separation. Lab Chip 2016;16:2791–802.
[30] Gao Y, Ota H, Schaler EW, Chen K, Zhao A, Gao W, et al. Wearable microfluidic diaphragm pressure sensor for health and tactile touch monitoring. Adv Mater 2017;29:1701985.
[31] Kim DH, Jung MC, Cho S-H, Kim SH, Kim H-Y, Lee HJ, et al. UV-responsive nano-sponge for oil absorption and desorption. Sci Rep 2015;5:12908.
[32] Souza R, Nobrega G, Afonso IS, Pereira J, Cardoso E, Marques F, et al. Thermal performance evaluation of pure PDMS and PDMS composites heat exchangers. J Therm Anal Calorim 2025;1–12.
[33] Zhang Y, Yang S, Liu Y, Gu T, Liu F. Dual network structures of PDMS-based composite foam via anchoring liquid metal nanoparticles for improved thermal conductivity and electromagnetic interference shielding performances. J Mater Chem A 2024;12:27527–39.
[34] Zhai G, Qi L, He W, Dai J, Xu Y, Zheng Y, et al. Durable super-hydrophobic PDMS@ SiO2@ WS2 sponge for efficient oil/water separation in complex marine environment. Environ Pollut 2021;269:116118.
[35] Liu F, Feng F, Ji Y, Peng J, He L, Cui J. Stretchable polydimethylsiloxane/aligned electrospun cellulose acetate nanofibers composites with high transparency and fracture resistance. Polym Compos 2024;45:3120–30.
[36] Huang C, Bian Z, Fang C, Zhou X, Song J. Experimental and theoretical study on mechanical properties of porous PDMS. J Appl Mech 2018;85:041009.
[37] Zhu J, Wang M, Zhang H, Yang S, Song K-Y, Yin R, et al. Effects of hydrophilicity, adhesion work, and fluid flow on biofilm formation of PDMS in microfluidic systems. ACS Appl Bio Mater 2020;3:8386–94.
[38] Liu H, Fu R, Su X, Wu B, Wang H, Xu Y, et al. Electrical insulating MXene/PDMS/BN composite with enhanced thermal conductivity for electromagnetic shielding application. Compos Commun 2021;23:100593.
[39] Rosales-Cuello N, Cárcamo C, Falcón C, Palza H. PDMS composites with carbon grease as reusable compliant electrodes for applications in artificial muscles based on dielectric elastomer actuators. Sens Actuators, A 2023;363:114710.
[40] Wang Z, Zhang J, Wang X, Wu J. A permeability membrane-type leak element based on PDMS. Vacuum 2024;220:112853.
[41] Lu C, Sun Y, Harley SJ, Glascoe EA. Modeling Gas Transport and Reactions in Polydimethysiloxane. Lawrence Livermore National Lab.(LLNL), Livermore, CA (United States); 2012.
[42] Greene T, House-Knight T, Gentry R, Clewell H. Silicones. Patty's Toxicology 2001:1–13.
[43] Kulyk K, Zettergren H, Gatchell M, Alexander JD, Borysenko M, Palianytsia B, et al. Dimethylsilanone generation from pyrolysis of polysiloxanes filled with nanosized silica and ceria/silica. ChemPlusChem 2016;81:1003–13.
[44] Izuka A, Winter HH, Hashimoto T. Molecular weight dependence of viscoelasticity of polycaprolactone critical gels. Macromolecules 1992;25:2422–8.
[45] Kolel-Veetii MK, Keller TM. Recent Advances in High-Temperature Network Polymers of Carboranylenesiloxanes and Silarylene-Siloxanes. Inorganic and Organometallic Macromolecules: Design and Applications. 2008:373-403.

[46] Wang J, Li G, Zhang Z, Huang Q, Niu B, Zhang Y, et al. Detailed insights of polydimethylsiloxane (PDMS) degradation mechanism via ReaxFF MD and experiments. Chem Eng J 2024;488:150728.
[47] Feng B, Bai L, Yan X, Liu X, Zheng J. A robust and thermally stable poly (dimethylsiloxane) elastomer with reprocessability based on dynamic silyl ether linkages. Macromol Chem Phys 2022;223:2200049.
[48] Tansel DZ, Brenneman J, Fedder GK, Panat R. Mechanical characterization of polydimethylsiloxane (PDMS) exposed to thermal histories up to 300 C in a vacuum environment. J Micromech Microeng 2020;30:067001.
[49] Mandal SK, Kumar R, Rizwee M, Kumar D. Tuning thermal and structural properties of nano-filled PDMS elastomer. Polym Compos 2024;45:14832–44.
[50] Revesz A, Gibbs G. Structural and bond flexibility of vitreous SiO2 films. the physics of MOS insulators. Elsevier; 1980. p. 92–6.
[51] Lu S, Cai W, Cao N, Qian H-j, Lu Z-y, Cui S. Understanding the extraordinary flexibility of polydimethylsiloxane through single-molecule mechanics. ACS Mater Lett 2022;4:329–35.
[52] Mohamed NS, Theng KC. Mechanical properties of graded polydimethylsiloxane for flexible electronics. Journal of Physics: Conference Series: IOP Publishing 2019:012030.
[53] Martin S, Bhushan B. Transparent, wear-resistant, superhydrophobic and superoleophobic poly (dimethylsiloxane)(PDMS) surfaces. J Colloid Interface Sci 2017;488:118–26.
[54] Zahid A, Dai B, Hong R, Zhang D. Optical properties study of silicone polymer PDMS substrate surfaces modified by plasma treatment. Mater Res Express 2017;4:105301.
[55] Ozkan M, Wang M, Ozkan C, Flynn R, Esener S. Optical manipulation of objects and biological cells in microfluidic devices. Biomed Microdevices 2003;5:61–7.
[56] Shakeri A, Khan S, Didar TF. Conventional and emerging strategies for the fabrication and functionalization of PDMS-based microfluidic devices. Lab Chip 2021;21:3053–75.
[57] Saha T, Mukherjee S, Dickey MD, Velev OD. Harvesting and manipulating sweat and interstitial fluid in microfluidic devices. Lab Chip 2024;24:1244–65.
[58] Nomoni M, May JM, Kyriacou PA. Novel polydimethylsiloxane (PDMS) pulsatile vascular tissue phantoms for the in-vitro investigation of light tissue interaction in photoplethysmography. Sensors 2020;20:4246.
[59] Goldfain AM, Lemaillet P, Allen DW, Briggman KA, Hwang J. Polydimethylsiloxane tissue-mimicking phantoms with tunable optical properties. J Biomed Opt 2022;27. 074706 -.
[60] Jenne S, Zappe H. Multiwavelength tissue-mimicking phantoms with tunable vessel pulsation. J Biomed Opt 2023;28. 045003 -.
[61] Tian K, Chen C, Xiong L, Chen X, Fu Q, Deng H. Self-Roughed Transparent Superhydrophobic Coating Enabled by Controlled-Crosslinking of Polydimethylsiloxane Droplets. Available at SSRN 4528140.
[62] Feng C, Li Y, Luo Y, Zhang L, Zong Y, Zhao K. Mechanisms of hydrophobic recovery of poly (dimethylsiloxane) elastomers after plasma/corona treatments: a minireview. Langmuir 2024;40:23598–605.
[63] Neves LB, Afonso IS, Nobrega G, Barbosa LG, Lima RA, Ribeiro JE. **A review of methods to modify the PDMS surface wettability and their applications**. Micromachines 2024;15:670.
[64] Kim T-H, Kim D-E. Tribological properties of polydimethylsiloxane grafted with poly (ethylene glycol) methyl ether methacrylate under water lubrication. Lubricants 2024;12:426.
[65] Mark JE. Polymer data handbook. (No Title) 2009.
[66] Reidy TM, Luo D, Rana P, Huegel B, Cheng X. Transparency of PDMS based microfluidic devices under temperature gradients. J Micromech Microeng 2018;29:015014.
[67] Shimura T, Jin Y, Kubyama K, Araki T, Kamimura N, Masai E, et al. Improved thermal properties of polydimethylsiloxane by copolymerization and thiol–ene crosslinking of 2-pyrone-4, 6-dicarboxylic acid moiety. Polym Chem 2025;16:45–51.
[68] Deshpande G, Rezac ME. Kinetic aspects of the thermal degradation of poly (dimethyl siloxane) and poly (dimethyl diphenyl siloxane). Polym Degrad Stab 2002;76:17–24.
[69] Kuo AC. Poly (dimethylsiloxane). Polymer data handbook 1999;1999:411–35.
[70] Liu C, Wu W, Chen Q, Wang Y, Cui S, Yang H. 3D expanded graphite frameworks for dual-functional polymer composites with exceptional thermal conductive and electromagnetic interference shielding capabilities. ACS Appl Electron Mater 2022;4:707–17.
[71] Ruben B, Elisa M, Leandro L, Victor M, Gloria G, Marina S, et al. Oxygen plasma treatments of polydimethylsiloxane surfaces: effect of the atomic oxygen on capillary flow in the microchannels. Micro Nano Lett 2017;12:754–7.
[72] Hu S, Ren X, Bachman M, Sims CE, Li G, Allbritton N. Surface modification of poly (dimethylsiloxane) microfluidic devices by ultraviolet polymer grafting. Anal Chem 2002;74:4117–23.
[73] Armani D, Liu C, Aluru N. Re-configurable fluid circuits by PDMS elastomer micromachining. In: Technical Digest IEEE International MEMS 99 Conference Twelfth IEEE International Conference on Micro Electro Mechanical Systems (Cat No 99CH36291): IEEE; 1999. p. 222–7.
[74] Müller A, Wapler MC, Wallrabe U. A quick and accurate method to determine the Poisson's ratio and the coefficient of thermal expansion of PDMS. Soft Matter 2019;15:779–84.
[75] Xu H, Ding L, Song Y, Wang W. Rheology of end-linking polydimethylsiloxane networks filled with silica. J Rheol 2020;64:1425–38.
[76] Liu J, Yao Y, Li X, Zhang Z. Fabrication of advanced polydimethylsiloxane-based functional materials: Bulk modifications and surface functionalizations. Chem Eng J 2021;408:127262.
[77] Li S, Zhang J, He J, Liu W, Wang Y, Huang Z, et al. Functional PDMS elastomers: bulk composites, surface engineering, and precision fabrication. Adv Sci 2023;10.
[78] Gu H, Liu C, Zhu J, Gu J, Wujcik EK, Shao L, et al. Introducing advanced composites and hybrid materials. Adv Compos Hybrid Mater 2018;1:1–5.
[79] Tavakoli S, Nemati S, Kharaziha M, Akbari-Alavijeh S. Embedding CuO nanoparticles in PDMS-SiO2 coating to improve antibacterial characteristic and corrosion resistance. Colloid Interface Sci Commun 2019;28:20–8.
[80] Karabchevsky A, Mosayyebi A, Kavokin AV. Tuning the chemiluminescence of a luminol flow using plasmonic nanoparticles. Light Sci Appl 2016;5. e16164 -e.
[81] del Bosque A, Sánchez-Romate XF, Sánchez M, Ureña A. Easy-scalable flexible sensors made of carbon nanotube-doped polydimethylsiloxane: analysis of manufacturing conditions and proof of concept. Sensors 2022;22:5147.
[82] Gong X, He S. Highly durable superhydrophobic polydimethylsiloxane/silica nanocomposite surfaces with good self-cleaning ability. ACS Omega 2020;5:4100–8.
[83] Maia R, Sousa P, Pinto VC, Lima R, Minas G, Rodrigues R. Development and Characterization of Porous PDMS Microneedles2023.
[84] Atazadeh A, Ameri E. Synthesis of PMHS–PDMS composite membranes embedded with silica nanoparticles and their application to separate of DMSO from aqueous solutions. Polym Bull 2021;78.
[85] Antonov E, Sosnin I, Tiwari A, Prasolov N, Dorogin L. Metal nanoparticles as an electromagnetic microwave heat-cure agent for polydimethylsiloxane elastomers. Letters on Materials 2022;12:49–53.
[86] Łapińska A, Grochowska N, Antonowicz J, Michalski P, Dydek K, Dużyńska A, et al. Influence of the filler distribution on PDMS-graphene based nanocomposites selected properties. Sci Rep 2022;12:19038.
[87] Raj R. Characterizing polydimethylsiloxane–carbon nanotubes composites manufactured using material extrusion additive technology: a rheological and mechanical analysis. Mater Lett 2024;360:136019.
[88] Borah B, Dash R. Improved dielectric properties of rGO/PDMS composites by incorporation of Ag nanoparticles. J Mater Sci Mater Electron 2022;33.
[89] Jeronimo K, Koutsos V, Cheung R, Mastropaolo E. PDMS-ZnO piezoelectric nanocomposites for pressure sensors. Sensors 2021;21:5873.
[90] Cutroneo M, Havranek V, Mackova A, Malinsky P, Silipigni L, Slepicka P, et al. Synthesis of porous polydimethylsiloxane gold nanoparticles composites by a single step laser ablation process. Int J Mol Sci 2021;22.
[91] Ketikis P, Tsalas I, Klonos PA, Pilatos G, Giannakopoulou T, Kyritsis A, et al. Preparation and characterization of graphene and carbon nanotube hybrid polydimethylsiloxane composites for protective coating applications. Journal of Composites Science 2024;8:499.

[92] Onyekanne MC, Oyewole O, Salifu A, Obayemi J, Anye VC, Nwazojie C, et al. Mechanical and thermal properties of polydimethylsiloxane/magnetite nanocomposites for cancer treatment by localized hyperthermia and photothermal ablation. J Appl Polym Sci 2022;139.
[93] Huang S-Y, Wu T-I, Chou C-M, Hsiao V. Tailoring mechanical and electrical properties of polydimethylsiloxane nanocomposites with graphene and carbon nanotubes for wearable electronics. Polym Polym Compos 2023;31.
[94] Salemi F, Karimzadeh F, Abbasi M-H, Moradi F, Song J, Latif M, et al. Surface patterning of polydimethylsiloxane (PDMS): graphene nanocomposites for application in triboelectric nanogenerators2022.
[95] Vanskeviče I, Kinka M, Banys J, Macutkevič J, Schaefer S, Selskis A, et al. Dielectric and ultrasonic properties of PDMS/TiO2 nanocomposites. Polymers 2024;16:603.
[96] Colijn I, Postma E, Fix R, van der Kooij HM, Schroën K. Particle dispersion governs nano to bulk dynamics for tailored nanocomposite design. J Colloid Interface Sci 2024;658:354–61.
[97] Li C, Yang Z, Zhang X, Ru Y, Gao D, Wu D, et al. Ultrasonic-assisted method for the preparation of carbon nanotube-graphene/polydimethylsiloxane composites with integrated thermal conductivity, electromagnetic interference shielding, and mechanical performances. Int J Mol Sci 2022;23:15007.
[98] Mugemana C, Moghimikheirabadi A, Arl D, Addiego F, Schmidt DF, Kröger M, et al. Ionic poly(dimethylsiloxane)-silica nanocomposites: dispersion and self-healing. MRS Bull 2022;47:1185–97.
[99] Park K, Woo M-A, Lim J-A, Kim Y-R, Choi S-W, Lim M-C. In situ synthesis of directional gold nanoparticle arrays along ridge cracks of PDMS wrinkles. Colloids Surf A Physicochem Eng Asp 2018;558:186–91.
[100] Ahmed SR, Kim J, Tran VT, Suzuki T, Neethirajan S, Lee J, et al. In situ self-assembly of gold nanoparticles on hydrophilic and hydrophobic substrates for influenza virus-sensing platform. Sci Rep 2017;7:44495.
[101] Yang J, Yoo J, Yu WS, Choi MK. Polymer-assisted high-resolution printing techniques for colloidal quantum dots. Macromol Res 2021;29:391–401.
[102] Jalajamony HM, Aliyana AK, De S, Diallo F, Stylios G, Fernandez RE. Plasma-aided direct printing of silver nanoparticle conductive structures on polydimethylsiloxane (PDMS) surfaces. Sci Rep 2024;14:31154.
[103] Paghi A, Corsi M, Corso S, Mariani S, Barillaro G. In situ controlled and conformal coating of polydimethylsiloxane foams with silver nanoparticle networks with tunable piezo-resistive properties. Nanoscale Horiz 2022;7:425–36.
[104] Kim JH, Park H, Seo SW. In situ synthesis of silver nanoparticles on the surface of PDMS with high antibacterial activity and biosafety toward an implantable medical device. Nano Convergence 2017;4:33.
[105] Reifarth M. (Sub-) microscale patterning via microcontact printing (μCP): Recent Advances, Applications and Future Perspectives. Soft Matter. 2025.
[106] Qiu S, Ji J, Sun W, Pei J, He J, Li Y, et al. Recent advances in surface manipulation using micro-contact printing for biomedical applications. Smart Mater Med 2021;2:65–73.
[107] Redolat J, Camarena-Perez M, Griol A, Kovylina M, Xomalis A, Baumberg JJ, et al. Accurate transfer of individual nanoparticles onto single photonic nanostructures. ACS Appl Mater Interfaces 2022;15:3558–65.
[108] Xie T, Cao Z, Li Y, Li Z, Zhang F-L, Gu Y, et al. Highly sensitive SERS substrates with multi-hot spots for on-site detection of pesticide residues. Food Chem 2022;381:132208.
[109] Lin G, Zhu J, Wang Y, Yang B, Xiong S, Zhang J, et al. Fabrication of polydimethylsiloxane (PDMS)-based flexible surface-enhanced raman scattering (sers) substrate for ultrasensitive detection. Journal of Visualized Experiments (JoVE) 2023. e65595.
[110] Schnee VP, Henry N, Huynh Q. Anti-reflective coating by 3D PDMS stamping using two-photon lithography master. Opt Mater 2021;111:110715.
[111] Park H, Kim S, Lee J, Kim K, Na H, Kim Y, et al. Facile strategy for uniform gold coating on silver nanowires embedded PDMS for soft electronics. npj Flexible Electron 2024;8:63.
[112] Gao R, Qian H, Weng C, Wang X, Xie C, Guo K, et al. A SERS stamp: Multiscale coupling effect of silver nanoparticles and highly ordered nano-micro hierarchical substrates for ultrasensitive explosive detection. Sens Actuators B 2020;321:128543.
[113] Ahn J, Jang H, Jeong Y, Choi S, Ko J, Hwang SH, et al. Illuminating recent progress in nanotransfer printing: core principles, emerging applications, and future perspectives. Adv Sci 2024;11:2303704.
[114] Kumar A, Thomas N, Swaminathan P. Plasma-tailored polydimethylsiloxane substrates for eventing of single molecules using wrinkle-enhanced raman spectroscopy. ACS Appl Nano Mater 2025;8:4625–35.
[115] Kelarakis A. In situ generation of nanoparticles on and within polymeric materials. Polymers 2024;16:1611.
[116] Cordoba A, Cauich-Rodríguez JV, Vargas-Coronado RF, Velázquez-Castillo R, Esquivel K. A novel in situ sol-gel synthesis method for PDMS composites reinforced with silica nanoparticles. Polymers 2024;16:1125.
[117] Cordoba A, Vargas-Coronado RF, Velázquez-Castillo R, Cauich-Rodríguez JV, Esquivel K. Mechanical and thermal performance of in-situ synthesized PDMS-SiO2 composite as electrical insulating coatings. Molecules 2025;30:2107.
[118] Kaur H, Chaudhary S, Kaur H, Chaudhary M, Jena KC. Hydrolysis and condensation of tetraethyl orthosilicate at the air–aqueous interface: implications for silica nanoparticle formation. ACS Appl Nano Mater 2021;5:411–22.
[119] Wang Y, Yan L, Ling Y, Ge Y, Huang C, Zhou S, et al. Enhanced mechanical and adhesive properties of PDMS coatings via in-situ formation of uniformly dispersed epoxy reinforcing phase. Prog Org Coat 2023;174:107319.
[120] Harun-Ur-Rashid M, Foyez T, Krishna SBN, Poda S, Imran AB. Recent advances of silver nanoparticle-based polymer nanocomposites for biomedical applications. RSC Adv 2025;15:8480–505.
[121] Vinnacombe-Willson GA, Conti Y, Stefancu A, Weiss PS, Cortés E, Scarabelli L. Direct bottom-up in situ growth: a paradigm shift for studies in wet-chemical synthesis of gold nanoparticles. Chem Rev 2023;123:8488–529.
[122] Figueira RB. Hybrid sol–gel coatings for corrosion mitigation: a critical review. Polymers 2020;12:689.
[123] Melnyk IV, Tomina VV, Stolyarchuk NV, Václavíková M. Sol-Gel technique to design hybrid materials and their application in water purification. In: Nanoscience and Nanotechnology in Security and Protection against CBRN Threats. Springer; 2020. p. 67–73.
[124] Rex A, dos Santos JHZ. The use of sol–gel technology to produce nanomaterials for air and water purification. Nanomaterials for Air-and Water Purification 2024:197–216.
[125] Barrino F. Hybrid organic–inorganic materials prepared by sol–gel and sol–gel-coating method for biomedical use: study and synthetic review of synthesis and properties. Coatings 2024;14:425.
[126] Hasan MZ, Dipti TT, Liu L, Wan C, Feng L, Yang Z. coating Metal–organic frameworks (MOFs) and associated composites on electrodes, thin film polymeric materials, and glass surfaces. Nanomaterials 2025;15:1187.
[127] Bakar NHA, Ismail WNW, Yusop HM, Zulkifli NFM. Synthesis of a water-based TEOS–PDMS sol–gel coating for hydrophobic cotton and polyester fabrics. New J Chem 2024;48:933–50.
[128] Kierat O, Dudek A. Sol–gel-derived vinyltrimethoxysilane (VTMS)/tetraetoxysilane (TEOS) hybrid coatings on titanium materials for use in medical applications. Materials 2025;18:2273.
[129] Pellegrini C, Duluard S, Gressier M, Turq V, Ansart F, Menu M-J. Development of multifunctional hybrid coatings (mechanically resistant and hydrophobic) using methyltrimethoxysilane–diethoxydimethylsilane–tetraethoxysilane mixed systems. Materials 2024;17:368.
[130] Kuddushi M, Kanike C, Xu BB, Zhang X. Recent advances in nanoprecipitation: from mechanistic insights to applications in nanomaterial synthesis. Soft Matter 2025.
[131] Pagels RF, Edelstein J, Tang C, Prud'homme RK. Controlling and predicting nanoparticle formation by block copolymer directed rapid precipitations. Nano Lett 2018;18:1139–44.
[132] Ristroph KD, Pinkerton NM, Markwalter CE, D'Addio SM, Gindy ME, Pagels RF. 20 years of flash nanoprecipitation – from controlled precipitation to global medicine. Adv Drug Deliv Rev 2025;115700.
[133] Lteif S, Nosratabad NA, Wang S, Xin Y, Weigand SJ, Mattoussi H, et al. Inorganic Nanoparticles embedded in Polydimethylsiloxane Nanodroplets. Langmuir 2023;39:15748–55.

[134] Shen Y, Gwak H, Han B. Advanced manufacturing of nanoparticle formulations of drugs and biologics using microfluidics. Analyst 2024;149:614–37.
[135] Nathanael K, Kovalchuk NM, Simmons MJH. Comparison of microfluidic synthesis of silver nanoparticles in flow and drop reactors at low dean numbers. Micromachines 2025;16:75.
[136] Agha A, Waheed W, Stiharu I, Nerguizian V, Destgeer G, Abu-Nada E, et al. A review on microfluidic-assisted nanoparticle synthesis, and their applications using multiscale simulation methods. Discov Nano 2023;18:18.
[137] Qin X, Seder I, Guo Z, Li X, Wang W, Sun Y. Microfluidic instruments for nanoparticle synthesis. Biomedical Instrumentation 2025;1:100002.
[138] Fortuni B, Inose T, Uezono S, Toyouchi S, Umemoto K, Sekine S, et al. In situ synthesis of Au-shelled Ag nanoparticles on PDMS for flexible, long-life, and broad spectrum-sensitive SERS substrates. Chem Commun 2017;53:11298–301.
[139] Ariati R, Sales F, Souza A, Lima RA, Ribeiro J. Polydimethylsiloxane composites characterization and its applications: a review. Polymers 2021;13:4258.
[140] Blattmann CO, Pratsinis SE. Nanoparticle filler content and shape in polymer nanocomposites. Kona Powder Part J 2019;36:3–32.
[141] Noimark S, Colchester RJ, Blackburn BJ, Zhang EZ, Alles EJ, Ourselin S, et al. Carbon-nanotube–PDMS composite coatings on optical fibers for all-optical ultrasound imaging. Adv Funct Mater 2016;26:8390–6.
[142] Yue X, Xi Y, Hu C, He X, Dai S, Cheng L, et al. Enhanced output-power of nanogenerator by modifying PDMS film with lateral ZnO nanotubes and Ag nanowires. RSC Adv 2015;5:32566–71.
[143] Wang Y-W, Liu Y-L, Xu J-Q, Qin Y, Huang W-H. Stretchable and photocatalytically renewable electrochemical sensor based on sandwich nanonetworks for real-time monitoring of cells. Anal Chem 2018;90:5977–81.
[144] Jackson J, Chen A, Zhang H, Burt H, Chiao M. Design and near-infrared actuation of a gold nanorod–polymer microelectromechanical device for on-demand drug delivery. Micromachines 2018;9:28.
[145] Yan X, Martin-Gonzalez M. Strategies for Enhancing thermal Conductivity of PDMS in Electronic applications. Adv Mater Technol 2025. e01210.
[146] Yang G, Li Y, Zhu J, Ma L, Li Z, Wang J, et al. Highly robust, processable and multi-functional PDMS/graphene composite aerogel constructed by “soft-hard” interface engineering strategy. Compos B Eng 2025;288:111904.
[147] Murai J, Nakajima T, Matsuda T, Tsunoda K, Nonoyama T, Kurokawa T, et al. Tough double network elastomers reinforced by the amorphous cellulose network. Polymer 2019;178:121686.
[148] Bokobza L. Enhanced electrical and mechanical properties of multiwall carbon nanotube rubber composites. Polym Adv Technol 2012;23:1543–9.
[149] Liu YL, Qin Y, Jin ZH, Hu XB, Chen MM, Liu R, et al. A stretchable electrochemical sensor for inducing and monitoring cell mechanotransduction in real time. Angew Chem Int Ed 2017;56:9454–8.
[150] Saharudin K, Karim M, Sreekantan S. Preparation of a polydimethylsiloxane (PDMS)/graphene-based super-hydrophobic coating. Mater Today Proc 2019;17:752–60.
[151] Abdelhafeez IA, Zhou X, Yao Q, Yu Z, Gong Y, Chen J. Multifunctional edge-activated carbon nitride nanosheet-wrapped polydimethylsiloxane sponge skeleton for selective oil absorption and photocatalysis. ACS Omega 2020;5:4181–90.
[152] Lee Y-H, Yu L, Wang H, Fang W, Ling X, Shi Y, et al. Synthesis and transfer of single-layer transition metal disulfides on diverse surfaces. Nano Lett 2013;13:1852–7.
[153] Young RJ, Kinloch IA, Gong L, Novoselov KS. The mechanics of graphene nanocomposites: a review. Compos Sci Technol 2012;72:1459–76.
[154] Liu Z, Lu J, Xu M, Li S, Zhou A, Geng Y, et al. Properties of Vinyl-Grafted h-BN/PDMS Coatings and their protective Effects on Mortar Surfaces. J Mater Res Technol 2025.
[155] Gupta S, Ramamurthy PC, Madras G. Covalent grafting of polydimethylsiloxane over surface-modified alumina nanoparticles. Ind Eng Chem Res 2011;50:6585–93.
[156] Stiegman A. Thiol-ene polymer metal oxide nanoparticle high refractive index composites. Google Patents 2018.
[157] Zhang F, Sun Y, Guo L, Zhang Y, Liu D, Feng W, et al. Microstructural welding engineering of carbon nanotube/polydimethylsiloxane nanocomposites with improved interfacial thermal transport. Adv Funct Mater 2024;34:2311906.
[158] Lin B, Feng Y, Yang X, Huang Z, Zhai C, Li H, et al. Rapid self-healing and durable adhesion of imine-linked dynamic polymer and its thermally conductive composites. J Appl Polym Sci 2025;142:e57813.
[159] Lv C, Wang J, Li Z, Zhao K, Zheng J. Degradable, reprocessable, self-healing PDMS/CNTs nanocomposite elastomers with high stretchability and toughness based on novel dual-dynamic covalent sacrificial system. Compos B Eng 2019;177:107270.
[160] Cai Y, Wang Y, Long L, Zhou S, Yan L, Zhang J, et al. Fabrication of highly thermally resistant and self-healing polysiloxane elastomers by constructing covalent and reversible networks. Macromol Rapid Commun 2023;44:2300191.
[161] Pasquini M, Raos G. Tunable interaction potentials and morphology of polymer–nanoparticle blends. J Chem Phys 2020;152.
[162] Chen J, Peng Q, Peng X, Zhang H, Zeng H. Probing and manipulating noncovalent interactions in functional polymeric systems. Chem Rev 2022;122:14594–678.
[163] Hamer MJ, Iyer BV, Yashin VV, Balazs AC. Designing mechanomutable composites: reconfiguring the structure of nanoparticle networks through mechanical deformation. Nano Lett 2014;14:4745–50.
[164] Kalghatgi SR, Kumar SK, Mani E. Molecular dynamics study of the role of nanoparticle assemblies on polymer nanocomposite rheology. Macromolecules 2024;57:9555–64.
[165] Wei Z-Y, Ning N-Y, Tian M, Zhang L-Q, Mi J-G. Theoretical interpretation of conformation variations of polydimethylsiloxane induced by nanoparticles. Chin J Polym Sci 2018;36:505–13.
[166] Camenzind A, Schweizer T, Sztucki M, Sotiris EP. Structure and Strength of Silica-PDMS Nanocomposites. MRS Online Proc Libr 2011;1312:510.
[167] Cordoba A, Rivera-Muñoz EM, Velázquez-Castillo R, Esquivel K. PDMS/TiO2 and PDMS/SiO2 nanocomposites: mechanical properties’ evaluation for improved Insulating Coatings. Nanomaterials 2023;13:1699.
[168] Sowan N, Cox LM, Shah PK, Song HB, Stansbury JW, Bowman CN. Dynamic covalent chemistry at interfaces: development of tougher, healable composites through stress relaxation at the resin–silica nanoparticles interface. Adv Mater Interfaces 2018;5:1800511.
[169] Wen J, Mark JE. Sol–gel preparation of composites of poly (dimethylsiloxane) with SiO2 and SiO2/TiO2, and their mechanical properties. Polym J 1995;27:492–502.
[170] Pornea AGM, Choi K-I, Jung J-H, Hanif Z, Kwak C, Kim J. Enhancement of isotropic heat dissipation of polymer composites by using ternary filler systems consisting of boron nitride nanotubes, h-BN, and Al2O3. ACS Omega 2023;8:24454–66.
[171] Balachander N, Seshadri I, Mehta RJ, Schadler LS, Borca-Tasciuc T, Keblinski P, et al. Nanowire-filled polymer composites with ultrahigh thermal conductivity. Appl Phys Lett 2013;102.
[172] HIDA S, SHIGA T, MARUYAMA S, ELLIOTT JA, SHIOMI J. Influence of thermal boundary resistance and interfacial phonon scattering on heat conduction of carbon nanotube/polymer composites. TRANSACTIONS OF THE JAPAN SOCIETY OF MECHANICAL ENGINEERS Series B. 2012;78:634-43.
[173] Du J, Wu P, Kou H, Gao P, Cao Y, Jing L, et al. Self-healing superhydrophobic coating with durability based on EP+ PDMS/SiO2 double-layer structure design. Prog Org Coat 2024;190:108359.
[174] Guo X, Shao Z, Wang H, Cheng J, Jiang Z, Huang M, et al. Mechanically durable superhydrophobic coating of poly (ethyl cyanoacrylate)/SiO2/polydimethylsiloxane with superior abrasion resistance. Prog Org Coat 2024;186:108044.
[175] Eder T, Mautner A, Xu Y, Reithofer MR, Bismarck A, Chin JM. Transparent PDMS surfaces with covalently attached lubricants for enhanced anti-adhesion performance. ACS Appl Mater Interfaces 2024;16:10942–52.
[176] Algorri J, Poudereux D, García-Cámara B, Urruchi V, Sánchez-Pena JM, Vergaz R, et al. Metal nanoparticles-PDMS nanocomposites for tunable optical filters and sensors. Optical Data Processing and Storage 2016;2.
[177] Rodrigues MS, Meira DI, Lopes C, Borges J, Vaz F. Preparation of plasmonic Au-TiO2 thin films on a transparent polymer substrate. Coatings 2020;10:227.
[178] Cho H, Lee D, Hong S, Kim H, Jo K, Kim C, et al. Surface modification of ZrO2 nanoparticles with TEOS to prepare transparent ZrO2@ SiO2-PDMS nanocomposite films with adjustable refractive indices. Nanomaterials 2022;12:2328.

[179] Abedinzadeh R, Shirian H, Parhizkar J. Study on the wettability and optical properties of polydimethylsiloxane-SiO 2 nano-composite surfaces. International Journal of Advanced Design & Manufacturing Technology 2020;13.
[180] Greer HF, Briggs RM, Harried SS, Lee T, Lobaton R, Mirkhani V. Control of light scattering with nanoparticles and/or coatings. Google Patents 2020.
[181] Guglielmelli A, Mazzei R, Palermo G, Valente L, Tone CM, Giorno L, et al. Development of a photothermal regenerative plasmonic platform as a light-controlled interface. ACS Appl Mater Interfaces 2024;16:59586–96.
[182] Granata F, Pirillo N, Alabastri A, Schirato A, Bruno L, Costa R, et al. Synthesis of plasmonic gold nanoparticles on soft materials for biomedical applications. Micro Nano Eng 2023;19:100207.
[183] Bonyár A, Izsold Z, Himics L, Veres M, Csarnovics I. Investigation of PDMS-gold nanoparticle composite films for plasmonic sensors. In: 2017 IEEE 23rd International Symposium for Design and Technology in Electronic Packaging (SIITME). IEEE; 2017. p. 25–8.
[184] Spicer JB, Kang J, Patterson AL, Boctor EM. Polymer matrix nanocomposites as photoacoustic transmitters for epiretinal prosthetics. In: 2023 IEEE 23rd International Conference on Nanotechnology (NANO). IEEE; 2023. p. 133–6.
[185] Tian Y, Wu N, Sun K, Zou X, Wang X. Numerical simulation of fiber-optic photoacoustic generator using nanocomposite material. J Comput Acoust 2013;21:1350002.
[186] Chang W-Y, Huang W, Kim J, Li S, Jiang X. Candle soot nanoparticles-polydimethylsiloxane composites for laser ultrasound transducers. Appl Phys Lett 2015;107.
[187] Strong LE, West JL. Thermally responsive polymer–nanoparticle composites for biomedical applications. Wiley Interdiscip Rev Nanomed Nanobiotechnol 2011;3:307–17.
[188] Yan J, Cai Y, Zhang H, Han M, Liu X, Chen H, et al. Rapid thermochromic and highly thermally conductive nanocomposite based on silicone rubber for temperature visualization thermal management in electronic devices. ACS Appl Mater Interfaces 2024;16:7883–93.
[189] Sang Z, Ke K, Manas-Zloczower I. Interface design strategy for the fabrication of highly stretchable strain sensors. ACS Appl Mater Interfaces 2018;10:36483–92.
[190] Ding L, Lin Y, Yang C, Kong D. Strategies for Stretchable and Durable Metal Nanowire-Based Conductors: Recent Advances and Future Prospects. Advanced Materials Technologies. 2025:e01387.
[191] Ke K, Sang Z, Manas-Zloczower I. Stretchable elastomer composites with segregated filler networks: effect of carbon nanofiller dimensionality. Nanoscale Adv 2019;1:2337–47.
[192] Zhang Q, Liang J, Huang Y, Chen H, Ma R. Intrinsically stretchable conductors and interconnects for electronic applications. Mater Chem Front 2019;3:1032–51.
[193] Kim Y, Zhu J, Yeom B, Di Prima M, Su X, Kim J-G, et al. Stretchable nanoparticle conductors with self-organized conductive pathways. Nature 2013;500:59–63.
[194] Johnston ID, McCluskey DK, Tan CK, Tracey MC. Mechanical characterization of bulk Sylgard 184 for microfluidics and microengineering. J Micromech Microeng 2014;24:035017.
[195] Abou-Hussein R, Wu S, Zhang L, Mark JE. Effects of some structural features of poly (dimethylsiloxane) on its unusually high gas permeabilities. J Inorg Organomet Polym Mater 2008;18:100–3.
[196] Owen M. Interfacial activity of polydimethylsiloxane. Surfactants in Solution: Volume 6: Springer; 1986. p. 1557-69.
[197] Kong S, Mariatti M, Busfield J. Effects of types of fillers and filler loading on the properties of silicone rubber composites. J Reinf Plast Compos 2011;30:1087–96.
[198] Hajiali F, Shojaei A. Network structure and mechanical properties of polydimethylsiloxane filled with nanodiamond–effect of degree of silanization of nanodiamond. Compos Sci Technol 2017;142:227–34.
[199] Zhang Y, Zhu Y, Lin G, Ruoff RS, Hu N, Schaefer DW, et al. What factors control the mechanical properties of poly (dimethylsiloxane) reinforced with nanosheets of 3-aminopropyltriethoxysilane modified graphene oxide? Polymer 2013;54:3605–11.
[200] Ahir SV, Terentjev EM. Photomechanical actuation in polymer–nanotube composites. Nat Mater 2005;4:491–5.
[201] Ahir S, Squires A, Tajbakhsh A, Terentjev E. Infrared actuation in aligned polymer-nanotube composites. physical review b—condensed matter and materials. Physics 2006;73:085420.
[202] Lu S, Panchapakesan B. Photomechanical responses of carbon nanotube/polymer actuators. Nanotechnology 2007;18:305502.
[203] Lu S, Ahir S, Velasco V, King B, Xu P, Terentjev EM, et al. Photo-mechanical actuation of carbon nanotubes: mechanisms and applications in micro and nano-devices. J Micro-Nano Mechatronics 2009;5:29.
[204] Zhang R, Ying C, Gao H, Liu Q, Fu X, Hu S. Highly flexible strain sensors based on polydimethylsiloxane/carbon nanotubes (CNTs) prepared by a swelling/permeating method and enhanced sensitivity by CNTs surface modification. Compos Sci Technol 2019;171:218–25.
[205] Rybak A, Rybak A, Kaszuwara W, Boncel S. Poly (2, 6-dimethyl-1, 4-phenylene oxide) hybrid membranes filled with magnetically aligned iron-encapsulated carbon nanotubes (Fe@ MWCNTs) for enhanced air separation. Diam Relat Mater 2018;83:21–9.
[206] Park S, Nam G, Choi Y, Woo S, Uhm W, Park S, et al. Mechanoelectrical properties of a GnF/PDMS composite controlled by the aspect ratio and concentration of GnF. Compos Sci Technol 2018;159:77–86.
[207] Ha S, Choi Y, Lee W, Kim Y, Yoon S-H. Prediction of mechanical properties of graphite nanoflake/polydimethylsiloxane nanocomposites as affected by processing method. Compos B Eng 2021;224:109186.
[208] Baharkoosh A, Karbasi F, Baniasadi H. Fabrication of polydimethylsiloxane/zinc oxide/silica nanocomposite for steel coating: improving physical and mechanical properties of polydimethylsiloxane. Mater Today Commun 2025;42:111333.
[209] Katz S, Lachman N, Hafif N, Rosh L, Pevzner A, Lybman A, et al. Studying the physical and chemical properties of polydimethylsiloxane matrix reinforced by nanostructured TiO2 supported on mesoporous silica. Polymers 2022;15:81.
[210] Yang Q, Zhang Z, Qi Y, Zhang H. The antifouling and drag-reduction performance of alumina reinforced polydimethylsiloxane coatings containing phenylmethylsilicone oil. Polymers 2021;13:3067.
[211] Zhou S, Zhang H, Chen Q, Yuan Q-w, Zhang S-h, Bao N, et al. A High-Sensitive PDMS-Based sensor with a Wide Sensing Range by fabricating refined and reconstructable conductive network. Chem Eng J 2025;507:160626.
[212] Huang J, Cao L, Xue C-Y, Zhou Y-Z, Cai Y-C, Zhao H-Y, et al. Extremely soft, stretchable, and self-adhesive silicone conductive elastomer composites enabled by a molecular lubricating effect. Nano Lett 2022;22:8966–74.
[213] Yan X, Bai L, Feng B, Zheng J. Mechanically strong, thermally stable, and reprocessable poly (dimethylsiloxane) elastomers enabled by dynamic silyl ether linkages. Eur Polym J 2022;173:111267.
[214] Ma Z, Zhang X, Lu S, Yang H, Huang X, Qin L, et al. Tribological properties of flexible composite surfaces through direct ink writing for durable wearing devices. Surf Coat Technol 2022;441:128573.
[215] Wang H, Ni Y, Dong Z, Zhao Q. A mechanically enhanced metal-organic framework/PDMS membrane for CO2/N2 separation. React Funct Polym 2021;160:104825.
[216] Fan J, Wu W, Zeng X, Zhang J, Zhang H, He H. Dual reversible network nanoarchitectonics for ultrafast light-controlled healable and tough polydimethylsiloxane-based composite elastomers. ACS Appl Mater Interfaces 2023;15:38996–9007.
[217] Tao HQ, Yue DW, Li CH. A fast self-healing magnetic nanocomposite for magnetic actuators. Macromol Mater Eng 2022;307:2100649.
[218] Gao X, Zheng M, Yan X, Zhu M, Hou Y. Ultrahigh current density and fatigue stability in flexible energy harvester by designing delivery paths. Mater Today Phys 2021;19:100424.
[219] Riccucci G, Pezzana L, Lantean S, Tori A, Spriano S, Sangermano M. Investigation of the thermal conductivity of silicon-base composites: the effect of filler materials and characteristic on thermo-mechanical response of silicon composite. Appl Sci 2021;11:5663.
[220] Shishkin RA. Influence of the physical and chemical properties of particles on the thermal conductivity of polymer composite materials. High Temp 2023;61:163–72.

[221] Masraff MS, Rahman AMNAA, Ramli MR, Jamil MKM, Abdullah MK, Ali MZ, et al. Alignment of silver nanoparticles in polysiloxane crosslink network under direct electric field. Compos Sci Technol 2021;203:108611.
[222] Liu C, Wu W, Wang Y, Liu X, Chen Q, Xia S. Silver nanoparticle-enhanced three-dimensional boron nitride/reduced graphene oxide skeletons for improving thermal conductivity of polymer composites. ACS Appl Polym Mater 2021;3:3334–43.
[223] Achard F. James Clerk Maxwell, A treatise on electricity and magnetism, (1873). Landmark Writings in Western Mathematics 1640-1940: Elsevier; 2005. p. 564-87.
[224] Lee N, Park J, Jang N, Lee S, Kim D, Yun S, et al. Promoting thermal conductivity of alumina-based composite materials by systematically incorporating modified graphene oxide. Crystals 2024;14:490.
[225] Cheng SC, Vachon R. The prediction of the thermal conductivity of two and three phase solid heterogeneous mixtures. Int J Heat Mass Transf 1969;12:249–64.
[226] Okamoto S, Ishida H. A new theoretical equation for thermal conductivity of two-phase systems. J Appl Polym Sci 1999;72:1689–97.
[227] Yang X, Liang C, Ma T, Guo Y, Kong J, Gu J, et al. A review on thermally conductive polymeric composites: classification, measurement, model and equations, mechanism and fabrication methods. Adv Compos Hybrid Mater 2018;1:207–30.
[228] Ji Y, Sun J, Ren Y, Gao R, Qi H. Influence of gold nanoparticle concentration on photoacoustic response of Au-PDMS nanocomposite films. Colloids Surf A Physicochem Eng Asp 2025;710:136309.
[229] Fang H, Guo H, Hu Y, Ren Y, Hsu P-C, Bai S-L. In-situ grown hollow Fe3O4 onto graphene foam nanocomposites with high EMI shielding effectiveness and thermal conductivity. Compos Sci Technol 2020;188:107975.
[230] Zhao S, Zhu R, Fu Y. Piezothermic transduction of functional composite materials. ACS Appl Mater Interfaces 2019;11:4588–96.
[231] Hamilton RL, Crosser OK. Thermal conductivity of heterogeneous two-component systems. Industrial & Engineering chemistry fundamentals 1962;1:187–91.
[232] Moreira D, Braga Junior N, Benevides R, Sphaier L, Nunes L. Temperature-dependent thermal conductivity of silicone-Al2O3 nanocomposites. Appl Phys A 2015;121:1227–34.
[233] Nga DT, Phan AD, Julie T, Le NB, Ha CV. Photo-to-heat conversion of broadband metamaterial absorbers based on TiN nanoparticles under laser and solar illumination. Mater Today Commun 2023;35:105794.
[234] Agari Y, Uno T. Estimation on thermal conductivities of filled polymers. J Appl Polym Sci 1986;32:5705–12.
[235] Agari Y, Ueda A, Nagai S. Thermal conductivity of a polyethylene filled with disoriented short-cut carbon fibers. J Appl Polym Sci 1991;43:1117–24.
[236] Zhao Z-B, Du X-Y, Wang Y, Wang Z-Y, Zhang C, Liu J-D, et al. Preparation of a novel bi-layer modified alumina-based hybrid material and its effect on the thermal conductivity enhancement of polymer composites. Ceram Int 2022;48:15483–92.
[237] Hatta H, Taya M, Kulacki F, Harder J. Thermal diffusivities of composites with various types of filler. J Compos Mater 1992;26:612–25.
[238] Chen Y, Guo Y, Batra S, Unsal E, Wang E, Wang Y, et al. Large-scale R2R fabrication of piezoresistive films (Ni/PDMS) with enhanced through thickness electrical and thermal properties by applying a magnetic field. RSC Adv 2015;5:92071–9.
[239] Wang Y, Chang Z, Gao K, Li Z, Hou G, Liu J, et al. Designing high thermal conductivity of polydimethylsiloxane filled with hybrid h-BN/MoS2 via molecular dynamics simulation. Polymer 2021;224:123697.
[240] Huang Z, Wu W, Drummer D, Liu C, Wang Y, Wang Z. Multi-contact hybrid thermal conductive filler Al2O3@ AgNPs optimized three-dimensional thermal network for flexible thermal interface materials. J Appl Polym Sci 2021;138:50889.
[241] Zhao Z-B, Liu J-D, Du X-Y, Wang Z-Y, Zhang C, Ming S-F. Fabrication of silver nanoparticles/copper nanoparticles jointly decorated nitride flakes to improve the thermal conductivity of polymer composites. Colloids Surf A Physicochem Eng Asp 2022;635:128104.
[242] Wu W, Ren T, Liu X, Davis R, Huai K, Cui X, et al. Creating thermal conductive pathways in polymer matrix by directional assembly of synergistic fillers assisted by electric fields. Compos Commun 2022;35:101309.
[243] Yan J, Zhang H, Bai Y, Wei X, Zheng X, She M, et al. Nature loofah network-inspired rapid thermal-conductive and thermochromic-based nanocomposites for efficient heat management in advanced electronic devices. Polym Compos 2025;46:5685–93.
[244] Yan Y, Wu B, Qian G, Lan H, Alam MM, Xia R, et al. Ultra-wideband electromagnetic interference shielding effectiveness composite with elevated thermal conductivity. Compos A Appl Sci Manuf 2023;167:107430.
[245] Morawska-Chochół A, Szumera M, Młyniec A, Pielichowska K. The effect of Aging process conditions on the thermal properties of poly (dimethylsiloxane)-based silicone rubber. Materials 2024;17:5608.
[246] Soe HM, Kumar R, Matsuda A, Mariatti M. Surface-modification of silver nanoparticle–based polydimethylsiloxane composite for fabrication of strain sensor. Mater Today Commun 2023;36:106486.
[247] Sheshkar N, Verma G, Pandey C, Sharma AK, Gupta A. Enhanced thermal and mechanical properties of hydrophobic graphite-embedded polydimethylsiloxane composite. J Polym Res 2021;28:403.
[248] He M, Hu J, Yan H, Zhong X, Zhang Y, Liu P, et al. Shape anisotropic chain-like CoNi/polydimethylsiloxane composite films with excellent low-frequency microwave absorption and high thermal conductivity. Adv Funct Mater 2025;35:2316691.
[249] Hassanpour-Tamrin S, Sanati-Nezhad A, Sen A. A simple and low-cost approach for irreversible bonding of polymethylmethacrylate and polydimethylsiloxane at room temperature for high-pressure hybrid microfluidics. Sci Rep 2021;11:4821.
[250] Neves LB, Afonso IS, Barbosa LG, Nobrega G, Lima RA, Ribeiro JE. Optimizing parameters to improve PDMS surface wettability and the thermal conductivity analysis. J Mol Liq 2025;128204.
[251] Zhou L, Su C, Chen B, Zhao Q, Wang X, Zhao X, et al. Durable ER@ SiO2@ PDMS superhydrophobic composite designed by double crosslinking strategy for efficient oil-water separation. Polymer 2022;245:124722.
[252] Ariyanti D, Afiatin A, Shintawati PD, Purbasari A. TiO2-PDMS super hydrophilic coating with self-cleaning and antimicrobial properties. Jurnal Kimia Sains dan Aplikasi 2021;24:192–9.
[253] Guo X-J, Zhang D, Xue C-H, Liu B-Y, Huang M-C, Wang H-D, et al. Scalable and mechanically durable superhydrophobic coating of SiO2/polydimethylsiloxane/epoxy nanocomposite. ACS Appl Mater Interfaces 2023;15:4612–22.
[254] Lu L, Yang L, Xu Y, Luo J, Wang Y, Li W, et al. Preparation of composite superhydrophobic coatings for mortar utilizing polydimethylsiloxane as a hydrophobic interconnection. Journal of Building Engineering 2024;96:110635.
[255] Xia X, Liu J, Liu Y, Lei Z, Han Y, Zheng Z, et al. Preparation and characterization of biomimetic SiO2-TiO2-PDMS composite hydrophobic coating with self-cleaning properties for wall protection applications. Coatings 2023;13:224.
[256] Chen J, Yuan L, Shi C, Wu C, Long Z, Qiao H, et al. Nature-inspired hierarchical protrusion structure construction for washable and wear-resistant superhydrophobic textiles with self-cleaning ability. ACS Appl Mater Interfaces 2021;13:18142–51.
[257] Li X, Yan J, Yu T, Zhang B. Versatile nonfluorinated superhydrophobic coating with self-cleaning, anti-fouling, anti-corrosion and mechanical stability. Colloids Surf A Physicochem Eng Asp 2022;642:128701.
[258] Gao Y-N, Wang Y, Yue T-N, Weng Y-X, Wang M. Multifunctional cotton non-woven fabrics coated with silver nanoparticles and polymers for antibacterial, superhydrophobic and high performance microwave shielding. J Colloid Interface Sci 2021;582:112–23.
[259] Jin Z, Mei H, Pan L, Liu H, Cheng L. Superhydrophobic self-cleaning hierarchical micro-/nanocomposite coating with high corrosion resistance and durability. ACS Sustain Chem Eng 2021;9:4111–21.
[260] Niu H, Li J, Wang X, Luo F, Qiang Z, Ren J. Solar-assisted, fast, and in situ recovery of crude oil spill by a superhydrophobic and photothermal sponge. ACS Appl Mater Interfaces 2021;13:21175–85.
[261] Nguyen NB, Ly NH, Tran HN, Son SJ, Joo SW, Vasseghian Y, et al. Transparent oil–water separating spiky SiO2 nanoparticle supramolecular polymer superhydrophobic coatings. Small Methods 2023;7:2201257.
[262] Wang X, Ding H, Sun S, Zhang H, Zhou R, Li Y, et al. Preparation of a temperature-sensitive superhydrophobic self-cleaning SiO2-TiO2@ PDMS coating with photocatalytic activity. Surf Coat Technol 2021;408:126853.
[263] Cui Y, Li Y, Huan D, Zeng D, Yang Y, Zhu C, et al. Fabrication of silicone modified polyurethane matrix superhydrophobic coating with hydroxy-terminated polydimethylsiloxane modified SiO2 nanoparticles. Polym-Plast Technol Mater 2022;61:482–96.

[264] Kumar P, Ramesh M, Doddamani M. Fabrication and characterization of silicon dioxide-reinforced polydimethylsiloxane composite coating for corrosion protection of galvanized iron. SAE International Journal of Materials and Manufacturing 2024;17:319–28.
[265] Slepička P, Hurtuková K, Fajstavr D, Kasálková NS, Lyutakov O, Švorčík V. Carbon-gold nanocomposite induced by unique high energy laser single-shot annealing. Mater Lett 2021;301:130256.
[266] Li S, Huang L, Wang D, Zhou S, Sun X, Zhao R, et al. A review of 3D superhydrophilic porous materials for oil/water separation. Sep Purif Technol 2023;326:124847.
[267] Naseem M, Sultan M, ul Islam M, Kareem A, Ali N, Khan I, et al. Superhydrophilic wettability porous materials from construction tooil/water separation applications. Fuel 2025;386:134195.
[268] Selim MS, Yang H, Wang FQ, Fatthallah NA, Huang Y, Kuga S. Silicone/ZnO nanorod composite coating as a marine antifouling surface. Appl Surf Sci 2019;466:40–50.
[269] Zhang G-D, Wu Z-H, Xia Q-Q, Qu Y-X, Pan H-T, Hu W-J, et al. Ultrafast flame-induced pyrolysis of poly (dimethylsiloxane) foam materials toward exceptional superhydrophobic surfaces and reliable mechanical robustness. ACS Appl Mater Interfaces 2021;13:23161–72.
[270] Kuang M, Yang X, Huang Y, Xu K, Ye X. Preparation of durable superhydrophobic composite surface. Mater Today Commun 2023;36:106618.
[271] Zheng W, Teng L, Lai Y, Zhu T, Li S, Wu X, et al. Magnetic responsive and flexible composite superhydrophobic photothermal film for passive anti-icing/active deicing. Chem Eng J 2022;427:130922.
[272] Li E, Pan Y, Wang C, Liu C, Shen C, Pan C, et al. Multifunctional and superhydrophobic cellulose composite paper for electromagnetic shielding, hydraulic triboelectric nanogenerator and Joule heating applications. Chem Eng J 2021;420:129864.
[273] Zhang J, Zhang L, Gong X. Large-scale spraying fabrication of robust fluorine-free superhydrophobic coatings based on dual-sized silica particles for effective antipollution and strong buoyancy. Langmuir 2021;37:6042–51.
[274] Do V-T, Chun D-M. Fabrication of large-scale, flexible, and robust superhydrophobic composite films using hydrophobic fumed silica nanoparticles and polydimethylsiloxane. Polymer 2022;244:124630.
[275] Zimmermann C, Amouzou K, Ung B. Recent advances in PDMS optical waveguides: properties, fabrication, and applications. Adv Opt Mater 2024;13.
[276] Prajzler V, Nekvindova P, Spirkova J, Novotny M. The evaluation of the refractive indices of bulk and thick polydimethylsiloxane and polydimethyl-diphenylsiloxane elastomers by the prism coupling technique. J Mater Sci Mater Electron 2017;28:7951–61.
[277] Schneider F, Draheim J, Kamberger R, Wallrabe U. Process and material properties of polydimethylsiloxane (PDMS) for optical MEMS. Sens Actuators, A 2009;151:95–9.
[278] Zhang X, Qiu J, Li X, Zhao J, Liu L. Complex refractive indices measurements of polymers in visible and near-infrared bands. Appl Opt 2020;59:2337–44.
[279] Jang JW, Kim YE, Kwon OH, Kim JY, Shen W, Kim Y, et al. Polymer-encapsulated UV-curable stacked prismatic layers of all-halide phosphor composites for white luminescence. Mater Des 2022;224:111307.
[280] Yin Q, Xu R, Wang X, Li M, Huang X, Chen Z, et al. Precise laser-modulated anion exchange on ultraflexible perovskite films for multicolor patterns. ACS Appl Mater Interfaces 2024;16:48094–102.
[281] Dalod AR, Grendal OG, Blichfeld AB, Furtula V, Pérez J, Henriksen L, et al. Structure and optical properties of Titania-PDMS hybrid nanocomposites prepared by in situ non-aqueous synthesis. Nanomaterials 2017;7:460.
[282] Lamberti A, Virga A, Rivolo P, Angelini A, Giorgis F. Easy tuning of surface and optical properties of PDMS decorated by Ag nanoparticles. J Phys Chem B 2015;119:8194–200.
[283] Kaneko Y, Hayashi H, Ishii Y, Kada W, Nishikawa H. Refractive index change and thermo-optic effect in polydimethylsiloxane nanocomposites with oxide nanoparticles induced by proton beam writing. Nucl Instrum Methods Phys Res, Sect B 2019;459:94–7.
[284] Cutroneo M, Torrisi A, Ryukhtin V, Dopita M, Silipigni L, Mackova A, et al. Polydimethylsiloxane containing gold nanoparticles for optical applications. J Instrum 2020;15:C03044.
[285] Scarano S, Berlangieri C, Carretti E, Dei L, Minunni M. Tunable growth of gold nanostructures at a PDMS surface to obtain plasmon rulers with enhanced optical features. Microchim Acta 2017;184:3093–102.
[286] Dunklin JR, Forcherio GT, Roper DK. Geometric optics of gold nanoparticle-polydimethylsiloxane thin film systems. Optical Materials Express 2014;4:375–83.
[287] Liu J, Zong G, He L, Zhang Y, Liu C, Wang L. Effects of fumed and mesoporous silica nanoparticles on the properties of sylgard 184 polydimethylsiloxane. Micromachines 2015;6:855–64.
[288] Pastoriza-Santos I, Pérez-Juste J, Kickelbick G, Liz-Marzán LM. Optically active poly (dimethylsiloxane) elastomer films through doping with gold nanoparticles. J Nanosci Nanotechnol 2006;6:453–8.
[289] Huang X, Jain PK, El-Sayed IH, El-Sayed MA. Gold nanoparticles: interesting optical properties and recent applications in cancer diagnostics and therapy. Nanomed Nanotechnol Biol Med 2007;2:681–93.
[290] Shiohara A, Langer J, Polavarapu L, Liz-Marzán LM. Solution processed polydimethylsiloxane/gold nanostar flexible substrates for plasmonic sensing. Nanoscale 2014;6:9817–23.
[291] Liz-Marzán LM. Tailoring surface plasmons through the morphology and assembly of metal nanoparticles. Langmuir 2005;22:32–41.
[292] Berry Jr KR, Russell AG, Blake PA, Roper DK. Gold nanoparticles reduced in situ and dispersed in polymer thin films: optical and thermal properties. Nanotechnology 2012;23:375703.
[293] Lee S, Shin H-J, Yoon S-M, Yi DK, Choi J-Y, Paik U. Refractive index engineering of transparent ZrO 2–polydimethylsiloxane nanocomposites. J Mater Chem 2008;18:1751–5.
[294] Lu Q, Mullins ME. In situ synthesis of high refractive index PDMS/Metal oxide nanocomposites. MRS Online Proc Libr 2012;1400:23–8.
[295] Kim B-S, Oh G-H, Song Y, Lee Y-S, Kim S. Acid catalyzed microwave-assisted production of full-color light emissive carbon quantum dots for CCT-tunable WLEDs. Appl Surf Sci 2023;640:158301.
[296] Miroshnichenko AS, Deriabin KV, Baranov AI, Neplokh V, Mitin DM, Kolesnikov IE, et al. Lanthanide (III)-incorporating polysiloxanes as materials for light-emitting devices. ACS Appl Polym Mater 2022;4:2683–90.
[297] Moscoso FG, Rodriguez-Albelo LM, Ruiz-Salvador AR, Lopes-Costa T, Pedrosa J. Enhancement of the intrinsic fluorescence of ZIF-8 via post-synthetic cation exchange with Cd2+ and its incorporation into PDMS films for selective sulfide optical sensing. Mater Today Chem 2023;28:101366.
[298] Dong Y, Ma Z, Song D-P, Ma G, Li Y. Rapid responsive mechanochromic photonic pigments with alternating glassy-rubbery concentric lamellar nanostructures. ACS Nano 2021;15:8770–9.
[299] Lu Y, Xu Y, Chen S, Lin J, Zhu J, Wang S, et al. Ultra-narrowband emitting and highly stable CsPbX3@ glass@ PDMS (X3= Br3, Br1. 5I1. 5) monolithic composite film for backlit displays. Journal of Luminescence. 2022;248:118952.
[300] Cai J, Wang C, Hu X, Ye Y, Zhong L, Chen E, et al. Water-driven photoluminescence reversibility in CsPbBr3/PDMS-PUa composite. Nano Res 2022;15:6466–76.
[301] Li C, Gao Y, Ren Z, Xiong S, Li C, Wu J, et al. Highly efficient, ultra-stable multi-interlayer luminescent solar concentrators based on green and red-emitting perovskite nanocrystal composites. J Mater Chem C 2025;13:945–53.
[302] Liu Y, Yang S, Luo X, Long Z, Cao E, Li J, et al. Layered B2O3/CsPbBr3 perovskite composite embedded using glass as microreactor with enhanced stability and high-efficiency light extraction. Chem Eng J 2023;470:144383.
[303] Yang Z, Lin C-Q, Liu M-L, Wang H, Pan C-Y. Dual-emission Mn-doped CsPbCl3 QDs in collaboration with CsPbBr3 QDs applied in excitation-sensitive flexible anti-counterfeiting technologies. J Solid State Chem 2024;332:124584.
[304] Xiong P, Yang X, Shen J. Confinement reaction synthesis of CsPbBr3 quantum dots within long afterglow mesoporous materials as lighting equipment. Mater Today Commun 2024;39:108590.
[305] Han J, AM T, Kim S, Morales Florez G, Shrestha K, Nguyen DD, et al. Nanocomposite-based PCR reactors to enhance thermal rate and fluorescence intensity in hand-held qPCR device. Journal of Nanobiotechnology. 2025;23:240.
[306] Guan J, Park J-E, Deng S, Tan MJ, Hu J, Odom TW. Light–matter interactions in hybrid material metasurfaces. Chem Rev 2022;122:15177–203.

[307] Chandran Y, Thakur D, Sharma A, Gupta K, Ravishankar N, Balakrishnan V. Durable PDMS-interleaved WS2 monolayer composites for enhanced optical absorbance and in-situ strain sensing. Adv Funct Mater 2025. e13892.
[308] Borjanović V, Bistričić L, Vlasov I, Furić K, Zamboni I, Jakšić M, et al. Influence of proton irradiation on the structure and stability of poly (dimethylsiloxane) and poly (dimethylsiloxane)-nanodiamond composite. Journal of Vacuum Science & Technology B: Microelectronics and Nanometer Structures Processing, Measurement, and Phenomena 2009;27:2396–403.
[309] Luo X, Fan J, Zhang M, Qian C, Fan X, Zhang G. Degradation mechanism analysis for phosphor/silicone composites aged under high temperature and high humidity condition. In: 2017 18th International Conference on Electronic Packaging Technology (ICEPT). IEEE; 2017. p. 1331–6.
[310] Lansade D, Lewandowski S, Remaury S, Sierra G, Solé S, Perraud S, et al. Enhanced resistance to proton irradiation of poly (dimethylsiloxane) resins through surface embedding of silica photonic crystals. Polym Degrad Stab 2020;176:109163.
[311] Liang G, Tang Y, Huang J, Li J, Yuan Y, Yang S, et al. Optical performance and moisture stability enhancement of flexible luminescent films based on quantum-dot/epoxy composite particles. Nanomaterials 2021;11:2100.
[312] Borjanovic V, Lawrence WG, Hens S, Jaksic M, Zamboni I, Edson C, et al. Effect of proton irradiation on photoluminescent properties of PDMS–nanodiamondcomposites. Nanotechnology 2008;19:455701.
[313] Kwon Y-T, Lim G-D, Kim S, Ryu SH, Hwang T-Y, Park K-R, et al. Near-infrared absorbance properties of Cu 2–x S/SiO 2 nanoparticles and their PDMS-based composites. J Mater Chem C 2018;6:754–60.
[314] Gong Y, Shen J, Zhu Y, Yang X, Zhang L, Li C. Stretch induced photoluminescence enhanced perovskite quantum dot polymer composites. J Mater Chem C 2020;8:1413–20.
[315] Wu K, Du X, Liang G, Tang Y, Lu H, Li Z, et al. Study on optical performance and reliability of white light-emitting diodes by quantum-dots/epoxy composite particles. In: 2019 20th International Conference on Electronic Packaging Technology (ICEPT). IEEE; 2019. p. 1–4.
[316] Torrisi L, Cutroneo M, Silipigni L, Fazio B, Di Marco G, Slepicka P, et al. Light luminescence and trapping in polydimethylsiloxane foils with low concentration of gold nanoparticles. Radiat Eff Defects Solids 2022;177:40–56.
[317] Ghasemlou M, Mayes EL, Murdoch BJ, Le PH, Dekiwadia C, Aburto-Medina A, et al. Silicon-doped graphene oxide quantum dots as efficient nanoconjugates for multifunctional nanocomposites. ACS Appl Mater Interfaces 2022;14:7161–74.
[318] Yao Z, Li Y, Lv G, Chen D, Yang J, Guo S. Structural optimization of photoacoustic transducer with PDMS/CSNPs nanocomposite for fatigue crack detection using laser-induced nonlinear surface waves. Mater Des 2024;238:112635.
[319] Yang X, Chen Y-H, Xia F, Sawan M. Photoacoustic imaging for monitoring of stroke diseases: a review. Photoacoustics 2021;23:100287.
[320] Kratkiewicz K, Manwar R, Zafar M, Zhang R, Huang B, Dadashzadesh N, et al. Review of cost reduction methods in photoacoustic computed tomography. arXiv preprint arXiv:190209987. 2019.
[321] Wang Q, Zhou J, Wu X, Riaud A. Optimization of the synthesis conditions of gold nanoparticle–polydimethylsiloxane composites for ultrasound generation. Mater Adv 2022;3:2850–7.
[322] Lu S, Li C, Liu R, Liang T, Song X. High-consistent optical fiber photoacoustic generator with carbon nanoparticles-PDMS composite. Opt Lasers Eng 2023;169:107731.
[323] Yao Z, Feng H, Shang K, Deng X, Yang T. Skin-like strain sensors based on multiwalled carbon nanotube/polydimethylsiloxane composite films. ACS Appl Nano Mater 2023;6:6550–8.
[324] Vella D, Mrzel A, Drnovšek A, Shvalya V, Jezeršek M. Ultrasonic photoacoustic emitter of graphene-nanocomposites film on a flexible substrate. Photoacoustics 2022;28:100413.
[325] Sappati KK, Bhadra S. Temperature compensated differential acoustic sensor for CO2 sensing. Meas Sci Technol 2021;32:105103.
[326] Hajra S, Oh Y, Sahu M, Lee K, Kim H-G, Panigrahi BK, et al. Piezoelectric nanogenerator based on flexible PDMS–BiMgFeCeO 6 composites for sound detection and biomechanical energy harvesting. Sustainable Energy Fuels 2021;5:6049–58.
[327] Cui X, Ruan Q, Zhuo X, Xia X, Hu J, Fu R, et al. Photothermal nanomaterials: a powerful light-to-heat converter. Chem Rev 2023;123:6891–952.
[328] Baffou G, Quidant R, Girard C. Heat generation in plasmonic nanostructures: influence of morphology. Appl Phys Lett 2009;94.
[329] Linic S, Christopher P, Ingram DB. Plasmonic-metal nanostructures for efficient conversion of solar to chemical energy. Nat Mater 2011;10:911–21.
[330] Pelton M, Aizpurua J, Bryant G. Metal-nanoparticle plasmonics. Laser Photonics Rev 2008;2:136–59.
[331] Wiley BJ, Im SH, Li Z-Y, McLellan J, Siekkinen A, Xia Y. Maneuvering the surface plasmon resonance of silver nanostructures through shape-controlled synthesis. ACS Publications 2006:15666–75.
[332] Wiley BJ, Chen Y, McLellan JM, Xiong Y, Li Z-Y, Ginger D, et al. Synthesis and optical properties of silver nanobars and nanorice. Nano Lett 2007;7:1032–6.
[333] Huang J, Liu C, Zhu Y, Masala S, Alarousu E, Han Y, et al. Harnessing structural darkness in the visible and infrared wavelengths for a new source of light. Nat Nanotechnol 2016;11:60–6.
[334] Hosseinaee Z, Le M, Bell K, Reza PH. Towards non-contact photoacoustic imaging. Photoacoustics 2020;20:100207.
[335] Vella D, Pereira DA, Mrzel A, Vengust D, Drnovšek A, Arnaut LG, et al. Picosecond photoacoustic generation of ultrasounds with composites of graphene-decorated gold nanoparticles. Nano Energy 2024;131:110236.
[336] Zhang T, Li C-H, Li W, Wang Z, Gu Z, Li J, et al. A self-healing optoacoustic patch with high damage threshold and conversion efficiency for biomedical applications. Nano-Micro Letters 2024;16:122.
[337] Wang D, Zhou X, Song R, Fang C, Wang Z, Wang C, et al. Freestanding silver/polypyrrole composite film for multifunctional sensor with biomimetic micropattern for physiological signals monitoring. Chem Eng J 2021;404:126940.
[338] Zhu S, Lu Y, Wang S, Sun H, Yue Y, Xu X, et al. Interface design of stretchable and environment-tolerant strain sensors with hierarchical nanocellulose-supported graphene nanocomplexes. Compos A Appl Sci Manuf 2023;164:107313.
[339] Munkhbayar B, Nine MJ, Hwang S, Kim J, Bae K, Chung H, et al. Effect of grinding speed changes on dispersibility of the treated multi-walled carbon nanotubes in aqueous solution and its thermal characteristics. Chem Eng Process 2012;61:36–41.
[340] Sidhu JS, Misra A, Bhardwaj A. Development of flexible piezoresistive pressure sensors via direct ink writing of MWCNT/PDMS nanocomposite inks: rheological and electromechanical characterization. Nanoscale Adv 2025.
[341] Hou Y, Ashkenazi S, Huang S-W, O'Donnell M. An integrated optoacoustic transducer combining etalon and black PDMS structures. IEEE Trans Ultrason Ferroelectr Freq Control 2008;55:2719–25.
[342] Herdovics B, Cegla F. Long-term stability of guided wave electromagnetic acoustic transducer systems. Struct Health Monit 2020;19:3–11.
[343] Xu J, Wu S, Tao C, Liu X. Optical and ultrasonic dual-sensitive sensor and its application in photoacoustic microscopy. Appl Phys Express 2024;17:017003.
[344] Li C-H, Wang C, Keplinger C, Zuo J-L, Jin L, Sun Y, et al. A highly stretchable autonomous self-healing elastomer. Nat Chem 2016;8:618–24.
[345] Liu H, Su X, Fu R, Wu B, Chen X. The flexible film of SCF/BN/PDMS composites with high thermal conductivity and electrical insulation. Compos Commun 2021;23:100573.
[346] Luo T, Esfarjani K, Shiomi J, Henry A, Chen G. Molecular dynamics simulation of thermal energy transport in polydimethylsiloxane. J Appl Phys 2011;109.
[347] Mallon P, Berhane T, Greyling C, Vosloo W, Chen H, Jean YC. Corona treated polydimethylsiloxane (PDMS) surfaces studied by the slow positron beam technique. materials science forum. Trans Tech Publ; 2004. p. 322–4.
[348] Teowee G, McCarthy K, Baertlein C, Boulton J, Motakef S, Bukowski T, et al. Dielectric properties of organic-inorganic hybrids: PDMS-based systems. MRS Online Proc Libr 1996;435:559–64.
[349] Adachi H, Adachi K, Ishida Y, Kotaka T. Dielectric relaxation of polydimethylsiloxane. J Polym Sci Polym Phys Ed 1979;17:851–7.
[350] Panda S, Acharya B. PDMS/MWCNT nanocomposites as capacitive pressure sensor and electromagnetic interference shielding materials. J Mater Sci Mater Electron 2021;32:16215–29.
[351] Gao X, Huang Y, Liu Y, Kormakov S, Zheng X, Wu D, et al. Improved electrical conductivity of PDMS/SCF composite sheets with bolting cloth prepared by a spatial confining forced network assembly method. RSC Adv 2017;7:14761–8.

[352] Wu D, Li Z, Du Y, Zhang L, Huang Y, Sun J, et al. Compression-induced electrical percolation and enhanced mechanical properties of polydimethylsiloxane-based nanocomposites. J Mater Sci 2020;55:10611–25.
[353] Meddeb A, Ounaies Z, Lopez-Pamies O. Interfacial effects on the electrical behavior of elastomer nanoparticulate composites. Behavior and Mechanics of Multifunctional Materials XIII: SPIE; 2019. p. 124-32.
[354] Hu Y, Ishikawa K. Ultrahigh dielectric constant induced by the interfacial polarization between liquid crystal droplets and polymer matrix. Jpn J Appl Phys 2020;59:060901.
[355] Seo J-S, Kim D-H, Jung H-S, Kim H-D, Choi J, Kim M, et al. Effect of the particle size and layer thickness of GNP fillers on the dielectric properties and actuated strain of GNP–PDMS composites. Polymers 2022;14:3824.
[356] Anlin LK, Vijoy K, Pradeesh K, Thomas S, John H, Saji K. Effects of metal nanoparticles on the performance of PDMS based triboelectric nanogenerators. Phys B Condens Matter 2022;639:413952.
[357] He X, Wu J, Xuan S, Sun S, Gong X. Stretchable and recyclable liquid metal droplets embedded elastomer composite with high mechanically sensitive conductivity. ACS Appl Mater Interfaces 2022;14:9597–607.
[358] Kim M-G, Nam K-W, Kim W-J, Park S-H. Optimizing stretchability and electrical stability in bilayer-structured flexible liquid metal composite electrodes. Micromachines 2024;15:1467.
[359] Zhang C, Lv Z, Xu Z, Wu K, Morshuis P, Claverie A. The effect of nano TiO2 on space charge behaviour of silicone elastomer under DC electric field. In: 2023 International Symposium on Electrical Insulating Materials (ISEIM). IEEE; 2023. p. 195–8.
[360] Cao T, Shi X-L, Chen Z-G. Advances in the design and assembly of flexible thermoelectric device. Prog Mater Sci 2023;131:101003.
[361] Zhou Y, Zhang Y, Nie Y, Sun D, Wu D, Ban L, et al. Recent advances and perspectives in functional chitosan-based composites for environmental remediation, energy, and biomedical applications. Prog Mater Sci 2025;101460.
[362] Wu R, Zhu T, Cheng Y, Liu Z, Huang J, Wei Y, et al. Materials, structure design, performances of multifunctional flexible devices for healthcare. Prog Mater Sci 2025;101491.
[363] Schlingman K, D'Amaral GM, Carmichael RS, Carmichael TB. Intrinsically conductive liquid metal-elastomer composites for stretchable and flexible electronics. Adv Mater Technol 2023;8:2200374.
[364] Cheng Y, Wang R, Sun J, Gao L. A stretchable and highly sensitive graphene-based fiber for sensing tensile strain, bending, and torsion. Adv Mater 2015;27:7365–71.
[365] Silva JP, Sousa L, Vélez HAV, Coelho PH. Simulación de lapercolación eléctrica de nanotubos de carbono a través de una matriz de polimetilmetacrilato: análisis bidimensional y tridimensional usando elefecto de latortuosidad de los nanoaditivos. Revista de Ciencia y Tecnología. 2022:71-80.
[366] Yang T, Lin C, Huang M, Ying P, Zhang P, Wu J, et al. Self-healing and recyclable polyurethane/nanocellulose elastomer based on the diels–alder reaction. Polymers 2024;16:2029.
[367] Li X, Yuan F, Tian W, Dai C, Yang X, Wang D, et al. Heat transfer enhancement of nanofluids with non-spherical nanoparticles: a review. Appl Sci 2022;12:4767.
[368] Qureshi N, Dhand V, Subhani S, Kumar RS, Raghavan N, Kim S, et al. Exploring conductive filler-embedded polymer nanocomposite for electrical percolation via electromagnetic shielding-based additive manufacturing. Adv Mater Technol 2024;9:2400250.
[369] Gao D, Chang R, Lyu B, Ma J. Growth from spherical to rod-like SiO2: Impact on microstructure and performance of nanocomposite. J Alloy Compd 2019;810:151814.
[370] Markel VA. Introduction to the Maxwell Garnett approximation: tutorial. J Opt Soc Am A 2016;33:1244–56.
[371] Shi G, Zhao Z, Pai JH, Lee I, Zhang L, Stevenson C, et al. Highly sensitive, wearable, durable strain sensors and stretchable conductors using graphene/silicon rubber composites. Adv Funct Mater 2016;26:7614–25.
[372] Chen J, Zheng J, Gao Q, Zhang J, Zhang J, Omisore OM, et al. Polydimethylsiloxane (PDMS)-based flexible resistive strain sensors for wearable applications. Appl Sci 2018;8:345.
[373] Zhu J, Li J, Tong Y, Hu T, Chen Z, Xiao Y, et al. Recent progress in multifunctional, reconfigurable, integrated liquid metal-based stretchable sensors and standalone systems. Prog Mater Sci 2024;142:101228.
[374] Manjakkal L, Pereira L, Barimah EK, Grey P, Franco FF, Lin Z, et al. Multifunctional flexible and stretchable electrochromic energy storage devices. Prog Mater Sci 2024;142:101244.
[375] Zha J-W, Wang F, Wan B. Polymer composites with high thermal conductivity: theory, simulation, structure and interfacial regulation. Prog Mater Sci 2025;148:101362.
[376] Amjadi M, Pichitpajongkit A, Lee S, Ryu S, Park I. Highly stretchable and sensitive strain sensor based on silver nanowire–elastomer nanocomposite. ACS Nano 2014;8:5154–63.
[377] Qiu L, Zhu N, Feng Y, Michaelides EE, Żyła G, Jing D, et al. A review of recent advances in thermophysical properties at the nanoscale: from solid state to colloids. Phys Rep 2020;843:1–81.
[378] Rai A, Moore AL. Enhanced thermal conduction and influence of interfacial resistance within flexible high aspect ratio copper nanowire/polymer composites. Compos Sci Technol 2017;144:70–8.
[379] Mahapatra A, Chatterjee S, Rahman A, Sain A, Ganguly V, Bajpai A, et al. Thermodynamic Control of Nanoparticle Fabrication via Confined Dewetting. 2025.
[380] Shim H, Hwang S, Byun E, Choi M, Kim B, Song S. Inkjet patterning of plasmonic metal nanoparticles in silicone elastomers. Adv Mater Technol 2023;8:2201614.
[381] Silipigni L, Salvato G, Torrisi A, Cutroneo M, Slepicka P, Fajstavr D, et al. Pressure sensor based on porous polydimethylsiloxane with embedded gold nanoparticles. J Mater Sci Mater Electron 2021;32:8703–15.
[382] Cutroneo M, Havranek V, Mackova A, Malinsky P, Torrisi A, Silipigni L, et al. The characterisation of polydimethylsiloxane containing gold nanoparticles as a function of curing time. Surf Interface Anal 2021;53:618–26.
[383] Romanenko O, Slepička P, Malinsky P, Cutroneo M, Havránek V, Stammers J, et al. The influence of Au-nanoparticles presence in PDMS on microstructures creation by ion beam lithography. Surf Interface Anal 2020;52:1040–4.
[384] Toci G, Olgiati F, Pallavicini P, Diaz Fernandez YA, De Vita L, Dacarro G, et al. Gold nanostars embedded in PDMS films: a photothermal material for antibacterial applications. Nanomaterials 2021;11:3252.
[385] Coetzee D, Venkataraman M, Militky J, Petru M. Influence of nanoparticles on thermal and electrical conductivity of composites. Polymers 2020;12:742.
[386] Lu J, Mei M, Huang C. Influence of silicon dioxide nanoparticles on hydrophobicity and transparency of polydimethylsiloxanes coatings hybridized with silicon dioxide nanoparticles. Thin Solid Films 2025;140800.
[387] Sun J, Chen Y, Li J, Su J, Huang S, Zhang Y, et al. Synthesis of transparent and flexible superhydrophobic PDMS-EP/SiO2 coating with excellent mechanical and chemical durability. Appl Surf Sci 2025;163586.
[388] Ananthasubramanian P, Sahay R, Raghavan N. Investigation of the surface mechanical properties of functionalized single-walled carbon nanotube (SWCNT) reinforced PDMS nanocomposites using nanoindentation analysis. RSC Adv 2024;14:15249–60.
[389] Gilshteyn EP, Romanov SA, Kopylova DS, Savostyanov GV, Anisimov AS, Glukhova OE, et al. Mechanically tunable single-walled carbon nanotube films as a universal material for transparent and stretchable electronics. ACS Appl Mater Interfaces 2019;11:27327–34.